THE UNIVERSITY OF CALGARY

DYNAMIC MODELLING OF A SPOUTED BED REACTOR WITH A DRAFT TUBE USED FOR HYDROCARBON ULTRAPYROLYSIS

by

John Harvey Eng

A Thesis
Submitted to the Faculty of Graduate Studies in Partial
Fulfillment of the Requirements for the Degree of
Master of Science

Department of Chemical and Petroleum Engineering
Calgary, Alberta, Canada

June, 1988

ISBN 0-315-46589-1

THE UNIVERSITY OF CALGARY

FACULTY OF GRADUATE STUDIES

The undersigned certify that they have read, and recommend to the Faculty of Graduate Studies for acceptance, a thesis entitled,

"DYNAMIC MODELLING OF A SPOUTED BED REACTOR WITH A DRAFT TUBE USED FOR HYDROCARBON ULTRAPYROLYSIS"

submitted by John Harvey Eng in partial fulfillment of the requirements for the degree of Master of Science.

Leo Behie

Dr. L.A. Behie, Committee Chairman
Department of Chemical & Petroleum Engineering

Franco Berruti

Dr. F. Berruti
Department of Chemical & Petroleum Engineering

W. Svrcek

Dr. W.Y. Svrcek
Department of Chemical & Petroleum Engineering

Dr. B. Tinker
Vice-President Finance & Services

June 28, 1988

Date

ABSTRACT

Studies in the applications of spouted beds began over thirty years ago. At that time, the primary use of spouted beds was as dryers for agricultural products. Since then, they have been studied as catalytic reactors and have even been employed as hydrocarbon thermal cracking or pyrolysis reactors.

Early studies considered employing a conventional spouted bed as a pyrolysis reactor and found it to be well-suited for this purpose as extremely high heat-up rates could be achieved in the reactor. This idea was later expanded upon by incorporating a centrally-located draft tube within the spouted bed. Its purpose was to restrict the residence time distribution of the reactant gases and hence, improve selectivity of the product distribution obtained. Recent work tested this configuration for its feasibility as a pyrolysis reactor, and a steady state model describing the bed was developed.

In this study, understanding concerning this reactor was extended by the development of a dynamic model of a spouted bed reactor with a draft tube to predict responses in the bed to operational disturbances. In order to verify the model, computer simulations were compared with experimental data. These comparisons not only served to substantiate the model, but also enabled investigation of the hydrodynamic characteristics of particle

entrainment and spout gas divergence into the annulus.

The dynamic responses predicted by the model were characterized by two trends. For changes in the feed stream properties, an almost immediate "pseudo-steady state" appeared, followed by a slower approach to the final steady state. For fluctuations in the wall temperature of externally-heated beds, the response was typified by a slow migration of bed temperatures to the final steady state. The slow response to the final steady state in the case of each disturbance was attributed to the long time constants associated with thermal equilibrium of the annular solids.

Due to the lack of published information available regarding hydrodynamic properties in spouted beds, it was impossible to apply this model to any specific situation. It was therefore recommended that further research be first carried out in this respect. Following the study of spouted bed hydrodynamics, this model could then be applied very effectively in the control of such reactors.

ACKNOWLEDGEMENTS

In completing this work, the contributions of many must be recognized since their support, advice, ideas, humor, and company made this study much more worthwhile.

First of all, I would like to acknowledge the University of Calgary and the Natural Sciences and Engineering Research Council of Canada for their financial assistance during my studies.

To the Department of Chemical and Petroleum Engineering, I would also like to express my gratitude. In particular, I would like to thank my supervising professor, Dr. Leo Behie, for his support, enthusiasm, and humor (or at least what I interpreted as humor). I sincerely appreciate all that he did in my behalf.

I would also like to thank my associates during this time, especially Rudi Stocker, who assisted in so many ways and also put up with a great deal in assisting me, but always seemed willing to help. In addition, John McRae provided much needed support on many occasions with my computing work. Many graduate students with whom I shared an office, Ashutosh Rastogi, James Muir, Judy Fairburn, Gustav Oertzen and Mohammad Asif, offered many useful suggestions and also made life a little more enjoyable, not to mention being an outlet for my frustrations at times. In addition, many of the other graduate students have offered their assistance and friendship, which I would

also like to thank them for.

I would also like to thank my friends who were always a great relief in a time when a great deal of relief was needed. While I would like to express my gratitude to Suzanne West for her assistance with graphing routines, I am even more appreciative of all of their friendships, which I hope will last long after I have forgotten all of this work.

Most of all, I would like to thank my family for all their endless support. They have always been my examples in life and I would like to dedicate this thesis to them.

Table of Contents

List of Tables

List of Figures

Nomenclature

A - cross-sectional or surface area (m^2)

Ar - Archimedes number = $d_p^3 \cdot \rho_g(\rho_p - \rho_g)/\mu^2$

B_1 - entrainment rate correlation for bench-scale spouted bed (Equation 5.2 on page 86)

B_2 - entrainment rate correlation for bench-scale spouted bed (Equation 5.3 on page 86)

B_3 - entrainment rate correlation for bench-scale spouted bed (Equation 5.4 on page 86)

a_i - coefficients of approximation polynomial

C_D - drag coefficient

C_i - concentration of gaseous component i ($kmol/m^3$)

c_{p_i} - heat capacity of component i ($kJ/kmol \cdot K$)

D_b - diameter of bed (m)

D_{dt} - draft tube diameter (m)

D_{in} - diameter of inlet nozzle (m)

D_s - diameter of spout (m)

d_p - particle diameter (m)

F_{12} - view factor for surface 1 surrounding surface 2

F_i - flow rate of component i (kmol/s)

F_p - total particle entrainment (kg/s)

f_{loss_i} - spout gas divergence function for component i ($kmol/m \cdot s$)

g_L - total fractional molar gas bypass

H_{dt} - length of draft tube region (m)

H_i - enthalpy of component i (kJ/kmol)

ΔH_i - heat of reaction for reaction i (kJ/kmol)

H_m - maximum spoutable bed depth for conventional spouted bed (m)

H_t - total height of bed = $L_e + H_{dt}$ (m)

h_a - heat transfer coefficient for bed wall to bulk annulus heat transfer ($kW/m^2 \cdot K$)

h_p - heat transfer coefficient for particle to spout gas heat transfer ($kW/m^2 \cdot K$)

h_{rv} - heat transfer contribution due to radiation between adjacent void spaces

h_{rs} - heat transfer contribution due to radiation between adjacent particle surfaces

h_w - heat transfer coefficient for annular wall to spout gas heat transfer ($kW/m^2 \cdot K$)

h_{w_0} - heat transfer coefficient for turbulent flow ($kW/m^2 \cdot K$)

Δh_w - enhancement factor for heat transfer coefficient h_w

k - thermal conductivity ($kW/m \cdot K$)

L_e - length of entrainment region (m)

M_i - molecular weight of component i (kg/kmol)

MH - Mamuro-Hattori equation (Equation 2.2 on page 17)

N_c - number of gaseous components

N_1 - number of collocation points in entrainment region

N_2 - number of collocation points in draft tube region

P_1 - entrainment rate correlation for pilot-scale spouted bed (Equation 5.6 on page 87)

P_2 - entrainment rate correlation for pilot-scale spouted bed (Equation 5.7 on page 87)

Pr - Prandtl number = $c_p \cdot \mu / k$

R_a - thermal resistance of annular bed wall boundary layer ($m \cdot K/kW$)

R_k - thermal resistance of bulk annulus ($m \cdot K/kW$)

R_w - thermal resistance of draft tube wall boundary layer ($m \cdot K/kW$)

Re - Reynolds number = $\rho \cdot U \cdot D / \mu$

r_{ij} - reaction rate for component i in reaction j ($kmol/m^3 \cdot s$)

T - temperature (K)

T_c - critical temperature (K)

T_r - reduced temperature = T/T_c

t - time (s)

U - gas velocity (m/s)

U_{ms} - minimum spouting gas velocity (m/s)

U_w - overall heat transfer coefficient for heat transfer from annular wall to spout gas ($kW/m^2 \cdot K$)

V - particle velocity (m/s)

z - axial distance (m)

Δz - increment in axial distance (m)

Greek Characters

α - parameter in energy balance equation
also parameter used in Jacobi polynomials

β - parameter used in Jacobi polynomials

$\in$ - voidage

ϵ - emissivity

ρ - density (kg/m^3)

ζ - normalized axial distance

θ - normalized temperature

- or, included cone angle for conic-based beds (^{o})

μ - gas viscosity (Pa·s)

σ - Stefan-Boltzmann constant = $5.672 \times 10^{-11} kW/m^2 \cdot K^4$

ϕ - thermal conductivity enhancement parameter

Subscripts

a - annular

f - final (i.e. at top of draft tube)

g - gas

p - particle

s - spout

w - external wall

0 - inlet conditions

Superscripts

o - steady state

Chapter 1

INTRODUCTION

Spouted bed technology has been developing for over thirty years. It has been implemented over a wide range of applications as disparate as the drying of agricultural products, the granulation and coating of particles, the blending of solids, and the means for various chemical reactions to take place. The diversity in the manner in which a spouted bed can be employed stems from the basic features inherent in the nature of this type of a reactor.

A conventional spouted bed, as illustrated in Figure 1.1, consists of a bed of coarse particles into the base of which a high velocity jet of gas or liquid is injected. The injected stream entrains and vertically conveys particles up through a high-voidage spout region, located centrally within the bed, and into a fountain region. In the fountain region, which is located above the bed, the particles disengage from the upward-moving stream as the fluid diverges and then the particles fall onto the top of the descending annular bed of solids. Spouted beds are therefore typified by the

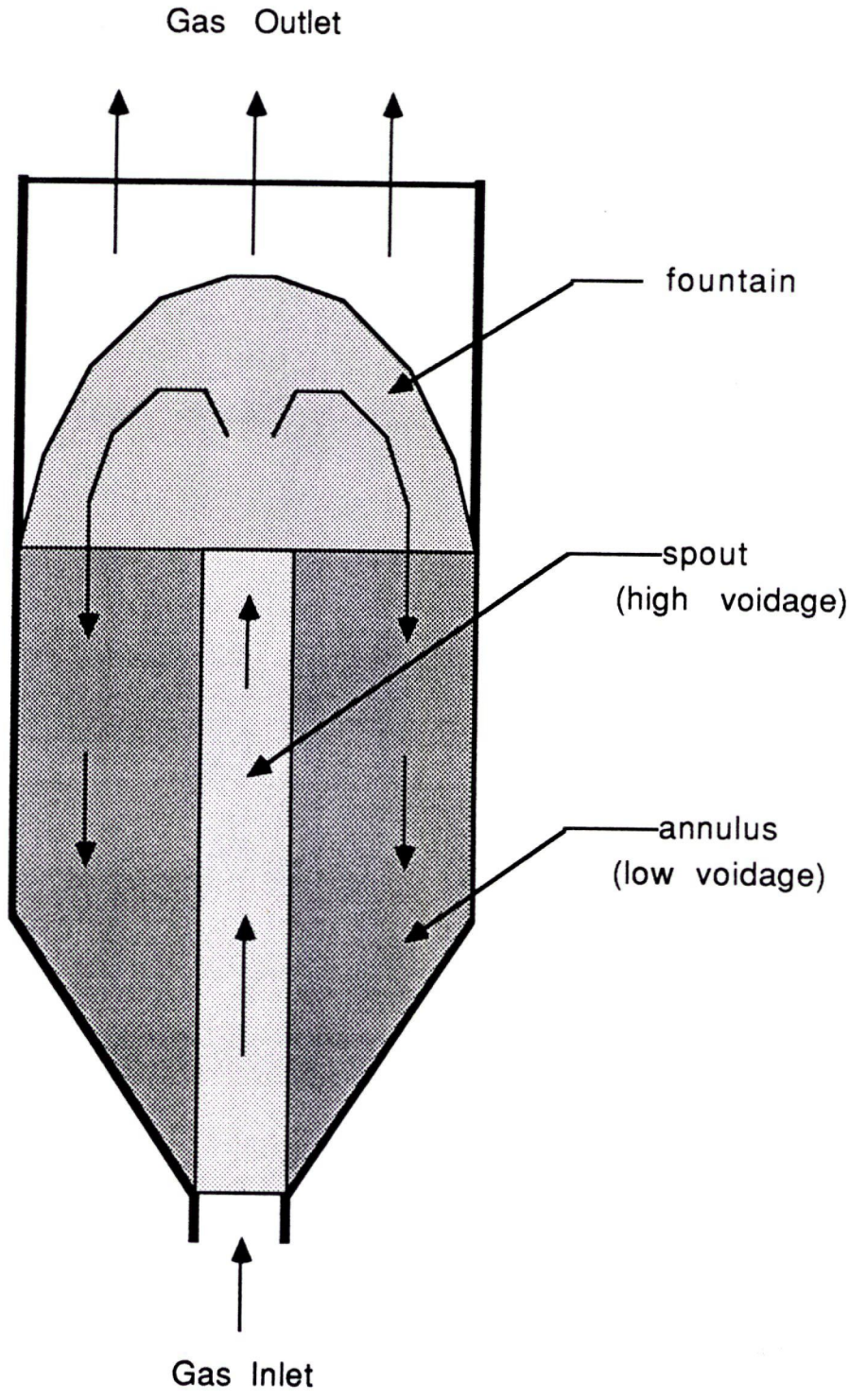

Fig.1.1 - Conventional Spouted Bed

dilute spout region, the downward-moving annular bed, and the fountain region in which particles are in transition between the two other regions.

The fluid-particle interactions accompanying spouted bed operation induce several effects. First of all, the particles are contacted with a highly turbulent fluid which results in large heat and mass transfer rates between the two phases. Secondly, the transport of particles up through the spout region causes high attrition as well as large solids recirculation rates. In many operations, the long residence time of particles in the downward-moving annular bed is also beneficial.

While spouted beds were first designed to take advantage of the high mass transfer characteristics necessary for the drying of grains, research indicated that it could also be useful in numerous other coarse-particle applications. Industrially, Mathur and Epstein (1974) found these applications to include granulation, drying of solids and solutions, tablet coating, fertilizer cooling, solids blending, and charcoal activation. In addition to these uses, however, Uemaki *et al.* (1970) have investigated the suitability of spouted beds in crude oil, heavy oil, and naphtha pyrolysis.

1.1 HYDROCARBON PYROLYSIS

The features of a spouted bed, in fact, make this technology particularly attractive for pyrolysis processes.

Hydrocarbon pyrolysis, or thermal cracking, has been determined to proceed by means of free radical reactions. These reactions are initiated by high activation-energy scission reactions in which molecules are divided into free radicals. Due to the high activation energies required by these reactions, temperatures generally in excess of 600° C are necessary to initiate cracking. The other pyrolysis reactions, generally categorized as propagation reactions, are characterized by low activation energies and can proceed as fast as gas-phase collision frequency. Consequently, residence times in pyrolysis reactions will strongly influence the product distributions obtained.

As an example, pyrolysis carried out under operating temperatures of less than 600° C typically require residence times in the order of minutes to hours in order to obtain conversions of 10 percent. As the operating temperature increases past 600° C, the required residence times of reactant gases is reduced to a range of one second for conversions of a comparable magnitude. In each of the previous cases, however, large amounts of undesirable byproducts, such as coke, are formed. Further increase of the operating temperature, with residence times in the range of hundreds of milliseconds, will result in fast initiation of the scission reactions. Moreover, the short residence times will minimize the extent of the propagation reactions, thus reducing the formation of undesirable byproducts while still achieving high conversions.

Ultrapyrolysis then, refers to that class of

pyrolysis characterized by operating temperatures in excess of 600^{o} C (depending upon the hydrocarbon feed), and residence times less than 500 milliseconds. Under such operating conditions, extremely high heat-up rates, typically in the range of 10^{5} K/s, are prevalent [Stocker (1987)].

1.2 SPOUTED BED REACTOR WITH A DRAFT TUBE

Since longer residence times shift the product distribution towards undesirable secondary products, reactors designed for thermal cracking should be capable of extremely high heat-up rates.

Improvements in pyrolysis yield distributions can thus be attained by incorporating spouted bed technology. The high temperatures can be obtained as the feed hydrocarbon is directly contacted with the heat-carrying bed particles. Since the heat transfer associated with this can cause temperature gradients in the range of 10^{5} K/s (Stocker, 1987), residence times at reaction temperature can be limited to several hundred milliseconds, and consequently higher selectivity can be achieved. Operational problems associated with coke deposition, a phenomenon which commonly occurs in pyrolysis, can also be overcome as the high surface area of the particles provides a means by which to remove the coke from the reaction region. Reheating of the bed particles can also be accomplished within an externally-heated spouted bed as the long particle residence times in the annulus allow them sufficient time to regain the heat lost to gases in the spout.

Consideration of the hydrodynamics of a conventional spouted bed, however, would lead to the observation of a deficiency with regards to the gas residence time distribution. Since cracked product gas yields are highly dependent upon gas residence times , the variation of these residence times should be carefully controlled. In a conventional spouted bed, though, a large discrepancy exists between the residence times of spout gases and those gases which diffuse into the annulus from the spout. To surmount this inadequacy, the inclusion of a centrally-located draft tube, as illustrated in Figure 1.2, could be used to inhibit the dispersion of gases into the annulus. Stocker (1987) illustrates the capability of this spouted bed configuration in propane pyrolysis. In addition, he proposes a steady state computer model for the prediction of temperature, pressure, velocity, and concentration profiles within this type of a reactor. In conclusion, he determines that a spouted bed with a draft tube is an ideal new generation reactor for the ultrapyrolysis (i.e. upgrading) of hydrocarbons.

1.3 RESEARCH OBJECTIVES

Steady state computer modelling of chemical reaction processes has found importance in the optimization of reactor design and operation. These models offer a preferable alternative to experimental trial-and-error techniques. In addition to the obvious economic benefits in the way of optimal design and operation, they also provide a means by which to better understand the pertinent characteristics of the reactor under varying operating conditions

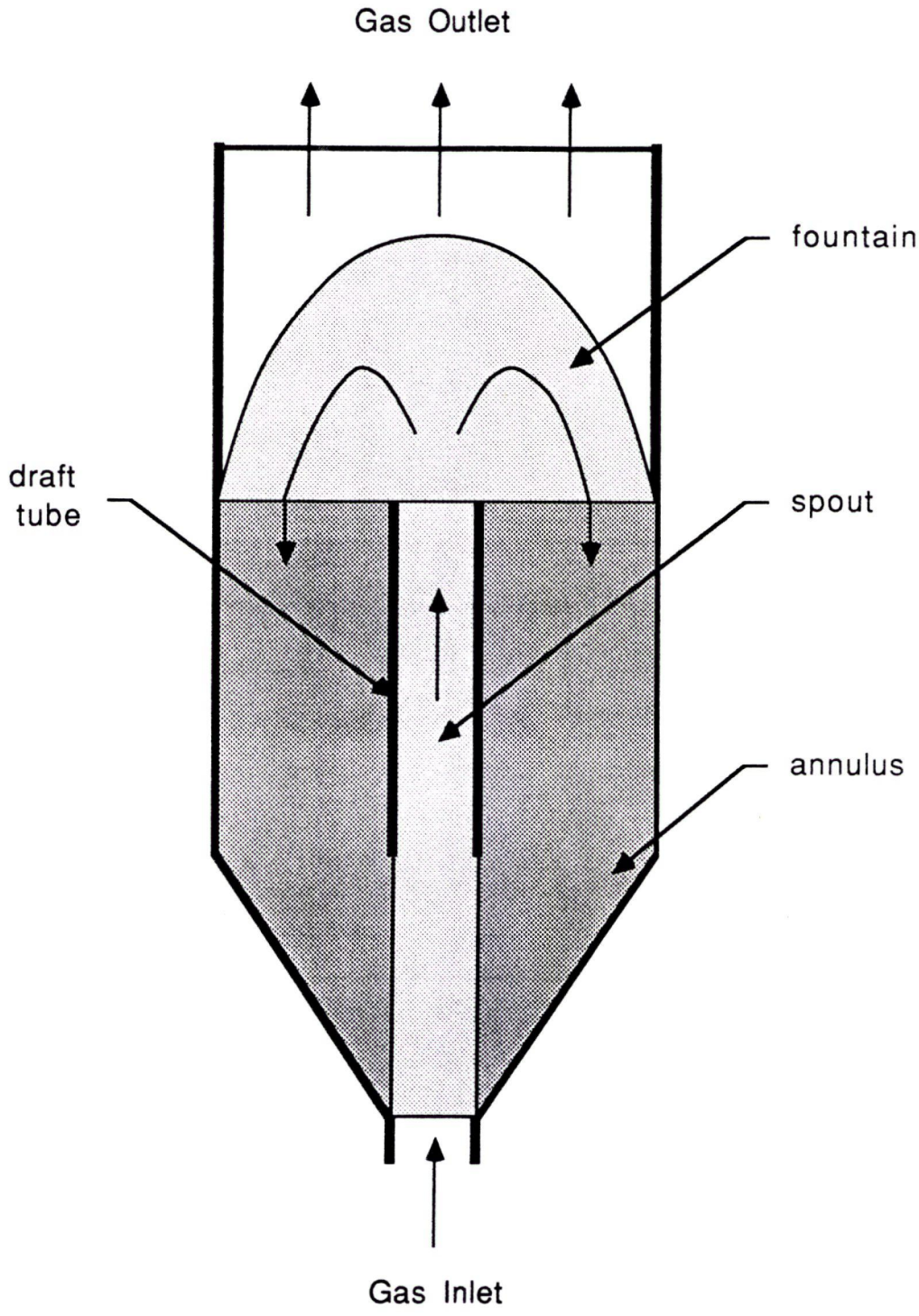

Fig.1.2 - Spouted Bed Reactor With a Draft Tube

While the advantages of accurate computer models may be quite apparent, insufficient work has been accomplished in the way of dynamic modelling of spouted bed reactors. With the advent of more sophisticated control strategies for chemical processes, the need for accurate dynamic models has increased. The aim of this work then, is to develop a dynamic model to simulate the response of a spouted bed reactor with a draft tube to changes in the operational conditions.

From the perspective of use as a pyrolysis reactor, this modelling work must be capable of predicting responses of heat transfer characteristics to operational disturbances. In order to establish the validity of this model then, comparisons are made with data obtained from experimental units. In addition, conclusions are drawn regarding the accuracy of present modelling work from the perspective of hydrodynamic correlations which must be used.

Chapter 2

LITERATURE REVIEW

In order to adequately model a spouted bed for use as a pyrolysis reactor, it is first necessary to define the features which will affect heat transfer. As portrayed in Figure 1.2 on page 7, the injected gas is initially contacted with hot particles situated at the base of the spouted bed and, due to the large temperature gradients that exist between the two stream components, large amounts of energy are transferred to the gas through the entire contacting surface of the particles. While the gas proceeds upward through the bed (i.e. in the spout), heat continues to be transferred to the gas not only from the entrained hot particles, but also from the annular wall of particles surrounding the spout. For an externally-heated spouted bed, the total heat transferred to the spouting gas stream is then also a function of the effective thermal conductivity of the annular moving bed of solids.

Efficacious modelling of a draft tube spouted bed reactor for hydrocarbon pyrolysis must then address all the hydrodynamic properties which most significantly influence heat

transfer in this type of a reactor.

2.1 HYDRODYNAMIC STUDIES

In analyzing the heating capabilities of a spouted bed, it becomes apparent that a large fraction of the total energy transferred to the reactant stream originates from the individual particles entrained in the gas stream. Particle entrainment into the spout is therefore a very significant factor which must be considered in modelling work.

2.1.1 PARTICLE ENTRAINMENT

While spouted beds have not been investigated extensively as high temperature reactors, they have been utilized in the drying of grains. In this capacity, particle entrainment or solids circulation also has a great influence on the operational effectiveness of the unit. Studies have therefore been carried out in an attempt to quantify the solids circulation in both conventional spouted beds and draft tube spouted beds. Although spouted bed dryers often do not employ a draft tube, entrainment phenomena are very similar between the two types of spouted beds and thus, a review of entrainment studies on conventional spouted beds would lend insight to that occurring in draft tube spouted beds.

Some of the earlier studies on conventional beds were carried out by Lefroy and Davidson (1969). In their work, they

observed entrainment effects along the length of the spout and noticed the continual collapse of the spout wall of particles as they were being swept into the jet stream at the inlet region and the collision of particles further up the spout which caused dislodging of some of the surrounding wall particles. Measurements made during experimentation indicated that the rate of particle entrainment into the spout per unit height was relatively constant throughout the bed. They then attempted to model the mechanism of entrainment by considering the collision of entrained particles with stationary spout wall particles; however, they were unable to adequately model the inlet region where they observed that particle-particle collisions were not the controlling entrainment mechanism and consequently, inaccurate entrainment rates were predicted from their model.

Chatterjee (1970) performed experimental work and attempted to correlate gas flow rate and bed particle properties to the solid circulation rate. The empirical correlation which he derived from his data predicted the solid circulation rate to be proportional to the incoming gas flow rate. His experimental approach for measuring entrainment rates, however, was put in question by Mann *et al.* (1972). They argued that Chatterjee's model, which measured particle circulation rates by tracer studies, did not realistically represent the actual flow of particles within the bed. Thus, Chatterjee's correlation could have been somewhat questionable.

Due to the difficulty in measuring entrainment rates in conventional spouted beds, the majority of information

available regarding them is qualitative. Observations made by numerous workers, though, all corroborate the early work of Thorley [Mathur and Epstein (1974)] who observed that total entrainment increases with corresponding increases in gas flow rate.

The only high temperature experimental results published were attributable to Wu *et al.* (1987). In their studies, they measured hydrodynamic properties in isothermal half-columns with operating bed temperatures ranging up to 420° C. While no data regarding entrainment rates were included in their paper, they did observe, by measuring particle velocities at the annulus wall, that the rates were not affected by bed temperature insofar as the same bed configuration was employed, the same size particles were used, and the ratio of U/U_{ms} was maintained constant. Consideration of the correlation which they derived for the minimum spouting velocity, U_{ms}, however, indicated that because of the thermal expansion of gases, lower molar feed rates were required at high temperatures to induce the same entrainment rate as that observed at lower bed temperatures.

With the inclusion of a draft tube, an additional parameter, that being the height in the bed at which the draft tube was situated, became significant. While the draft tube served as a restriction to gas flow into the annulus, it also prevented the favorable entrainment of solids into the spout. Studies performed by Buchanan and Wilson (1965), Claflin and Fane (1984), and Yang and Keairns (1983) all agreed that solid circulation rates increased as the length of the entrainment region, L_e, increased. With respect to the

effect of changes in the total feed gas flow rate, though, some disagreement arose. While Buchanan and Wilson, and Yang and Keairns observed the solids throughput in the spout to be proportional to the inlet volumetric gas flow rate to the power of 1.0, Claflin and Fane found the exponent to be 0.7.

In an attempt to theoretically describe entrainment phenomena, workers such as Massimilla *et al.* (1981), Filla *et al.* (1983), and Patrose and Caram (1984) compared jets in spouted beds to those in fluidized beds. Each of these workers approached the problem by outlining the governing mass and momentum balance equations involved. Experimental observations revealed the entrainment rates to be significantly different between the two types of jets. Since the system of equations developed to describe the two types of jets were still valid, these workers investigated the auxiliary equations upon which the solution of the problem was dependent, namely gas flows in and out of the jet. Further work illustrated that the description of gas flow in and out of the jet strongly influenced the particle entrainment trends. Thus, in order to correctly describe particle entrainment in a spouted bed, one must have also addressed the issue of gas bypassing into the annulus..

2.1.2 SPOUT GAS DIVERGENCE

For fast reactions such as the pyrolytic upgrading of hydrocarbons, narrow ranges of the gas residence times are preferable for optimum yields. In using spouted beds as reactors for

fast reactions then, and taking into account the aforementioned effect of gas divergence upon particle entrainment, it becomes apparent that an accurate estimation of the amount of gas diverging from the spout into the annulus is necessary. Awareness of its importance has stimulated many workers to investigate and attempt to correlate the extent of gas dispersion from the spout.

Early work in the area of analyzing gas flow patterns implemented the measurement of static pressure profiles for the calculation of annular flow rates. Workers such as Thorley [Mathur and Epstein (1974)] and Lefroy and Davidson (1969) calculated annular flow rates assuming the annular flows to be comparable to flows through loosely packed beds. They then deduced spout gas flow rates by consideration of the bed geometry. A second approach, the pitot tube method, was later employed by investigators such as Mamuro [Mathur and Epstein (1974)] and Van Velzen *et al.* (1974) to measure flow profiles in the spout.

Qualitative conclusions reached by researchers, however, seem to conflict somewhat. Epstein *et al.* (1978a), who performed experiments on small diameter beds ($D_b \leq 29.2$ cm), found annular gas velocities, U_a, to actually decrease for increases in the inlet gas velocity, U_o (sometimes called the spout velocity). Lim and Grace (1987), though, in their work on a 0.91 m diameter bed found that while U_a is not a strong function of U_o, slight increases in U_a may accompany increases in U_o. Buchanan and Wilson (1965) in commenting on this phenomenon as regards to draft tube spouted beds

concluded that for high values of U_o, the gas bypass occurring in the entrainment region would be equivalent to that occurring in a spouted bed of height L_e. Thus, for high gas flow rates, annular gas flow rates remained relatively constant regardless of fluctuations in U_o.

Attempts to theoretically model annular gas flow were commenced by Mamuro and Hattori [Mathur and Epstein (1974)]. Their analysis was based upon force balances in the annulus, the assumption of Darcy flow in the annulus, and the specification of proper boundary conditions. The boundary conditions which they used in the solution of the force balance differential equation as applied to a bed at the maximum spoutable bed height were

$$\text{at } z = 0 \qquad U_a = 0$$
$$\text{at } z = H_m \qquad U_a = U_{mf} \qquad (2.1)$$

where z = height in annulus
U_a = annular gas velocity
H_m = maximum spoutable bed height
U_{mf} = minimum fluidization velocity

Solution of the differential equation then yielded the following relationship for the annular gas velocity:

$$\frac{U_a}{U_{mf}} = 1 - \left(1 - \frac{z}{H_m}\right)^3 \qquad (2.2)$$

This equation, henceforth referred to as the MH equation, was criticized by later workers who questioned the validity of the Darcy

flow assumption, and the second boundary condition, and also pointed out discrepancies arising in the derivation of the differential equation. Despite the criticism, however, the MH equation held up well. For example, Epstein *et al.* (1978) attempted to incorporate a quadratic equation to relate pressure drop in the annulus to U_a in an attempt to improve upon the inaccuracy of the Darcy regime assumption. Calculations, though, indicated marginal improvement over the original equation. Consistency of predictions made by the MH equation led Piccinini *et al.* (1978) to the empirical equation

$$\frac{U_a}{U_{mf}} = 0.88 \left[1 - \left(1 - \frac{z}{H_m} \right)^3 \right] \qquad (2.3)$$

which they obtained by fitting the experimental data of Epstein *et al.* (1978a). Of note in this equation was the stipulation of the second boundary condition. Epstein *et al.* (1978) observed in their experimental studies that often fluidization was not achieved at the top of the annulus. Accordingly, the modified MH equation predicted the gas velocity at the top of the annulus to be 88 percent of the minimum fluidization velocity.

Stocker (1987), in his modelling work for a draft tube spouted bed, incorporated yet a different modification of the MH equation. This equation, originally proposed by Mamuro and Hattori for

beds with heights less than H_m, was of the following form:

$$\frac{U_a}{U_{aH}} = 1 - \left(1 - \frac{z}{H} \right)^3 \qquad (2.4)$$

where U_{aH} = maximum annular gas velocity

H = spouted bed height

While Mamuro and Hattori arbitrarily chose this modification, Stocker's computer modelling work indicated that it provided reasonable approximations.

Wu *et al.* (1987) also determined that annular gas velocities in high temperature spouted beds were well represented by the MH equation. Their experimental results, however, also reflected the observations of Epstein in that the annular gas velocities were consistently lower than U_{mf}. Perhaps another point of significance, hitherto unexamined, was the relationship which they derived for H_m and temperature. Their data indicated that H_m decreased significantly with temperature , a trend not predicted by the majority of correlations available at that time. The implication of this observation, while still unconfirmed, was that fluidization rather than spouting would occur for high temperature beds.

2.2 SPOUTED BED MODELS

After establishing a basic understanding of spouted bed hydrodynamics, mathematical models describing spouted beds were

attempted. While spouted beds were most popular as a means of drying coarse granular materials, the concept of using spouted beds as catalytic chemical reactors had not been investigated until the 1970's.

Having realized that many of the features of spouted beds were advantageous for gas-solid reactions, namely, intimate gas-solid contact and a high degree of gas and solids mixing, Mathur and Lim (1974) set out to model a spouted bed as a reactor for first order vapour phase catalytic reactions. Due to the limited amount of information available regarding the bed hydrodynamics, however, their modelling effort required the inclusion of several basic assumptions. First of all, they dealt with only an isothermal, isobaric reactor and thus density variations could be ignored. Secondly, the first order reactions would occur on the surfaces of porous catalyst beads where mass transfer resistances were assumed to be negligible. Thirdly, they divided the reactor into two regions, a spout region with a constant voidage of 0.95, and an annular region with a uniform voidage of 0.42. The reactant gas streams were then assumed to pass through each of these regions in plug flow. As the error associated with the first two assumptions was generally of a minor nature, the accuracy of the predictions of their model hinged more significantly on the accuracy of their last assumption. For gas-solid reactions, they predicted little reaction occurring within the high voidage spout region, as expected, and therefore, overall conversion in the reactor depended mainly upon the relative amount and residence time of reactant gases in the annulus. Hence, conditions which increased either of these achieved a higher overall conversion as

a result.

With the Mathur and Lim model serving as the benchmark in spouted bed reactor modelling, researchers undertook to improve the predictions of the model by revising the annular flow assumptions. Lim and Mathur (1976) proposed a streamtube model for annular gas flow which was developed in an endeavor to explain their experimental residence time distribution data. This model attempted to describe annular flows by defining streamlines along which gases would travel. An axial dispersion coefficient was then included to match experimental data. Expanding upon this streamtube model, Piccinini *et al.* (1979) investigated the decomposition of ozone and compared experimental results to both the Mathur and Lim model and the streamtube model. Their results, however, were inconclusive in discriminating between the two models due to the similarity of predictions calculated by both models for the spouted bed configuration employed. Littman *et al.* (1981) further analyzed these two models, but from the perspective of correlations utilized in the calculation of spouted bed parameters, in particular, the correlations describing gas velocities, voidages, spout diameter and maximum spoutable bed height. While this emphasis may be valid, insufficient experimental data to that point in time created difficulty in attempting to resolve a particular preference to any of the models.

In consideration of the lack of experimental data available, Rovero *et al.* (1983a) carried out additional experimental work on the decomposition of ozone in spouted beds of differing

diameter. Moreover, they also carried out radial concentration profile measurements to greater elucidate annular gas flow characteristics. Although reasonable predictions of the overall conversions were again calculated by the different models, insight into the adequacy of the models was provided by the radial concentration measurements. In the plug flow model, the assumed flat annular concentration gradient did not represent well the profile measured experimentally, while the streamtube model predicted too steep a gradient. Therefore, Rovero *et al.* (1983a) proposed that the streamtube model be revised to employ the added feature of radial dispersion. This model, however, has yet to be published.

Continuing along this modelling concept, Viswanathan (1984) postulated a "semicompartmental" model in order to describe axial gas dispersion in the annulus. This modelling technique involved representing the annulus as a number of continuously stirred tanks, CST's, in series. By then altering the number of CST's, they were able to match the overall conversion in the reactor. Similarly, Kumpinsky and Amundson (1984) considered this model for the combustion of char in a spouted bed. In total, they actually considered five different models for flow in the annulus.

While numerous workers were concerned with the implementation of a spouted bed as a catalytic reactor, Kursad and Kilkis (1983) carried out a more fundamental study in their model of spouted bed hydrodynamics. In developing their model, they first derived the material balance equations for the spout gases and the

annular gases while assuming a voidage profile in the spout and a constant voidage in the annulus. By then defining the momentum balance equations for the spout gases, the annular fluids, and the spout solids, they then evaluated the flow pattern and pressure distribution in both the spout and annulus.

The first researchers to attempt dynamic modelling of a nonisothermal spouted bed for chemical reaction also considered a first order catalytic reaction. Smith *et al.* (1982), in establishing the steady state model, again considered a two region model and then derived their energy balance equations by lumping the particles and gases in each of the spout and annular regions. By then simultaneously solving the material balance equations with these energy balance equations, they were able to determine the effect of design parameter changes on the conversion in the reactor. While their simplifying assumptions, which were similar to those of the first model of Mathur and Lim, may have introduced significant error, they served as the basis for the work of Arkun *et al.* (1983), who presented the results of their dynamic model. In this dynamic model, they considered the effect of changing the feed composition, the feed flow rate, and the reactor temperature on the temperature and concentration profiles present in the reactor. Their results indicated a common trend throughout. For any changes in the inlet reactant stream properties, an apparently immediate "pseudo-steady state" was achieved, after which the profiles slowly converged towards a final steady state. The initial "pseudo-steady state" corresponded with the short residence times of the gases in the reactor and the second steady state was due to the

much slower thermal equilibrium time constant associated with the annular solids. While the simplifying assumption of plug flow in the annulus may have led to errors in both the temperature and concentration gradients in the annulus, this initial dynamic model should serve as a basis upon which to develop more accurate models.

Even though much effort had been exerted on the modelling of conventional spouted beds, the first work related to draft tube spouted beds did not appear until much later. Claflin and Fane (1983,1984) considered implementing both a porous draft tube and a solid draft tube in a spouted bed for the thermal disinfestation of grains. In their modelling work then, they were concerned with the distribution of gases in each of the spout and annular regions, as well as the heat transfer associated with this configuration of reactor. Due to the addition of the draft tube, they were uncertain as to the applicability of correlations derived for conventional spouted beds. They therefore performed additional experimentation in order to estimate the total solids entrainment and the annular gas flow rates. With the empirical correlations which they derived, they developed their model by outlining the mass and momentum balances on the spout and annular gases. In developing their energy balance equation for a nonisothermal bed, they also accounted for intraparticle temperature gradients by modifying the heat transfer coefficients in conjunction with unsteady state heat transfer solutions for small spheres. With their steady state model they were able to investigate the effect of varying design parameters on gas distribution and heat transfer aspects of the bed.

The first attempt at modelling a draft tube spouted bed as a chemical reactor was carried out by Stocker (1987). In contrast to previous models of spouted beds as chemical reactors, however, he considered the extremely fast reaction of propane pyrolysis at high temperatures. Since the hydrocarbon thermal cracking reactions which occurred were controlled by high temperatures and short residence times (i.e. reactions did not require solid catalysts), he could not neglect the reactions occurring in the spout. In fact, gases travelling in the annulus had such high residence times that reactions in the annulus could actually be ignored as any desirable products degraded as a result of secondary reactions.

In order to account for the hydrodynamic effects in his steady state model, Stocker defined the applicable mass and momentum balance equations in a similar fashion to those derived by previous researchers. Due to the reactions occurring in the spout, however, it was necessary for him to also define the spout voidage profile by including an additional mass balance equation for the spout particles. Supplementing the hydrodynamic equations, he also simultaneously solved the energy balance equations in his model. While the inclusion of various hydrodynamic correlations already presupposed certain assumptions, it was also necessary for him to incorporate some additional simplifying assumptions. He, nevertheless, attempted to validate his assumptions, such as the assumption of lumping parameters in the annulus. In order to do this, he developed both a one-dimensional and a two-dimensional model to observe the radial temperature gradients in the annulus and concluded that from a heat

transfer point of view, a one-dimensional model would not introduce significant error. Because of the previously mentioned degradation of products in the annulus, radial concentration gradients could also be neglected with little loss of accuracy. For simplicity, he also ignored intraparticle gradients, but was unable to substantiate this assumption. His other major assumptions concern the manner in which he dealt with the particle entrainment and the gas bypassing. Limited solids entrainment data required that entrainment rates be estimated from tests performed on cold reactor units. The gas divergence into the annulus was assumed to follow profiles as estimated by the Mamuro-Hattori equation. This approximation, though, he found to be a reasonable representation.

The model which Stocker proposed was also compared with experimental results from both a bench-scale and a pilot-scale reactor. Results appeared to validate the model which he proposed. The effluent temperatures which he measured compare well with those which he predicted from his model. The product distributions of the propane pyrolysis runs also matched well.

2.3 DYNAMIC MODELS

Recently, more emphasis has been focussed on the dynamic modelling of reactors in order to provide better control during operation. A brief review of literature reveals that modelling has already been carried out for plug flow reactors, reactors which approximate the flow of gases in the spout of a spouted bed reactor.

Hansen and Jorgensen (1976) carried out the dynamic modelling of a gas phase catalytic fixed bed reactor. While this reactor differed considerably from a spouted bed reactor, it illustrated dynamic behaviour in flow reactors. In response to feed property changes, two periods were observed. Firstly, a fast dynamic time period was observed which corresponded to the residence time of reactants in the reactor. A second slower dynamic time period was then observed to occur due to a much longer thermal residence time. These same responses were observed in the modelling work of Arkun *et al.* (1983) for conventional spouted beds.

Kirkbir and Kisakurek (1986), who studied the dynamics of the thermal cracking of ethane in a tubular reactor, outlined the state of modelling work. In models developed, it was common to ignore transient effects of both the equation of motion and the continuity equation due to the extremely short time constants usually associated with these equations. Since computational time was a factor of considerable importance, one dimensional models were most often used, dispersion terms were ignored, fluid properties were assumed to be constant, and orthogonal collocation techniques were most often employed. In developing their model, however, they did not exclude the accumulation terms in the continuity equations. For simplicity, though, they did assume that pressure profiles, heat transfer coefficients, friction factors, and fluid properties were constant. While these assumptions did introduce error, and depending upon the disturbance considerable error, they allowed the much faster calculation of dynamic responses and provided a basis by which to

improve further computer simulations..

Chapter 3

DYNAMIC MODEL DEVELOPMENT

In the development of a dynamic model for a draft tube spouted bed reactor, the experience of previous researchers proves invaluable. Not only does the methodology which they employ assist in the evolution of future models, but also their results and conclusions indicate the validity of various assumptions and the directions toward which future studies should be aimed. In this regard, the efforts of Smith *et al.* (1982) and Stocker (1987), in particular, provide a good basis upon which to develop a dynamic model for a draft tube spouted bed.

Before actual mathematical modelling can begin, it is first necessary to decide upon a modelling concept. This means that the reactor must be divided into separate continuous regions, each of which can be modelled by a governing set of equations. In conventional spouted beds, for instance, the accepted scheme is to divide the reactor into two distinct regions, the spout and the annulus, with interactions occurring between them. In operating a draft tube spouted

bed as a pyrolysis reactor, Stocker also considers both the spout and annulus regions; however, since hydrodynamic properties which greatly affect the reactions change, he is required to consider these two regions both above and below the base of the draft tube. He also considers a fountain region, but assumes thermal equilibrium to exist and so consequently, he does not rigorously model it. In the development of the dynamic model of the draft tube spouted bed reactor then, the spout and annulus in both the entrainment and draft tube regions, as illustrated in Figure 3.1, are analyzed. Modelling of the fountain, however, is ignored because of the thermal equilibrium which Stocker finds to exist, and the added complexity which rigorous modelling of the fountain would entail.

In describing any reactor, it is also necessary to understand the actual nature of the reaction occurring, such as whether the reaction is catalyzed or whether it is thermally initiated. For thermal cracking reactions which are considered in this study, the areas of interest within the reactor are those at which high reactant gas temperatures are achieved, but for only very short residence times. Consequently, the regions of greatest concern from a pyrolysis reactor viewpoint, are those in the spout. In fact, annular gas flows are ignored from a conversion viewpoint because the high temperatures and residence times of annular reactant gases cause them to deteriorate to coke, aromatics, methane, and hydrogen.

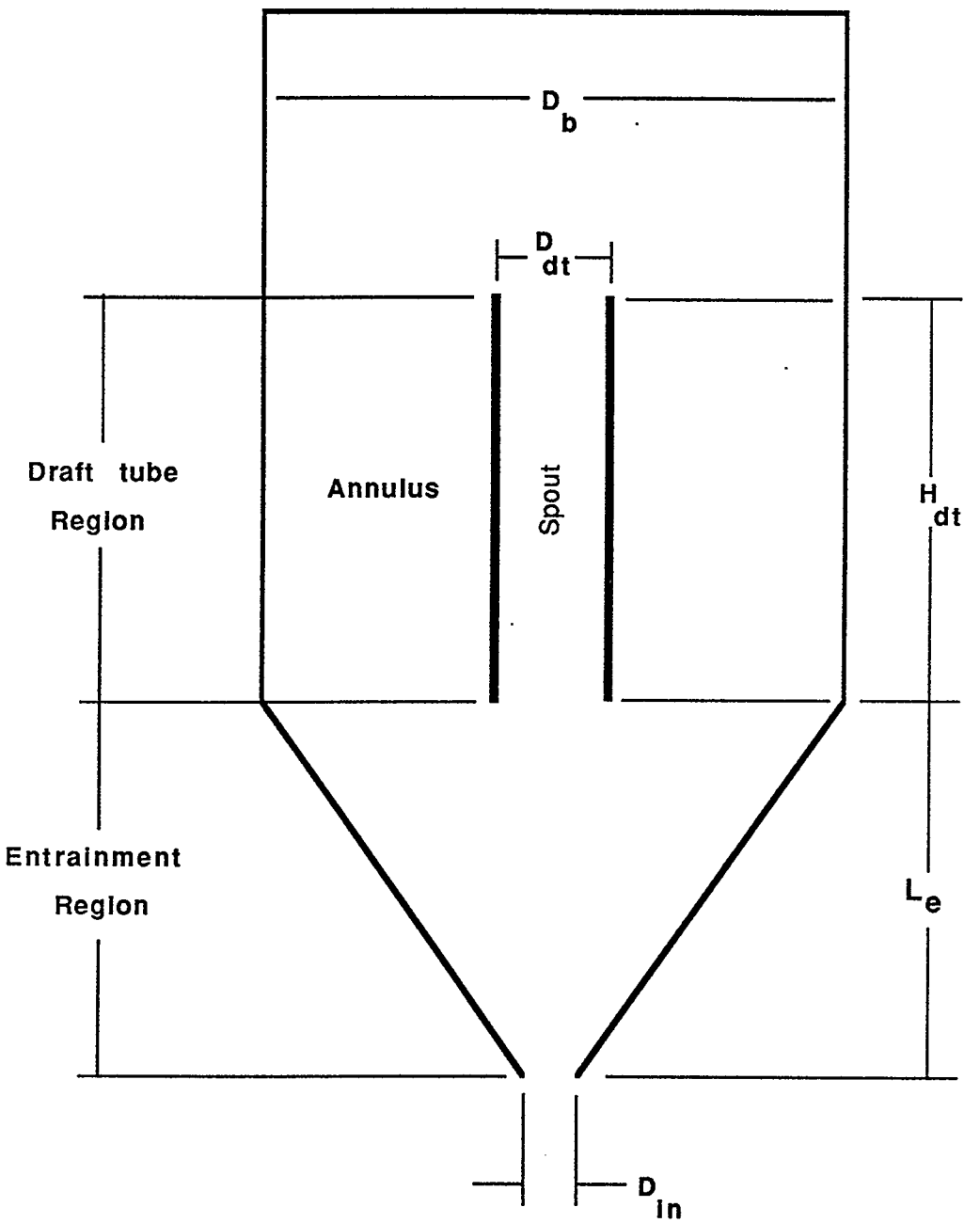

Fig. 3.1 - Spouted Bed Modelling Regions

3.1 MATERIAL BALANCE EQUATIONS

While it is obvious that the most important component within a noncatalytic reactor is the reactant itself, a spouted bed reactor also contains large quantities of particles. When these particles are contacted with the reactant gases, large amounts of heat or mass transfer may occur dependent upon the respective driving forces present. Most available simulations, however, either make an assumption regarding the solids in the spout, such as assuming a constant voidage, or neglect it altogether. While this assumption may not be detrimental for the purposes which they are considering, such an assumption would produce highly spurious results when modelling a spouted bed as a thermal cracking reactor. The first step in dynamic model development then, is the derivation of the material balance equations while ensuring that the solids in the spout are accounted for.

Due to computational difficulties encountered, as discussed later in this chapter, it is necessary to include an additional assumption regarding the flow profiles in the reactor. As observed by numerous researchers, dynamic responses to disturbances in the feed properties in nonisothermal reactors are often characterized by sudden "pseudo steady states" brought about by the short time constants associated with mass residence in the reaction zone. Because of the short residence times of gaseous and solid components in the spout, they are therefore assumed to be at steady state at all times. Hence, the accumulation terms of their respective material balance

equations are ignored.

3.1.1 GAS MATERIAL BALANCES

By assuming steady state profiles to exist in the spout, the mass balance equations describing the flow of each component in the gas stream in the spout can be derived by assuming plug flow. This plug flow assumption is reasonable as particle Reynolds numbers in the spout are of the order of magnitude of 10^5. Thus, the material balance equations for each of the gas stream components, N_c, are

$$\frac{dF_i}{dz} = A_s \cdot \epsilon_s \cdot \sum_{j=1}^{N_r} r_{ij} - f_{loss_i}(z) \qquad i = 1, N_c \qquad (3.1)$$

with the boundary conditions specified by the feed conditions as follows:

$$\text{at} \quad z = 0 \qquad F_i = F_{i_0} \qquad i = 1, N_c \qquad (3.2)$$

The form of Equation 3.1 is very familiar in that the first term on the right represents the change in molar flow due to reaction as in the equation for a plug flow reactor. The second term, however, may be somewhat unfamiliar. This term represents the amount of gases diverging into the annulus. Above the entrainment height, L_e, this term reduces to zero because of the physical constriction provided by the solid draft tube. Below the draft tube, though, an approximation must be made to estimate this function. This

approximation is made in view of the observation of Buchanan and Wilson (1965), in which they discover that gas divergence in the entrainment region is similar to that occurring in a conventional spouted bed of height L_e. The annular gas velocity at the top of the entrainment region is then calculated using the modified Mamuro-Hattori equation:

$$\frac{U_{aH}}{U_{mf}} = 0.88 \left[1 - \left(1 - \frac{L_e}{H_m} \right)^3 \right] \qquad (3.3)$$

In order to evaluate the annular gas velocity, additional expressions are required for both the minimum fluidization velocity, U_{mf}, and the maximum spoutable bed depth, H_m. For U_{mf}, the following expression [Littman *et al.* (1981)] is used:

$$U_{mf} = 42.857 \frac{(1-\epsilon_{mf}) \cdot \mu}{d_p \cdot \rho_g} \left[\left(1 + (3.111 \times 10^{-4}) \frac{\epsilon_{mf}^3 \cdot Ar}{(1-\epsilon_{mf})^2} \right)^{0.5} - 1 \right] \qquad (3.4)$$

Note that in employing the above expression, vapor properties at annular conditions at height L_e are used.

The decision regarding the expression for H_m is somewhat more difficult. Numerous correlations are available, but no expression has been shown to be markedly superior to the others. As observed in the MH equation, specification of H_m strongly influences the value of the annular gas velocity and hence, the total gas bypass and should therefore be predicted as accurately as possible. Referring to the work of Stocker (1987) then, the correlation which he employed

and found to predict reasonable values is given by [Mathur and Epstein (1974)]

$$H_m = 0.72 \left[\frac{D_b^2}{D_s} \right] \qquad (3.5)$$

Subsequent calculation of U_{aH} then defines the gas velocity in the draft tube region of the annulus. The gas divergence profile below the draft tube, however, must still be specified. For this, the work of Stocker is again referred to in which he found the following modification of the MH equation to be valid:

$$U_a = U_{aH} \left[1 - \left(1 - \frac{z}{L_e} \right)^3 \right] \qquad (3.6)$$

Manipulation of this equation then reduces to a function for the molar flow of gas out of the spout per unit height, assuming as in the original derivation of the MH equation, that flow is in a cylindrical, isothermal bed:

$$f_{loss_i}(z) = \frac{3 \cdot F_{i_0} \cdot g_L}{L_e} \left(1 - \frac{z}{L_e} \right)^2 \qquad (3.7)$$

where g_L = total fractional molar gas bypass

Implications of the validity of Equation 3.7 as incorporated into the mass balance equations are discussed in Chapter 5.

3.1.2 SOLIDS MATERIAL BALANCE

Making a similar plug flow assumption for the spout solids results in the following expression

$$\frac{d\epsilon_s}{dz} = \frac{(1-\epsilon_s)}{V_s}\cdot\frac{dV_s}{dz} + \frac{(1-\epsilon_s)}{A_s}\cdot\frac{dA_s}{dz} - \frac{F_p}{V_s \cdot A_s \cdot \rho_p \cdot L_e} \qquad (3.8)$$

with a corresponding boundary condition of

$$\text{at} \quad z = 0 \qquad \epsilon_s = 1.0 \qquad (3.9)$$

In actual computations, however, the spout voidage is set at 0.999 at the base of the bed. While this stipulation does not introduce significant error, it does reduce singularity problems and thus considerably eases the computing effort.

Analysis of Equation 3.8 reveals that the first term on the right hand side represents spout voidage changes resulting from particle velocity gradients.

The second term is due to changes in the spout diameter. While the exact shape of the spout is still unclear, a simple first approximation that the spout diameter increases linearly from the inlet to the draft tube is made. The cross-sectional area of

the spout in the entrainment region is then given by

$$A_s = \frac{\pi}{4}\left[(D_{dt} - D_{in}) \left(\frac{z}{L_e} \right) + D_{in} \right]^2 \qquad (3.10)$$

The axial change in cross-sectional area is obtained from differentiation of this equation:

$$\frac{dA_s}{dz} = \frac{\pi (D_{dt}-D_{in})}{2 \cdot L_e}\left[(D_{dt} - D_{in}) \left(\frac{z}{L_e} \right) + D_{in} \right] \qquad (3.11)$$

Note that the equations for A_s and its axial gradient apply only in the entrainment region, after which A_s becomes constant and the gradient reduces to zero.

The third term in the solids material balance equation also applies only in the entrainment region and represents the particle entrainment into the spout. The lack of information regarding this phenomenon necessitates the incorporation of additional assumptions. The first of these being that the rate of particle entrainment into the spout is a constant value per unit height. Secondly, values of the total solids entrained, F_p, are assumed in order to match experimental data, but are maintained within the ranges observed in half-bed plexiglass units.

3.2 MOMENTUM BALANCE EQUATION

As noted in Equation 3.8, the voidage in the spout

is dependent upon the particle velocity profile. This profile is determined by the solids momentum balance equation. Lefroy and Davidson (1969) carry out this approach which is similar to the force balance method employed by Thorley [Mathur and Epstein (1974)]. In developing these equations, again assumptions are required. First of all, it is assumed that the velocities of all particles travelling in the spout at a particular height are equal and that the particles entering the spout at that height attain this velocity instantaneously. Secondly, pressure changes are ignored. It has been observed that pressure differentials across a spouted bed are typically quite small (less than 10 kPa), and so consequently, this assumption will not introduce much error. A third assumption made is that particle-wall and particle-particle effects are negligible, a assumption which is reasonable since spout voidages are found to exceed 98 percent.

The particle momentum balance equation, which supplies the expression for the particle velocity profile as required in Equation 3.8, is then given by

$$\frac{dV_s}{dz} = \frac{1}{V_s}\left[\frac{3 \cdot C_D \cdot \rho_g (U_s - V_s)^2}{4 \cdot d_p \cdot \rho_p} + \frac{(\rho_g - \rho_p) g}{\rho_p}\right] \qquad (3.12)$$

with a boundary condition of

$$\text{at} \quad z = 0 \qquad V_s = 0 \qquad (3.13)$$

For reasons similar to that for the spout voidage, V_s is set to 0.1 m/s at the base of the bed in order to minimize singularity problems

without introducing significant error.

The form of Equation 3.12 illustrates the dominant accelerating forces acting on the particles. The second term accounts for the gravitational effects exerted on the particles.

The other dominant force, caused by the frictional drag of the passing spout fluids, is accounted for by the first term on the right hand side of Equation 3.12. In order to calculate this force, however, the drag coefficient must be evaluated. This coefficient is quantified by using the correlations of Clift *et al.* (1983). These correlations, which are shown in Table 3.1, are developed to match experimental data for fluids flowing past single spheres.

3.3 ENERGY BALANCE EQUATIONS

Since pyrolysis reactions are highly temperature dependent, predictions of temperatures within the draft tube spouted bed reactor are of utmost importance if any control over the product distribution is to be maintained. In order to predict temperatures at points within the reactor then, energy balance equations are derived for incremental elements in the bed.

3.3.1 SPOUT GAS ENERGY BALANCE

By assuming radial uniformity of the temperatures

Table 3.1 - Drag Coefficients For Flow Past Rigid Spheres

$w = \log_{10}Re$ [Clift *et al.* (1978)]

Range	Correlation
$20 \le Re \le 260$	$C_D = \frac{24}{Re}\left(1 + 0.1935 \cdot Re^{0.6305}\right)$
$260 \le Re \le 1500$	$\log_{10}C_D = 1.6435 - 1.1242 \cdot w + 0.1558 \cdot w^2$
$1500 \le Re \le 12000$	$\log_{10}C_D = -2.4571 + 2.5558 \cdot w - 0.9295 \cdot w^2 + 0.1049 \cdot w^3$
$12000 \le Re \le 44000$	$\log_{10}C_D = -1.9181 + 0.6370 \cdot w - 0.0636 \cdot w^2$
$44000 \le Re \le 3.38\times10^5$	$\log_{10}C_D = -4.3390 + 1.5809 \cdot w - 0.1546 \cdot w^2$
$3.38\times10^5 \le Re \le 4\times10^5$	$C_D = 29.78 - 5.3 \cdot w$
$4\times10^5 \le Re \le 10^6$	$C_D = 0.1 \cdot w - 0.49$

within the spout, an energy balance over an elemental volume in the spout yields the following expression for the dynamic behavior of the spout gas temperature:

$$\frac{\partial T_g}{\partial t} = \frac{1}{\epsilon_s \sum_{i=1}^{N_c} C_i \cdot c_{p_i}} \left[\frac{4U_w(T_a - T_g)}{D_s} + \frac{6h_p(1-\epsilon_s)(T_p - T_g)}{d_p} \cdots \right.$$

$$\left. - \epsilon_s \sum_{j=1}^{N_r} r_j(\Delta H_j) - \frac{\sum_{i=1}^{N_c} F_i \cdot c_{p_i}}{A_s} \frac{\partial T_g}{\partial z} \right] \qquad (3.14)$$

The accompanying boundary conditions are

$$\text{at} \quad z = 0 \qquad T_g = T_{g_0}$$

$$\text{at} \quad t = 0 \qquad T_g(z) = T_g^o(z) \qquad (3.15)$$

The initial temperature profile, $T_g^o(z)$, is determined from steady state calculations as described later in this chapter.

The first term on the right-hand side in Equation 3.14 addresses the heat transferred to the gas from the annular wall. While a wall of annular particles will exhibit different heat transfer characteristics than will a draft tube, the heat transfer coefficient correlations used are assumed to be valid for both cases. The overall heat transfer coefficient, U_w, is a function of the heat transfer

coefficient in the annulus, h_a, and that in the spout, h_w. By neglecting the thermal resistance of the draft tube, which is a reasonable assumption considering the relatively high conductivity and the thinness of the draft tube materials commonly employed, the overall heat transfer coefficient is simply expressed as,

$$U_w = \left(\frac{1}{h_w} + \frac{1}{h_a} \right)^{-1} \qquad (3.16)$$

The heat transfer coefficient for the turbulent flow of gases in a cylindrical pipe, neglecting entrance effects and radial gradients, is calculated by the Seider-Tate equation [McCabe and Smith (1976)]:

$$h_{w_0} = \frac{0.023\ k_g}{D_s} \cdot Re^{0.8} \cdot Pr^{0.333} \qquad (3.17)$$

This correlation is then augmented by an enhancement factor suggested by Sadek (1972), which accounts for the mechanical disruption of the boundary layer resulting from particle collisions, to arrive at an expression for the heat transfer coefficient for the energy transfer from the draft tube wall to the spout gases:

$$h_w = (1 + \Delta h_w) \cdot h_{w_0} \qquad (3.18)$$

$$\Delta h_w = 0.2 \left(\frac{6\ (1-\epsilon_s)\ D_s}{\pi \cdot \epsilon_s \cdot d_p} \right) \qquad (3.19)$$

The effective annular heat transfer coefficient, h_a, is given by Equation 3.29 and is discussed in greater detail in

Section 3.3.3.

The second term in Equation 3.14 quantifies the energy transfer from the entrained particles to the spout gases. In developing this expression, the intraparticle temperature gradients are assumed to be negligible. While the validity of this has been questioned [Stocker (1987)], it is made here to reduce computational difficulties. This point is further discussed in Chapter 5.

The particle-to-gas heat transfer coefficient is calculated from the equation of Rowe and Claxton [Mathur and Epstein (1974)], which applies to cases in which particle Reynolds numbers exceed 1000:

$$h_p = \frac{k_g}{D_s}\left[A + B \cdot Re_p^{0.8} \cdot Pr^{0.333} \right] \qquad (3.20)$$

$$\text{where} \quad A = \frac{1}{1 - (1-\epsilon_s)^{0.333}}$$

$$B = \frac{2}{3\epsilon_s}$$

The third term in Equation 3.14 represents the heat of reaction term, while the fourth is in consideration of the enthalpy of the flowing fluids.

In high temperature operations, radiation heat transfer must often be considered. Consequently, the dynamic model

developed in this study is initially tested with radiation energy transferring between the draft tube walls and the spout gases. The fractional contribution of radiation to the total heat transferred to the gas, however, is less than 1 percent for wall temperatures of 1200 K and is therefore ignored in subsequent modelling. This insignificance of radiation to spout fluids is also noted by Stocker (1987).

In the computational process, values must be assigned to the fluid properties in order to evaluate the heat transfer coefficients. This is carried out by making use of the mixing rules shown in Table 3.2, as suggested by Reid *et al.* (1977).

3.3.2 SPOUT PARTICLE ENERGY BALANCE

In a likewise manner to the derivation of the gas energy balance, the particle energy balance over an incremental element is derived by considering a mass-averaged temperature for all of the particles in the spout at a given height. This balance is given by the

Table 3.2 - Rules for Calculating Properties

of Gas Mixtures

Heat capacity mixing rule :

$$c_{p_g} = \frac{\sum_{i=1}^{N_c} \left(F_i \, c_{p_i} \right)}{\sum_{i=1}^{N_c} F_i} \qquad (3.21)$$

where $c_{p_i} = a_i + b_i \cdot T_g + c_i \cdot T_g^{\,2} + d_i \cdot T_g^{\,3}$

[coefficients as given in Reid *et al.* (1977)]

Viscosity mixing rule :

$$\mu_g = \frac{\sum_{i=1}^{N_c} \left[F_i \cdot M_i^{0.5} \frac{\left(4.61 T_r^{0.618} - 2.04 e^{(-0.449 T_r)} + 1.94 e^{(-4.058 T_r)} + 0.1 \right)}{\xi_i} \right]}{\sum_{i=1}^{N_c} F_i \cdot M_i^{0.5}}$$

where $\xi_i = T_{c_i}^{1/6} \cdot M_i^{-1/2} \cdot P_{c_i}^{-2/3}$ (3.22)

Thermal conductivity mixing rule :

$$k_g = \frac{\sum_{i=1}^{N_c} \left(F_i \cdot M_i^{0.5} 10^{-6} \cdot c_{p_i} \frac{(14.52 \cdot T_r - 5.14)^{2/3}}{\xi_i \cdot M_i} \right)}{\sum_{i=1}^{N_c} F_i \cdot M_i^{0.5}} \qquad (3.23)$$

following equation

$$\frac{\partial T_p}{\partial t} = - V_s \frac{\partial T_p}{\partial z} - \frac{6 \cdot h_p (T_p - T_g)}{c_{p_p} \cdot \rho_p \cdot d_p} + \frac{4 \cdot \sigma \cdot F_{ap} (T_a^4 - T_p^4)}{D_s \cdot c_{p_p} \cdot \rho_p (1-\epsilon_s)} \cdots$$

$$+ \frac{F_p (T_a - T_p)}{\rho_p \cdot L_e \cdot A_s (1-\epsilon_s)} \qquad (3.24)$$

The boundary conditions associated with this P.D.E. are

$$\text{at} \quad z = 0 \qquad T_p = T_{a_0}$$

$$\text{at} \quad t = 0 \qquad T_p(z) = T_p^o(z) \qquad (3.25)$$

These boundary conditions are somewhat more difficult to specify. Since the particles entering the spout must originate from the annulus, they must have the same temperature as the particles at the base of the annulus. That temperature, T_{a_0}, however, must be calculated, since it is dependent upon the temperature of particles further up the annulus. This calculation procedure is described more fully later in this chapter. Calculation of the initial particle temperature profile is also discussed later in this chapter.

As in all flow systems, Equation 3.24 has a term, the first on the right hand side, accounting for the enthalpy of the flowing particles.

In order to account for the energy transferred to the spout gases, the second term is included.

Radiation is compensated for by the third term in Equation 3.24, which implements the Stefan-Boltzmann law. In order to make use of this law, the assumption is made that both the particles and the draft tube are gray surfaces. The overall interchange factor, F_{ap}, is then given by the equation below [McCabe and Smith (1976)] when appropriate expressions for pertinent surface areas are included:

$$F_{ap} = \left[\left(\frac{1}{\epsilon_w} \right) + \frac{2 \cdot d_p}{3 \cdot D_s (1-\epsilon_s)} \left(\frac{1}{\epsilon_p} - 1 \right) \right]^{-1} \qquad (3.26)$$

The fourth term in Equation 3.24 applies only in the entrainment region, after which it reduces to zero. This is due to the fact that this term represents the influx of energy associated with particles entraining from the annulus. Since the entering particles may have a different temperature from the average of those already in the spout, this term must be included.

3.3.3 ANNULAR ENERGY BALANCE

As previously mentioned, heat transfer through the annulus plays an important role in the function of a draft tube spouted bed as a pyrolysis reactor. Its importance is realized in two facets. First of all, the effective thermal conductivity of the annulus determines the amount of energy which is transferred from the external

heat source by conduction, convection, and radiation to the spout. Secondly, as the particles travel down the length of the draft tube, they slowly regain energy which will again be transferred to the gas as the particles return upwards through the spout. Consequently, accurate prediction of the annular temperatures is also extremely important.

Calculation of the annular temperatures is also carried out by means of energy balances over elemental volumes. In doing so, additional assumptions are made. As pointed out by Stocker (1987), radial gradients in the annulus are not significant. While this assumption is further examined in Chapter 5, it has been utilized here in order to reduce the complexity of the dynamic model. Another assumption made is that the enthalpy of the annular gases is negligible with respect to the enthalpy of the annular solids. This assumption is again substantiated by the modelling work of Stocker.

The partial differential equation outlining the lumped annular temperature is then given by the following equation:

$$\frac{\partial T_a}{\partial t} = \frac{4}{(1-\epsilon_a)\rho_p \cdot c_{p_p} (D_b^2 - D_{dt}^2)} \left[D_b \cdot h_a (T_w - T_a) - D_{dt} \cdot U_w (T_a - T_g) \cdots \right.$$

$$\left. - \sigma \cdot D_s \cdot F_{ap} (T_a^4 - T_p^4) + \sigma \cdot D_b \cdot F_{wa} (T_w^4 - T_a^4) + \frac{\alpha \cdot F_p \cdot c_{p_p}}{\pi} \frac{\partial T_a}{\partial z} \right]$$

(3.27)

The accompanying boundary conditions for this P.D.E. are

$$\text{at} \quad z = L_e + H_{dt} \qquad T_a = T_{p_f}$$

$$\text{at} \quad t = 0 \qquad T_a(z) = T_a^o(z) \qquad (3.28)$$

The first of these boundary conditions is proposed in view of the observation of thermal equilibrium in the fountain region. Since the particles exiting from the top of the spout settle on the top of the annulus, their temperatures, based upon this observation, are equal. Again the implementation of this boundary condition is discussed later in this chapter.

As the first term in Equation 3.27 indicates, the heat flux into the bed is dictated by the wall-to-annulus heat transfer coefficient, h_a. This heat transfer coefficient is calculated using the correlation of Epstein and Mathur (1971), which is based on the analysis of heat transfer proceeding through a thin thermal boundary layer:

$$h_a = 1.129\left[\frac{V_a \cdot (1-\epsilon_a) \cdot \rho_p \cdot c_{p_p} \cdot k_a}{L_e + H_{dt} - z}\right]^{0.5} \qquad (3.29)$$

In this equation, which is developed in a manner analogous to that derived for a moving bed, the annular particle velocity is specified as a function of the total entrainment rate by the following continuity

equation:

$$V_a = \frac{4 \cdot F_p}{(1-\epsilon_a)\rho_p \cdot \pi (D_b^2 - D_{dt}^2)} \qquad (3.30)$$

The other term which must be considered in Equation 3.29 is k_a, the effective thermal conductivity of the annulus. For this, reference is made to the work of Kunii and Smith (1960). Their work involves the prediction of effective thermal conductivities in beds of unconsolidated particles containing stagnant fluids. Given the low annular velocities, these criteria are approximately satisfied. The correlation which they derive then accounts for conductive and radiative heat transfer between the particles and the interstitial fluid, each mode of which occurs in the annulus:

$$\frac{k_a}{k_g} = \epsilon_a \left(1 + 0.895 \frac{h_{rv} \cdot d_p}{k_g} \right) + \frac{0.895(1-\epsilon_a)}{\frac{\phi \cdot k_g}{k_g + \phi \cdot d_p \cdot h_{rs}} + \frac{2 \cdot k_g}{3 \cdot k_p}} \qquad (3.31)$$

As is apparent from Equation 3.31, the effective conductivity of the annulus is a function of the thermal conductivities of the gases and particles, the voidage in the annulus, the particle diameter, and three other quantities ϕ, h_{rv}, and h_{rs}. The first of these parameters, ϕ, represents the enhanced thermal conductivity occurring between particles due to the presence of gases near particle-particle contact

points. It is given by Equation 3.32:

$$\phi = \frac{\frac{1}{3}\left(\frac{k_p - k_g}{k_p}\right)^2}{\ln\left(\frac{k_p}{k_g} - \frac{k_p - k_g}{k_g \cdot \sqrt{3}}\right) - \frac{k_p - k_g}{k_p}\left(1 - \frac{1}{\sqrt{3}}\right)} - \frac{2 \cdot k_g}{3 \cdot k_p} \qquad (3.32)$$

The second and third parameters, h_{rv} and h_{rs}, refer to the relative contributions of radiation between adjacent void spaces and adjacent particle surfaces, respectively. These quantities are calculated through the correlations of Yagi and Kunii (1957):

$$h_{rv} = \left[\frac{0.1952}{1 + \frac{\epsilon_a(1-\epsilon_p)}{2 \cdot \epsilon_p(1-\epsilon_a)}}\right] \cdot \left[\frac{T_a}{100}\right]^3 \qquad (3.33)$$

$$h_{rs} = \left[\frac{0.1952 \cdot \epsilon_p}{2 - \epsilon_p}\right] \cdot \left[\frac{T_a}{100}\right]^3 \qquad (3.34)$$

The second and third terms in Equation 3.27 reflect the previously discussed heat transfer to spout gases and particles, respectively.

The fourth term in Equation 3.27 represents the radiative heat transfer from the outer wall of the bed to the annulus. With the high temperatures involved in thermal cracking processes, heat transfer by radiation becomes increasingly dominant. The expression

for the view factor is derived making the same assumptions as for the case of radiation in the draft tube. A similar expression, with appropriate terms for applicable surface areas, to Equation 3.26 is therefore employed.

The fifth term in Equation 3.27 is due to the flow of particles down the annulus. An additional parameter, α, is included in this term which represents the fractional flow of solids down the annulus and as such, equals $^{z}/_{L_e}$ in the entrainment zone and one in the draft tube section.

In the modelling process, axial conduction is also considered; however, it is found to be negligible in comparison with the much higher energy flux associated with the moving bed of particles. It is therefore disregarded in the dynamic model in order to further minimize computational effort.

3.4 METHOD OF SOLUTION

Review of literature concerning the solution of coupled partial differential equations (P.D.E.'s) reveals several approaches to the calculation of the solution. In classical chemical engineering applications, the most common computer technique is the method of finite differences combined with a method for the solution of simultaneous ordinary differential equations, otherwise referred to as the method of lines.

3.4.1 NUMERICAL METHODS FOR PARTIAL DIFFERENTIAL EQUATIONS

In order to implement the aforementioned method of lines, the spatial domain is first discretized into N grid points. The derivatives at each of the grid points are then estimated by means of techniques such as the central finite differencing scheme shown in Equations 3.35 and 3.36:

$$\frac{dT_i}{dz} = \frac{T_{i+1} - T_{i-1}}{2 \cdot \Delta z} \qquad (3.35)$$

$$\frac{d^2T_i}{dz^2} = \frac{T_{i+1} - 2 \cdot T_i + T_{i-1}}{(\Delta z)^2} \qquad (3.36)$$

While differencing schemes are relatively simple to implement, inherent inadequacies in these schemes exist. Since the derivative approximations of finite differencing formulas are based upon truncated Taylor series expansions, truncation errors will arise dependent upon the function and the value of the interval, Δz. In approximating steep gradients, smaller intervals must be employed in order to obtain sufficient accuracy. This, however, greatly increases the computational effort required to calculate the solution.

In order to circumvent the shortcomings of finite differencing techniques, recent modelling work [Arkun *et al.* (1982), Hansen and Jorgensen (1976), Kirkbur and Kisakurek (1986)] has implemented the method of orthogonal collocation. This method, as outlined by Finlayson (1972) and Villadsen and Michelsen (1978),

employs a polynomial approximation approach for calculating the derivatives of various functions. In this approach then, a function is expressed as a summation of polynomial terms or a summation of powers of the spatial variable as shown in Equation 3.37:

$$y(z_j) = \sum_{i=1}^{N+1} a_i z_j^{2i-2} \qquad (3.37)$$

With constant coefficients, a_i, the first and second derivatives at any point, z_j, can be determined by differentiation of Equation 3.37 as performed in order to obtain Equations 3.38 and 3.39.:

$$\left.\frac{dy}{dz}\right|_{z_j} = \sum_{i=1}^{N+1} \left.\frac{dz^{2i-2}}{dz}\right|_{z_j} a_i \qquad (3.38)$$

$$\left.\frac{d^2y}{dz^2}\right|_{z_j} = \sum_{i=1}^{N+1} \nabla^2\left(z^{2i-2} \right)\Big|_{z_j} a_i \qquad (3.39)$$

The forms of Equations 3.38 and 3.39 are still difficult to incorporate into a computer program due to the presence of the unknown coefficients, a_i. By rearranging Equation 3.37, however, the coefficients can be expressed as functions of y_i and x_i. First consider Equation 3.37 expressed in matrix form:

$$\bar{y} = \bar{Q} \cdot \bar{a} \qquad \text{where } \bar{Q}_{ij} = z_j^{2i-2}$$

$$\text{or} \quad \bar{a} = \bar{Q}^{-1} \cdot \bar{y} \qquad (3.40)$$

Similar consideration of Equations 3.38 and 3.39 and the substitution of Equation 3.40 yields the following equations for the first and

second derivatives:

$$\frac{\overline{dy}}{dz} = \overline{C}\cdot\overline{a} = \overline{C}\cdot\overline{Q}^{-1}\cdot\overline{y} = \overline{A}\cdot\overline{y} \qquad (3.41)$$

$$\frac{\overline{d^2y}}{dz^2} = \overline{D}\cdot\overline{a} = \overline{D}\cdot\overline{Q}^{-1}\cdot\overline{y} = \overline{B}\cdot\overline{y} \qquad (3.42)$$

Note that in Equations 3.41 and 3.42, the first and second derivatives, respectively, are expressed solely as functions of z_i and y_i. Hence, by defining the axial points, z_i, and thus the matrices $\overline{A}$ and $\overline{B}$, the derivatives can be calculated as functions of the solutions, y_i, at these points. In order to implement orthogonal collocation techniques, two additional queries must be addressed. First of all, what types of functions can be used, and, secondly, where should the points z_i be located.

In regards to the matter of what polynomial functions can be used, it can be seen from the derivations presented that the summations of these functions must be capable of transforming into a summation series of powers of z, such as that shown in Equation 3.37. Properties of families of polynomials reveal that orthogonal polynomials may be expressed in this way. In this modelling work then, the orthogonal Jacobi polynomials are employed due to their versatility. These polynomials derive their versatility from the fact that they are functions of two parameters, α and β. Details regarding the description of these polynomials are found in Villadsen and

Michelsen (1978).

The answer regarding where to locate the axial points, z_i, stems from an error minimization consideration. Previous work indicates that minimum error is obtained when the values of z_i are chosen as the roots of the N^{th} order polynomial equation. These roots are referred to as collocation points. In using the Jacobi polynomials then, these collocation points are defined by the values assigned to the parameters α and β.

Implementation of the method of lines and orthogonal collocation in the development of the dynamic simulation of a draft tube spouted bed reactor involves discretization of two regions. First of all, the entrainment region is divided into N_1 collocation points. In calculating the temperature gradients in the spout, the final temperatures predicted in the entrainment region become the lower boundary values for the draft tube section. The draft tube section is then discretized into N_2 collocation points, totalling (N_1+N_2-1) collocation points for the entire length of the reactor. It is noted that in the solution of the hyperbolic P.D.E.'s, differencing schemes may be unstable unless the direction of fluid flow is considered. What this infers, in this case, is that the base annular temperature in the draft tube section must be used as the upper boundary condition for the entrainment region since flow in the annulus is downwards.

Once the number of collocation points in each

region and the values of α and β are specified, the matrices $\bar{A}$ and $\bar{B}$, as given in Equations 3.41 and 3.42 can be calculated. The subroutines outlined in Villadsen and Michelsen (1978) are used in these computations.

An additional problem arises in the solution of the simultaneous P.D.E.'s in this particular study. In the entrainment region, relatively steep axial gradients are encountered in the gas, particle, and annular temperature profiles. These gradients, however, appear at different axial locations in the bed. In order to approximate a steep gradient by an N^{th} order polynomial, however, points must be chosen along the gradient, otherwise the polynomial will predict an oscillatory curve to match the "step change". In this particular study, steep gradients in the annular temperature profile are present at the bottom of the entrainment region, while the gradients in the gas temperature profile occur later in this region. Consequently, precise selection of the parameters α and β is necessary to strategically place collocation points along each of these gradients. Since this trial and error approach for obtaining values for α and β is very time-consuming, a modification of the orthogonal collocation method is employed. In this modification, a forward finite differencing scheme is applied in the entrainment region of the annulus, while orthogonal collocation is used in all other regions of the bed. Since the gradients in the annular temperatures occur at the base of the bed, collocation points are defined such that small axial increments are present in this region. The accuracy of the finite differencing scheme is then evaluated by increasing the number of

collocation points (i.e. reducing the finite difference truncation error) until changes in the calculated temperatures become negligible.

After discretization of the P.D.E.'s by the orthogonal collocation-finite differencing schemes developed, the resulting set of simultaneous ordinary differential equations (O.D.E.'s) is solved. The algorithm used to carry out this integration is Gear's method as set out in the IMSL subroutine DGEAR. This method is particularly suited to solving sets of stiff O.D.E.'s. Stiffness in solving simultaneous O.D.E.'s occurs when the difference between the largest and smallest eigenvalues is great. In other words, the time constants of each of the differential equations differ by several orders of magnitude. This is the case in this study in attempting to solve the three temperature equations, as the time constants for the spout gas temperature equations are in the order of milliseconds, while the time constants for the annular temperature equations are in the order of minutes.

3.4.2 QUASI-STEADY STATE APPROACH

In addition to the solution of the P.D.E.'s describing temperature profiles in the bed, the hydrodynamic characteristics, namely, the gas flow rates, the spout voidage, and the particle velocity, are also known to affect the reactor operation. While each of the mass balance and momentum balance equations can be derived to include their respective accumulation terms, a problem with stiffness becomes more pronounced. As previously mentioned, stiffness

arises when the time constants associated with the solution of various O.D.E.'s differ by several orders of magnitude. Consideration of the time constants associated with the hydrodynamic equations, indicates them to be of a magnitude comparable to the residence time of the spout fluids or, in other words, their time constants are very short. Contrasting this with the large time constants associated with thermal equilibrium of the annular solids illustrates the inevitable problems to be encountered with stiffness. This problem is circumvented by means of a quasi-steady state approach.

Due to the extremely short residence times associated with the equations describing flows in the spout then, they are assumed to be at equilibrium for a given gas temperature profile. In the case of the dynamic simulation developed in this study, the gas flows, voidage, and particle velocity profiles are calculated from instantaneous gas temperature profiles. The time interval between quasi-steady state calculations is specified as large as possible, without causing significant error, so that computational time is minimized

The quasi-steady state calculations, for a given gas temperature profile, are performed by integration of Equations 3.1, 3.8, and 3.12 with their respective boundary conditions. With the implementation of orthogonal collocation, spout gas temperatures are easily calculated at any point in the reactor by interpolation of the polynomial equation.

In addition to the calculation of gas flow, voidage, and particle velocity profiles, other parameters are also calculated on a quasi-steady state basis. These parameters include the heat transfer coefficients, h_a, h_p, and h_w, the annular thermal conductivity, and the gas properties of heat capacity, thermal conductivity, and viscosity. This simplification is also employed in an effort to reduce computational effort. Results indicate that accuracy is not sacrificed when these parameters are calculated on a quasi-steady state basis, but that program run times, in terms of cpu minutes, can decrease by as much as a factor of fifteen, depending upon the time intervals chosen.

3.4.3 STEADY STATE ALGORITHM

In order to calculate the dynamic response of the draft tube spouted bed reactor to disturbances, steady state temperature profiles are required. These may be calculated in one of two manners. The first method, as employed in the majority of steady state models, is to set the accumulation terms of each of the P.D.E.'s to zero and then solve the resulting set of O.D.E.'s. As elucidated by Stocker (1987), however, difficulty in meeting the boundary conditions of the particle and annular temperature equations, given by Equations 3.25 and 3.28, necessitates a computational intensive trial-and-error approach.

A second method, the one employed in this work, is to implement the dynamic model. By initiating the program at a steady

state condition of room temperature, the steady state profiles are then calculated by introducing slow changes until the operating conditions are achieved. The dynamic algorithm, shown in Figure 3.2, is actually followed. In this manner, the boundary conditions are satisfied and the trial-and-error approach is avoided. Consequently, the need for accurate initial guesses is eliminated and the computational effort is reduced by as much as 50 percent.

3.4.4 DYNAMIC MODEL ALGORITHM

Before calculation of dynamic responses commences, model variables are normalized. This normalization is carried out in accordance with the following equations:

$$
\begin{aligned}
\zeta &= z \cdot L_e && 0 \le z \le L_e \\
\zeta &= z \cdot H_{dt} + L_e && L_e \le z \le L_e + H_{dt} \\
\theta_g &= \Delta T \cdot T_g + T_{g_0} \\
\theta_p &= \Delta T \cdot T_p + T_{g_0} \\
\theta_a &= \Delta T \cdot T_a + T_{g_0}
\end{aligned}
\qquad (3.43)
$$

In order to calculate the dynamic response of the draft tube spouted bed reactor using the methods stated then, the first step is to transform the variables in accordance with Equations 3.43. The next step is to define the collocation points by setting the Jacobi polynomial parameters, α and β. The matrices $\bar{A}$ and $\bar{B}$, as specified in Equations 3.41 and 3.42, are then calculated.

Once the variables are normalized and the grids are

set up, the steady state temperature profiles are entered, whether they have been previously calculated or whether they are set at room temperature. The quasi-steady state calculations are then carried out to determine the flow profiles of each gaseous component, the voidage profile, the particle velocity profile, and the heat transfer terms, k_a, h_a, h_p, and h_w, at each of the grid points. It should also be mentioned that if particle entrainment rates or gas bypassing rates are allowed to change, they are corrected during quasi-steady state calculations as well.

Finally, dynamic calculations are started. As mentioned, Gear's method is employed to integrate the dynamic equations over a specified time interval. After integration is completed for this time interval, quasi-steady state calculations are again carried out. This process is completed until a specified time is reached or until steady state is achieved. This algorithm is illustrated in the flow diagram of Figure 3.2.

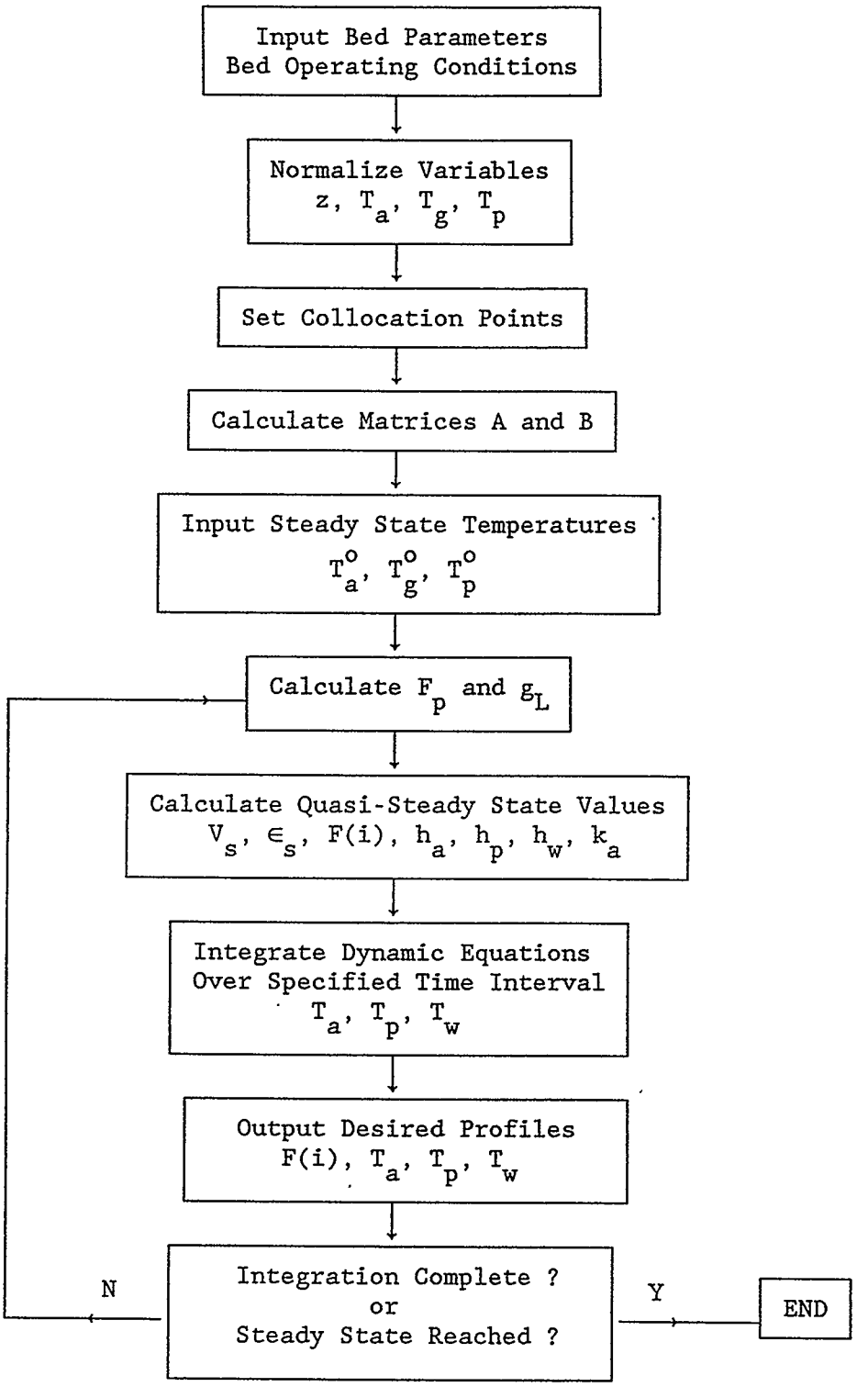

Figure 3.2 Dynamic Model Flow Diagram

Chapter 4

EXPERIMENTAL EQUIPMENT

While computer simulations may be verified in all theoretical aspects, the true value of a simulation lies in its ability to accurately predict responses in physical situations. With this in mind, comparisons are made with yet unpublished work of Stocker (1987). Although his work does not include data describing transient hydrocarbon pyrolysis runs, it does include dynamic temperature responses during spouting runs. Matching of these responses, however, should still indicate the validity of this model since the most dominant factors affecting pyrolysis are those of temperature and residence time.

The experimental runs are performed in one of two high temperature reactors. The first of these is a flat-bottomed, semi-cylindrical, bench-scale spouted bed reactor with a draft tube as illustrated in Figure 4.1 and with bed dimensions as listed in Table 4.1. Temperature measurements are obtained by means of thermocouples which are mounted through the flat face of the bed. Heating is provided by means of an external furnace. Data obtained from this

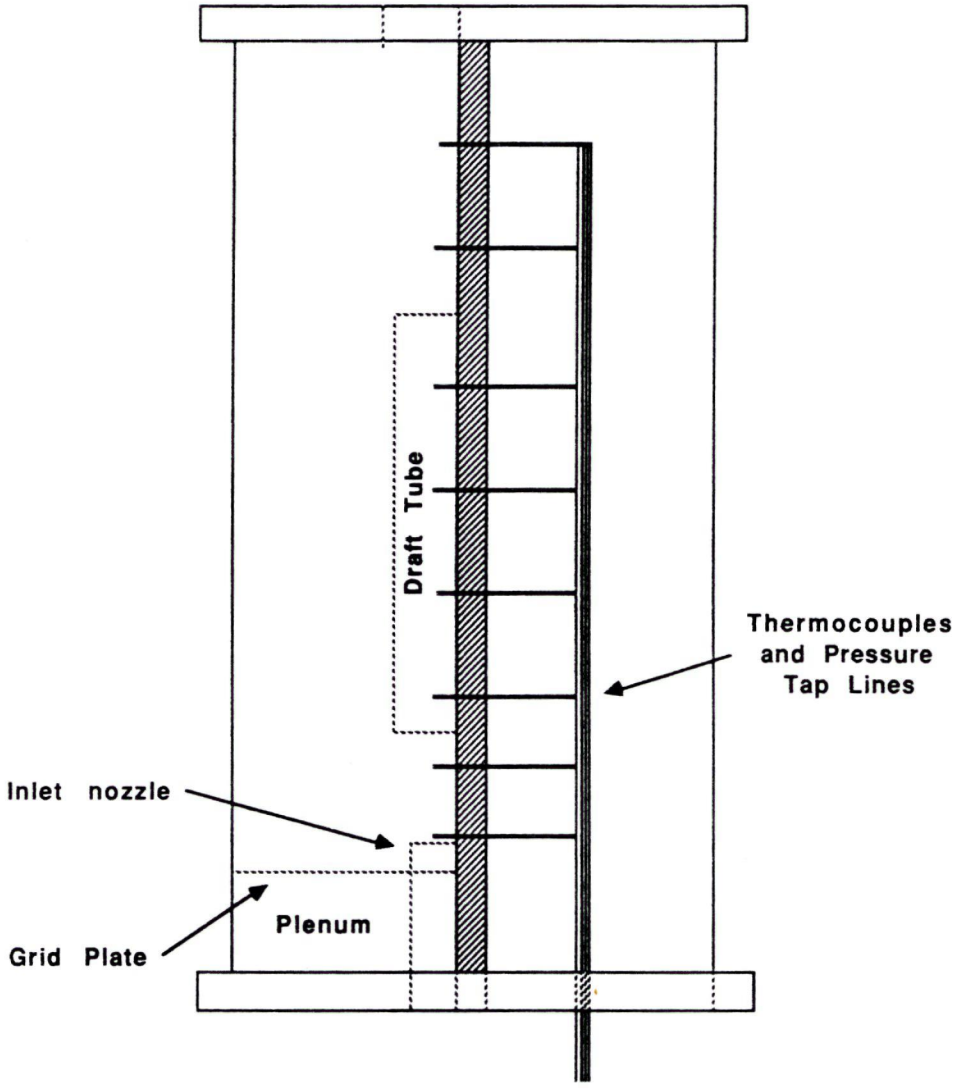

Fig. 4.1 - Schematic of Bench-Scale Spouted Bed With a Draft Tube [Stocker (1987)]

Table 4.1

Experimental Spouted Bed Dimensions

	Bench-Scale Bed	Pilot-Scale Bed
D_b(m)	0.1143	0.20
D_{in} (m)	0.0191	0.0254
D_{dt}(m)	0.0254	0.04
θ (^{o})	180	60
L_e(m)	0.067	0.151
H_{dt}(m)	0.30	0.60

reactor include dynamic responses within the bed to wall temperature changes in a low temperature range.

The second reactor from which data is derived is a conic-based, cylindrical, pilot-scale spouted bed reactor with a draft tube. This larger reactor, as shown in Figure 4.2, has the dimensions listed in Table 4.1, and is capable of much higher temperatures. It is therefore useful in ascertaining the validity of this model in predicting responses at thermal cracking conditions. Runs carried out on this reactor again include responses to wall temperature changes with bed temperatures in the range typical of thermal cracking reactions.

Each of the beds described contained silica sand having a mean particle diameter of 1.03 mm and a density of 2635 kg/m^3. Further description of both of these reactors is included in Stocker (1987).

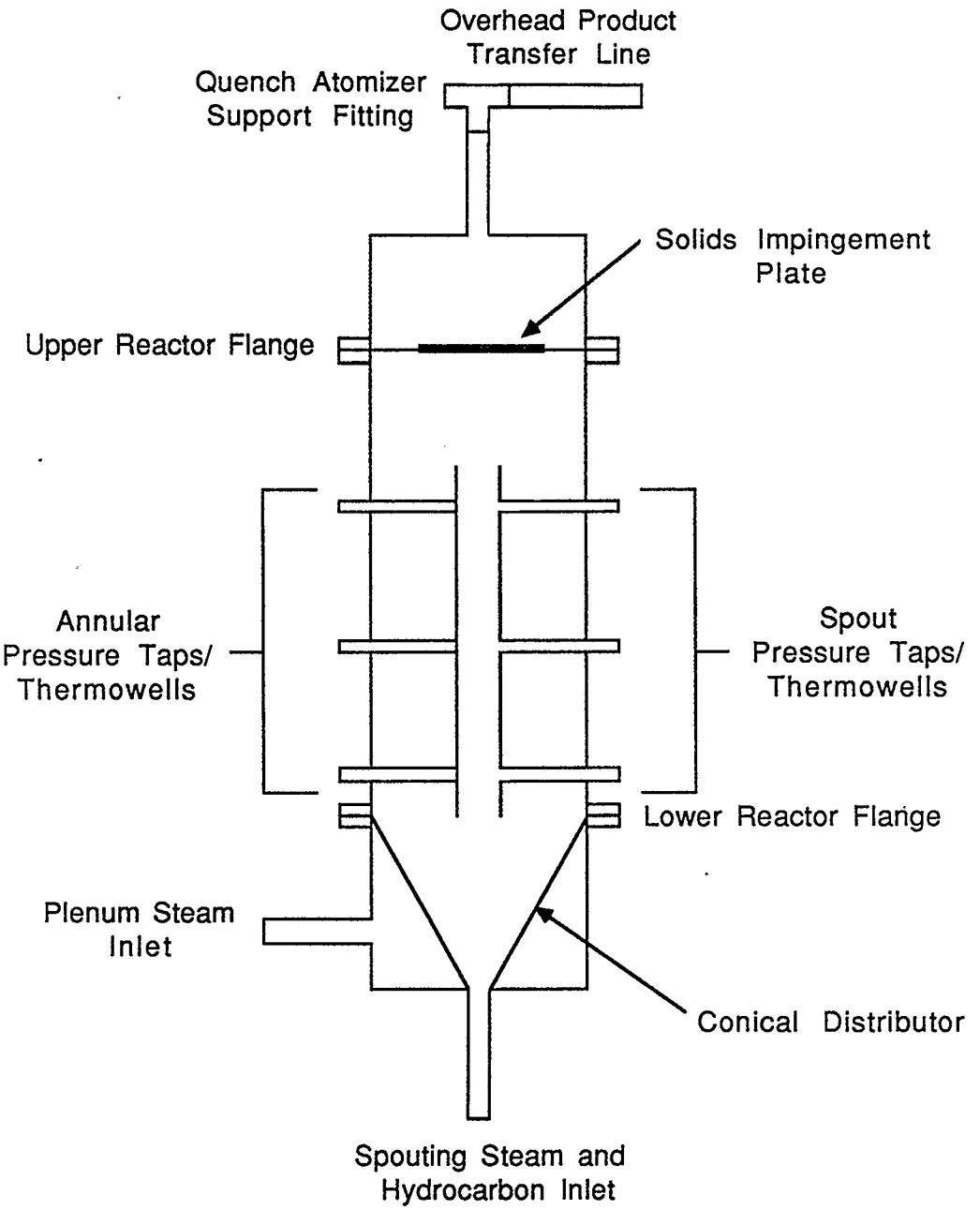

Fig. 4.2 - Schematic of Pilot-Scale Spouted Bed With a Draft Tube [Stocker (1987)]

Chapter 5

RESULTS AND DISCUSSION

While the computer modelling in this study is valuable in predicting the dynamic behavior of a spouted bed with a draft tube, it is first studied in terms of the various assumptions made in its development. The first objective then, is to ascertain the correctness of the assumptions required in the derivation of the equations, as well as the validity and accuracy of numerical methods employed. In conjunction with this analysis, results are compared with experimental data to both confirm the validity of the computer simulation presented in this study and to also examine various hydrodynamic correlations. Finally, simulation runs are carried out to investigate the effects of various disturbances on reactor performance. Each of the aforementioned investigations are carried out using a Honeywell DPS 8/70 mainframe computer.

5.1 ANALYSIS OF ASSUMPTIONS

As is common in all mathematical modelling,

assumptions are required in the development of the governing differential and algebraic equations incorporated into the computer model. The major assumptions made in this study are addressed and their applicability analyzed.

The first assumption which is addressed is the question of lumped parameters in the annulus. The work of Malek and Lu [Epstein and Mathur (1971)] illustrates that heat transfer in a conventional spouted bed is characterized by a thin thermal boundary layer no greater than 1 cm in thickness from the bed wall. Moreover, Stocker (1987) develops a two-dimensional model for the draft tube section of a draft tube spouted bed and also finds that thermal boundary layers at the contacting surfaces of the annulus account for the majority of the thermal resistance and consequently, temperatures in the bulk of the annulus are relatively uniform at a given height in the bed.

From a more fundamental approach of thermal resistance considerations, the one-dimensional modelling approach is analyzed. For this approach, an electrical analogy in which electrical resistances are compared with thermal resistances as illustrated in Figure 5.1 is considered.

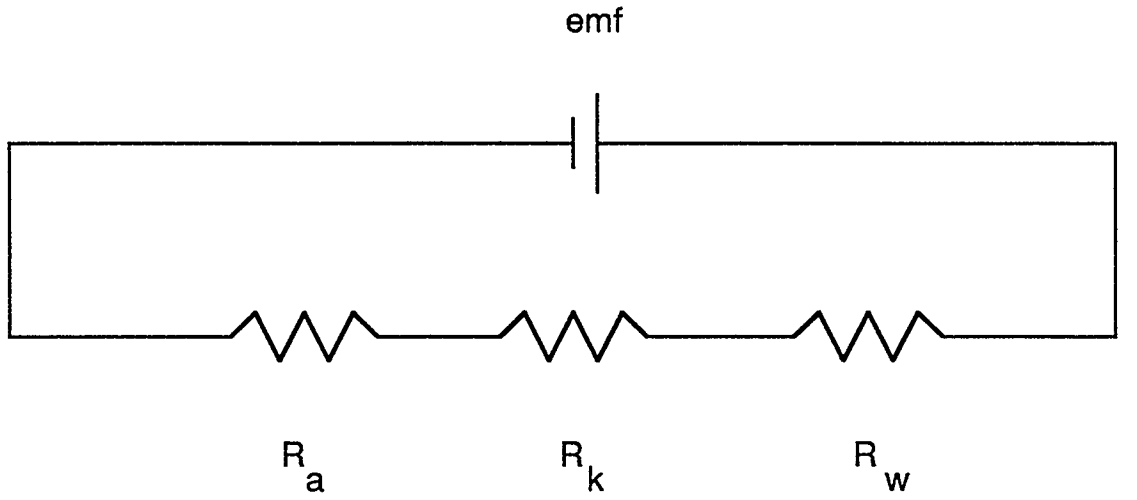

Fig. 5.1 - Electrical Analogue to Heat Transfer Resistances

The thermal resistance of the annular bed wall boundary layer, R_a, is proportional to $(D_b \cdot h_a)^{-1}$, while the thermal resistance of the bulk annulus, R_k, is proportional to $\ln(D_b/D_{dt})/(2 \cdot k_a)$ and the thermal resistance of the boundary layer at the draft tube wall, R_w, is proportional to $(D_{dt} \cdot U_w)^{-1}$. From this analogy, the voltage drop across each resistance is proportional to its fractional resistance of the total. In terms of thermal loads, the temperature differential across each thermal resistance is proportional to its relative resistance. Calculations obtained from this modelling work indicate the heat transfer coefficients and thermal conductivities to be in the ranges shown in Table 5.1.

Table 5.1 Ranges in Heat Transfer Properties

h_a ($kW/m^2 \cdot K$)	h_p ($kW/m^2 \cdot K$)	h_w ($kW/m^2 \cdot K$)	k_a ($kW/m \cdot K$)
0.033-0.039	0.782-1.140	0.060-0.125	0.00028-0.00034

For the heat transfer coefficients and thermal conductivities listed in Table 5.1, the greatest thermal resistance is found to be due to the low thermal conductivity of the annulus itself, which accounts for greater than 80 percent of the total resistance.

The thermal resistance study appears to indicate inaccuracy in the lumped annular assumption; however, the electrical analogue approach is unable to consider the effect of the moving bed characteristics of the annulus. This is significant because of the high energy flows associated with the downward-flowing particles. Since particles resting on the top of the annulus originate from the spout, they will have approximately the same temperatures throughout an entire horizontal cross-section. The effect of this is to produce flatter profiles throughout the length of the annulus. A brief investigation of the relative energy flows corroborates this point.

The energy flux associated with the flowing

particles is a function of the particle entrainment rate and the axial annular temperature gradient, while the energy flow in the radial direction is a function of the heat transfer coefficients and the radial temperature gradients (refer to Equation 3.27 on page 46). Comparison of these quantities, as calculated using a steady state simulation, reveals that the energy flux associated with the flowing particles is over 800 times that of the energy flow due to the radial temperature gradients. Subsequent evaluations made, indicate that the high energy flows associated with the flowing particles are due mainly to the high heat capacity of the annulus. Consequently, large amounts of heat input to the annulus are reflected by only small axial temperature gradients. Because of the boundary condition at the top of the annulus and these small axial temperature gradients, the radial gradients will tend to be dampened leading to conclusions more similar to those found by Stocker (1987).

From a more practical consideration, the one-dimensional approach is required in order to ease computational difficulty. As outlined in Chapter 3, the number of grid points along the length of the reactor equals (N_1+N_2-1). The corresponding number of simultaneous ordinary differential equations which are then solved in the one-dimensional model are $3\cdot(N_1+N_2-1)$. In order to implement a two-dimensional model, however, this number increases by (N_1+N_2-1) for each radial grid included in the model. The associated increase in computational time makes the model infeasible for use in any controls application. Therefore, although error is introduced with the annular lumped parameter assumption, it is a necessary to make this assumption

in order to utilize the resulting dynamic model in controls applications.

Using a similar electrical analogue, the assumption of negligible intraparticle temperature gradients is studied. In this case, the heat transfer resistance due to the thermal conductivity of the particle is proportional to $(2 \cdot k_p)^{-1}$, while the thermal resistance due to the external heat transfer coefficient is proportional to $(d_p \cdot h_p)^{-1}$. With the values for the particle heat transfer coefficient as shown in Table 5.1, the relative magnitudes of the resistances are approximately 60 percent to 40 percent respectively, or in other words, the temperature differential from the center of the spherical particle to the outer surface of the particle accounts for 60 percent of the total temperature difference between the maximum particle temperature and the bulk gas temperature. This indicates that the intraparticle temperature gradients are not negligible. In this analysis, however, the surface temperature of the particles is also affected by radiation, which is not considered in the electrical analogue. Radiation from the draft tube wall to the particles tends to increase the temperature at the surface of the particles causing a more even temperature profile in the particles.

Again, the practical consideration of computational time restricts the inclusion of additional differential equations to account for the intraparticle temperature gradients. Thus, the particle lumped parameter assumption is included in this work.

A third simplifying assumption proposed in the dynamic model development, is that of thermal equilibrium in the fountain. In Figure 5.2, typical axial spout gas, spout particle, and annular temperature profiles for the bench-scale spouted bed reactor, with air as the spouting medium, are presented. As illustrated, the spout gases in this bed increase in temperature at rates up to 5.8×10^4 K/s. At these rates, thermal equilibrium between the spout gases, spout particles, and annular solids is quickly achieved. Thus, the assumption of thermal equilibrium for cases of low temperature operating conditions is valid.

Figure 5.3 illustrates typical axial temperature profiles in the pilot-scale reactor. From this graph, heat-up rates of magnitudes in the vicinity of 2.6×10^4 K/s are achieved for spout gases in the entrainment region. Surprisingly, these rates are somewhat lower than those obtained in the bench-scale reactor; however, this is due to the absence of a heating source for the entrainment region of the bed (external heating source extends only to the base of the draft tube). Even with these lower heating rates, though, the difference between temperatures at the top of the bed are only approximately 100° C. Since this difference continues to decrease as heating rates are increased (i.e. higher operating temperatures and/or higher particle entrainment rates), the assumption of thermal equilibrium in the fountain region is reasonable as a first approximation. With the extremely complicated hydrodynamics associated with the fountain region, this approximation is also made to eliminate the inclusion of a significantly more complicated boundary condition.

Fig. 5.2 – Typical Axial Temperature Profiles in Bench–Scale Spouted Bed
(Inlet gas flowrate = 0.00533 kg/s air,
T_w = 490 K, F_p = 0.193 kg/s)

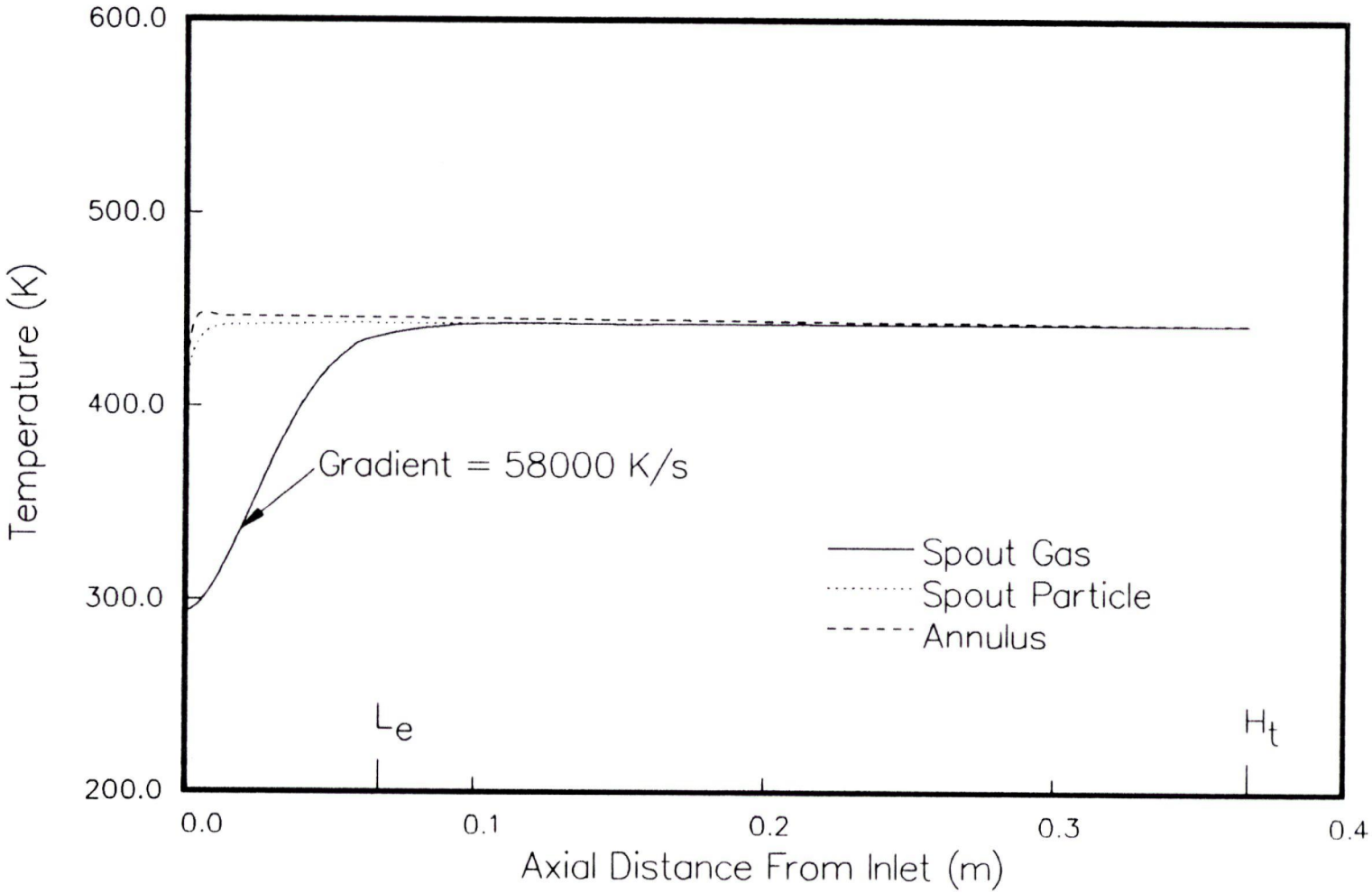

Fig. 5.3 – Typical Axial Temperature Profiles in Pilot–Scale Spouted Bed
(Inlet gas flowrate = 0.0107 kg/s steam,
T_w = 1214 K, F_p = 0.06 kg/s)

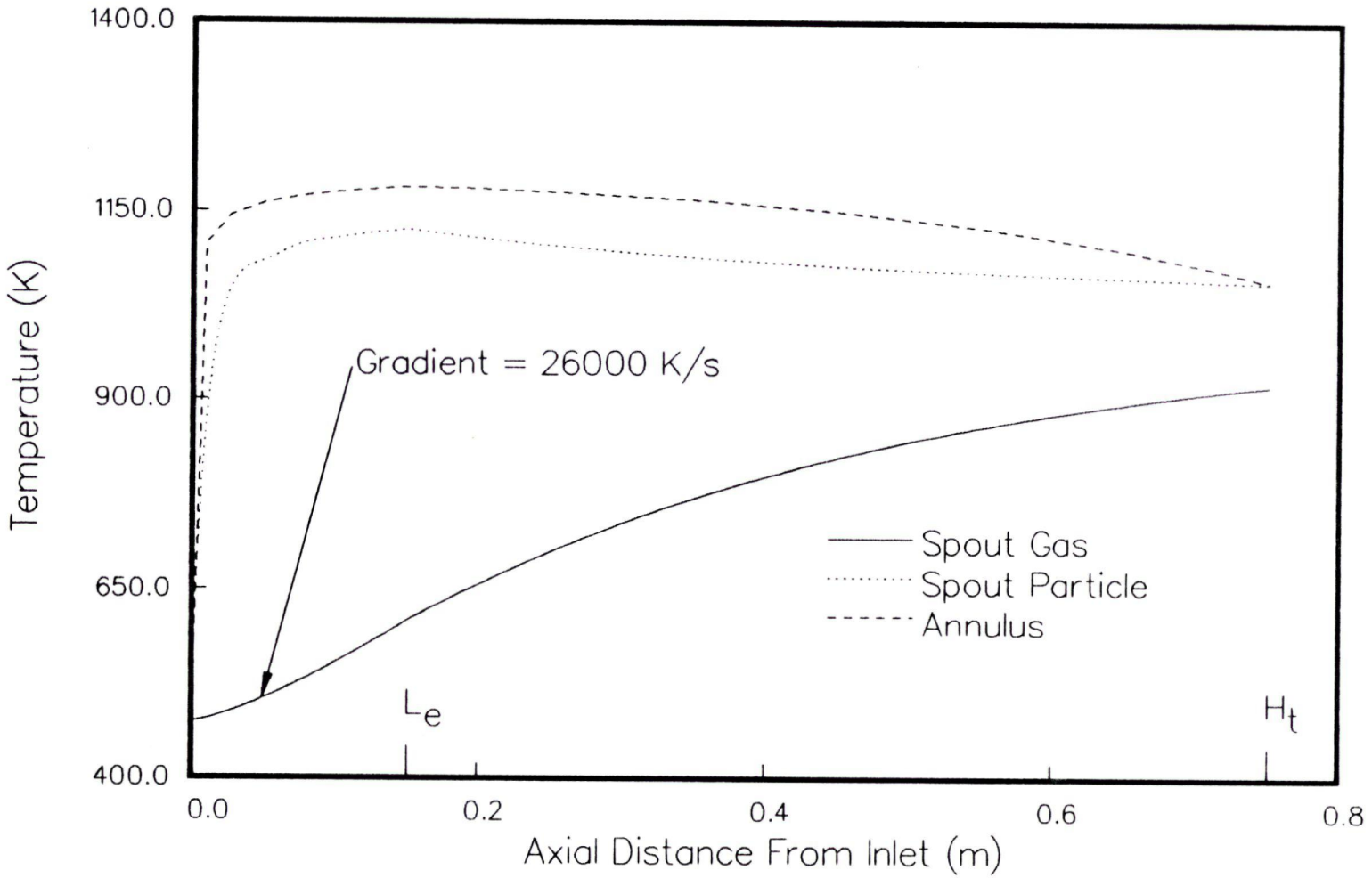

5.2 NUMERICAL METHOD CONSIDERATIONS

In implementing any numerical methods in the solution of P.D.E.'s, the errors associated with the approximation techniques must be considered. In this case, truncation errors resulting from finite differencing schemes and errors arising from orthogonal collocation applications appear to be of most concern. First of all, however, it is noted that in the derivation of the orthogonal collocation method, the residuals, or errors, at each of the collocation points are zero. Errors associated with collocation methods are therefore more dependent upon the order of the polynomial approximating function or the number of collocation points selected. In view of this, errors in both of the spacial discretizing techniques reduce as the number of grid points increases. Simulation runs are therefore carried out using as few grid points as necessary while not sacrificing accuracy.

In these runs the number of grid points in each of the entrainment and draft tube sections is specified to be equal in order to reduce the number of parameters which may be varied between runs. By then adjusting the number of grids, the dependence of the solution upon this parameter is observed. This dependence is illustrated in Figure 5.4. The differences in solutions associated with a reduction in the number of grid points is obvious. While the tendency is initially to attribute this difference to inadequacies of the differencing techniques, it should actually be ascribed to another more significant factor. This factor stems from the highly coupled

Fig. 5.4 – Axial Spout Gas Temperature Profiles
in Pilot–Scale Reactor For Various Numbers of Grids (N)
(Inlet gas flowrate = 0.0107 kg/s steam,
T_w = 1214 K, F_p = 0.06 kg/s)

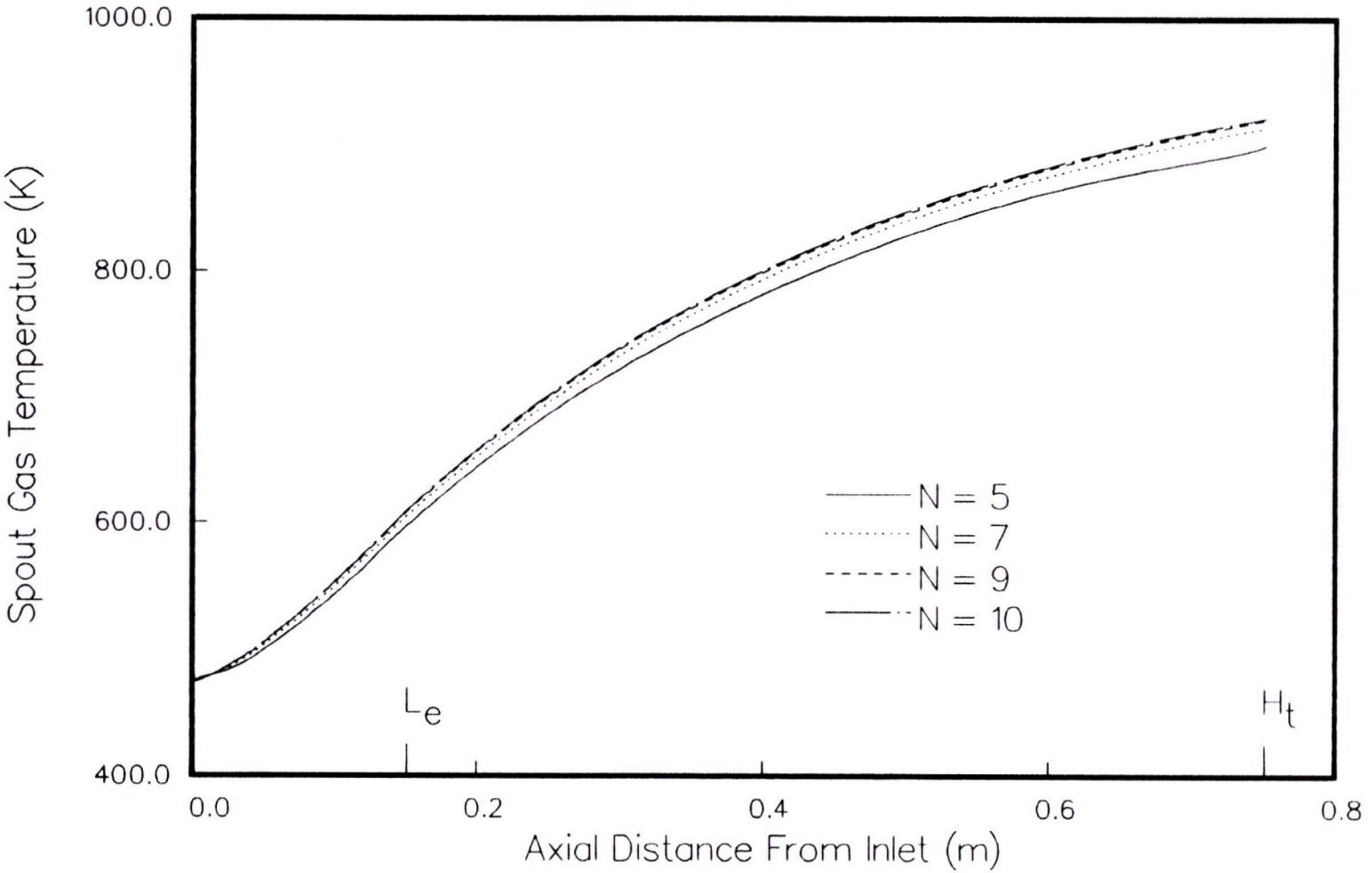

nature of the three energy balance equations. The number of grid points selected may increase the accuracy of the axial gradient calculations, but, more importantly, they determine the degree of interdependence of the partial differential equations in the spacial domain. Hence, while truncation errors may be negligible for a specified number of grids, the number of grid points used in calculations may actually be higher in order to correctly describe the interaction between the three dependent variables.

In addition to the specification of the number of grid points in each section of the reactor, the time intervals specified between quasi-steady state calculations is also a significant parameter. Selection of too high a value for this parameter may not only yield inaccurate solutions, but may actually introduce step changes of such a magnitude as to render the solution of the resulting problem incalculable. Even if the resulting problem is solvable, the large step changes create numerical difficulties. Hence, the CPU time of the computer may increase as these time intervals are specified either too long or too short.

Another difficulty in defining the length of the quasi-steady state time intervals is that the nature of the dynamic response must be understood. For instance, changes to the inlet gas properties cause sudden responses in the reactor and consequently, time intervals are specified to be extremely short initially. Changes in the wall temperature of an externally heated spouted bed, however, are accompanied by a much slower response and so much longer time intervals

are chosen.

In this study, insofar as errors do not become significant, the quasi-steady state time intervals are stipulated to be as large as possible in order to minimize the calculation time. Figure 5.5 illustrates the effect of decreasing the time intervals by a factor of 50 percent. As shown in this graph, the difference between the two predictions is negligible; however, the runs carried out with the smaller time intervals require 43 minutes of CPU time as opposed to 27 minutes with the longer time intervals.

5.3 EXPERIMENTAL COMPARISONS

In order to first verify the dynamic model proposed in this study, comparisons are made with experimental data obtained from the bench-scale reactor. This data is a record of the internal bed temperatures resulting from an increase in the wall temperature. The experimentally measured wall temperatures are entered into the simulation and the resulting temperature profiles are compared with those measured experimentally. These results are shown in Figure 5.6. As illustrated in this graph, predictions of temperatures further up within the bed match very well with those measured experimentally, noting the consistent offset predicted at all times. Since this offset is a function of the initial particle entrainment rate entered into the program, it can be reduced by adjustment of this parameter. In the entrance or entrainment region, inaccuracies in the particle entrainment or gas divergence profiles can be the cause of the

Fig. 5.5 – Effect of Quasi–Steady State Time Intervals on Dynamic Response of Exit Gas Temperature in Pilot–Scale Bed

(Inlet gas flowrate = 0.0107 kg/s steam, T_w and F_p as given in Equations 5.5 and 5.7)

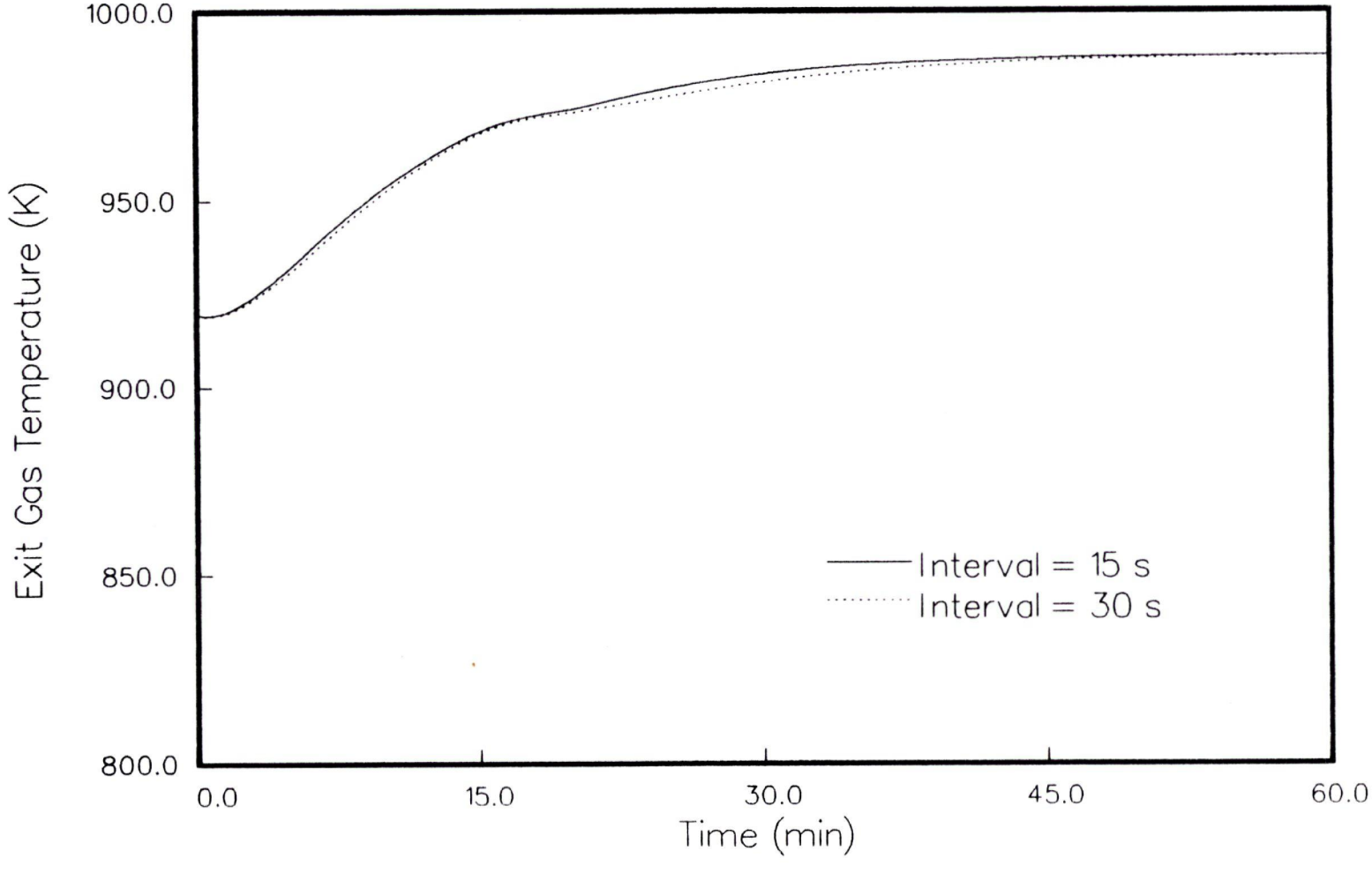

Fig. 5.6 – Transient Spout Gas Temperature Profiles in Bench–Scale Spouted Bed For Change in Wall Temperature
(Inlet gas flowrate = 0.00533 kg/s air, T_w and F_p as given in Equations 5.1 and 5.4)

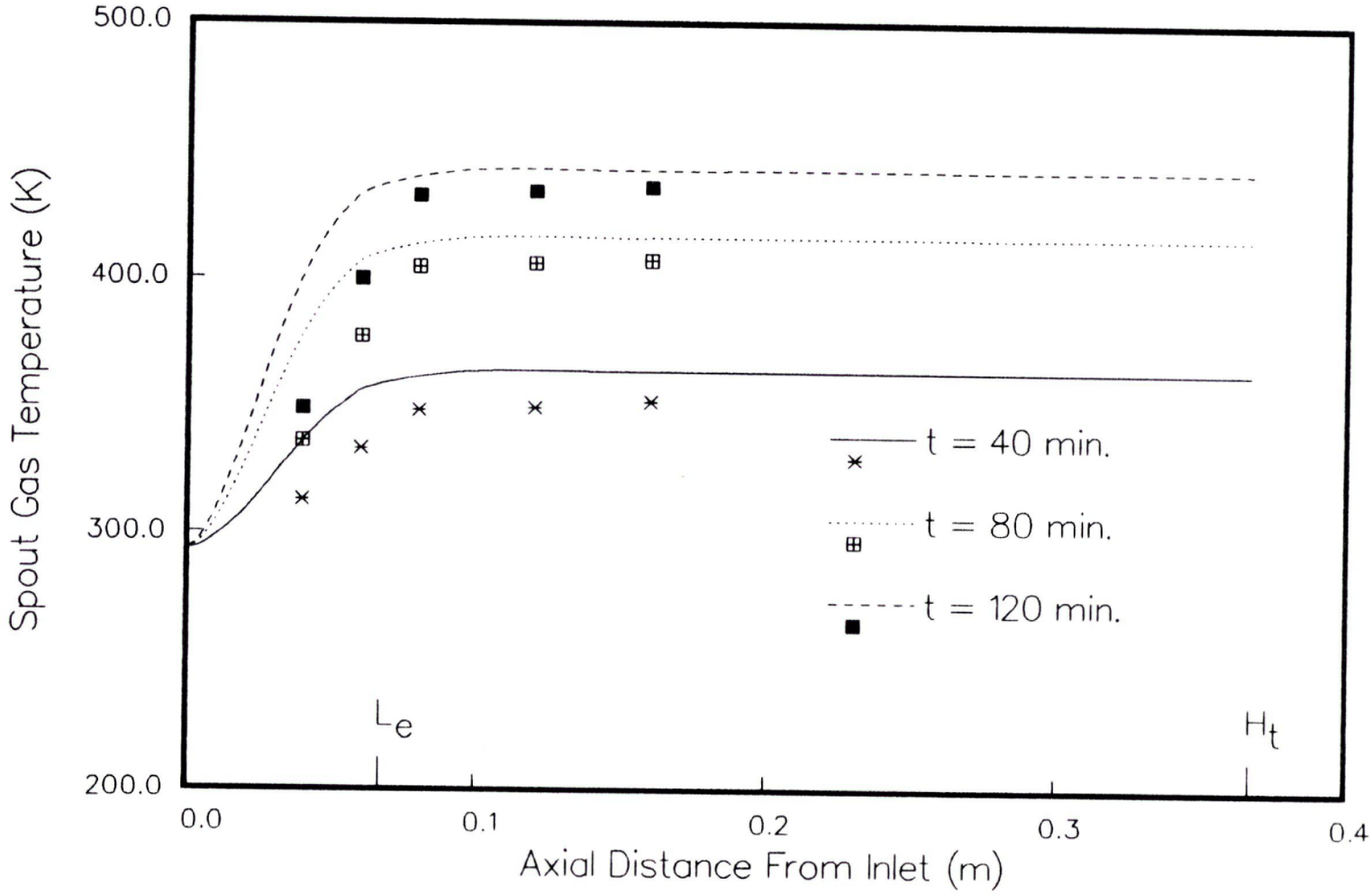

discrepancies between model predictions and experimental results. In general then, the comparisons can be observed to qualitatively substantiate the dynamic model predictions.

While calculation of accurate dynamic responses are the purpose of the model developed in this study, steady state simulations are also possible. These steady state simulations provide valuable insight regarding the significance of various hydrodynamic correlations. For instance, one of the most important of the hydrodynamic parameters, spout gas divergence into the annulus, is highly dependent upon the accuracy of presently available correlations. Although the pattern of divergence along the length of the spout, $f_{loss_i}(z)$, is found to alter the temperature profiles negligibly, the maximum spoutable bed height correlation, as discussed in Chapter 3, has a considerably greater affect. Figure 5.7 indicates the difference in steady state spout gas temperature profiles calculated using three different correlations. The McNab and Bridgwater correlation, which Wu *et al.* (1987) find to be valid for high temperature operations, results in predictions which differ notably from those obtained utilizing either the Lefroy and Davidson correlation or the Malek and Lu correlation. The discrepancy lies in the prediction of overall gas bypass into the annulus, the McNab and Bridgwater correlation predicting higher values of approximately 32 percent as compared with values of 13 to 16 percent using the other two correlations. Unfortunately, distinction as to which correlation is correct is impossible due to the limited amount of experimental information available regarding gas divergence phenomena and the concurrent

Fig. 5.7 – Effect of Various H_m Correlations on Steady State Gas Temperature Profile in Pilot–Scale Bed

(Inlet gas flowrate = 0.0107 kg/s steam, T_w = 1214 K, F_p = 0.06 kg/s)

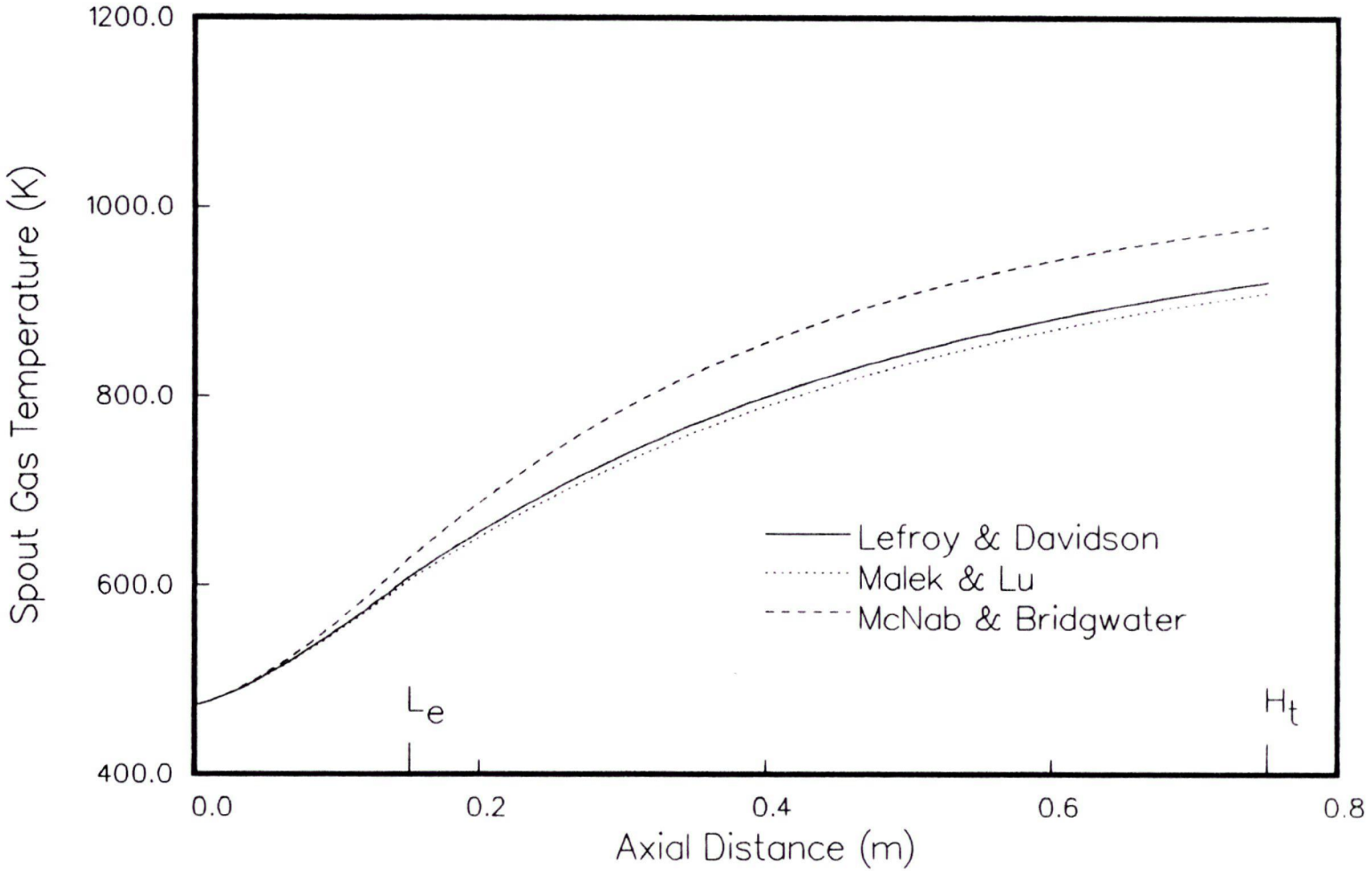

interaction of a second hydrodynamic parameter, the particle entrainment.

Knowledge concerning particle entrainment rates is also minimal, at best, for isothermal operations. For high temperature beds, information is even more scarce. Nevertheless, trends in particle entrainment rates in spouted beds with draft tubes, as considered by Buchanan and Wilson (1965), Yang and Keairns (1983), and Claflin and Fane (1984), are studied by means of dynamic simulations.

First of all, however, it is noted that values of the particle entrainment rates entered into the dynamic model are uncertain. An approximate range for these values is available, though, from observations of particle travel times in a semi-cylindrical plexiglass unit. Using these values then, steady state profiles are calculated.

The added uncertainty, and consequently the necessity of the trends observed by the authors mentioned, arises in the dynamic simulations. Figure 5.8 compares the predicted exit gas temperature response in the bench scale reactor to experimental data for the following change in the external wall temperature (expression obtained from fitting experimentally-measured values):

$$T_w = 523.2 - 250 \cdot e^{-t/3600} \qquad (5.1)$$

As observed in this graph, a base case for comparison in which a constant entrainment rate is assumed (correlation B_1), underpredicts

Fig. 5.8 – Effect of Various Entrainment Correlations on Transient Exit Gas Temperature in Bench–Scale Spouted Bed
(Inlet gas flowrate = 0.00533 kg/s air,
T_w given by Equation 5.1)

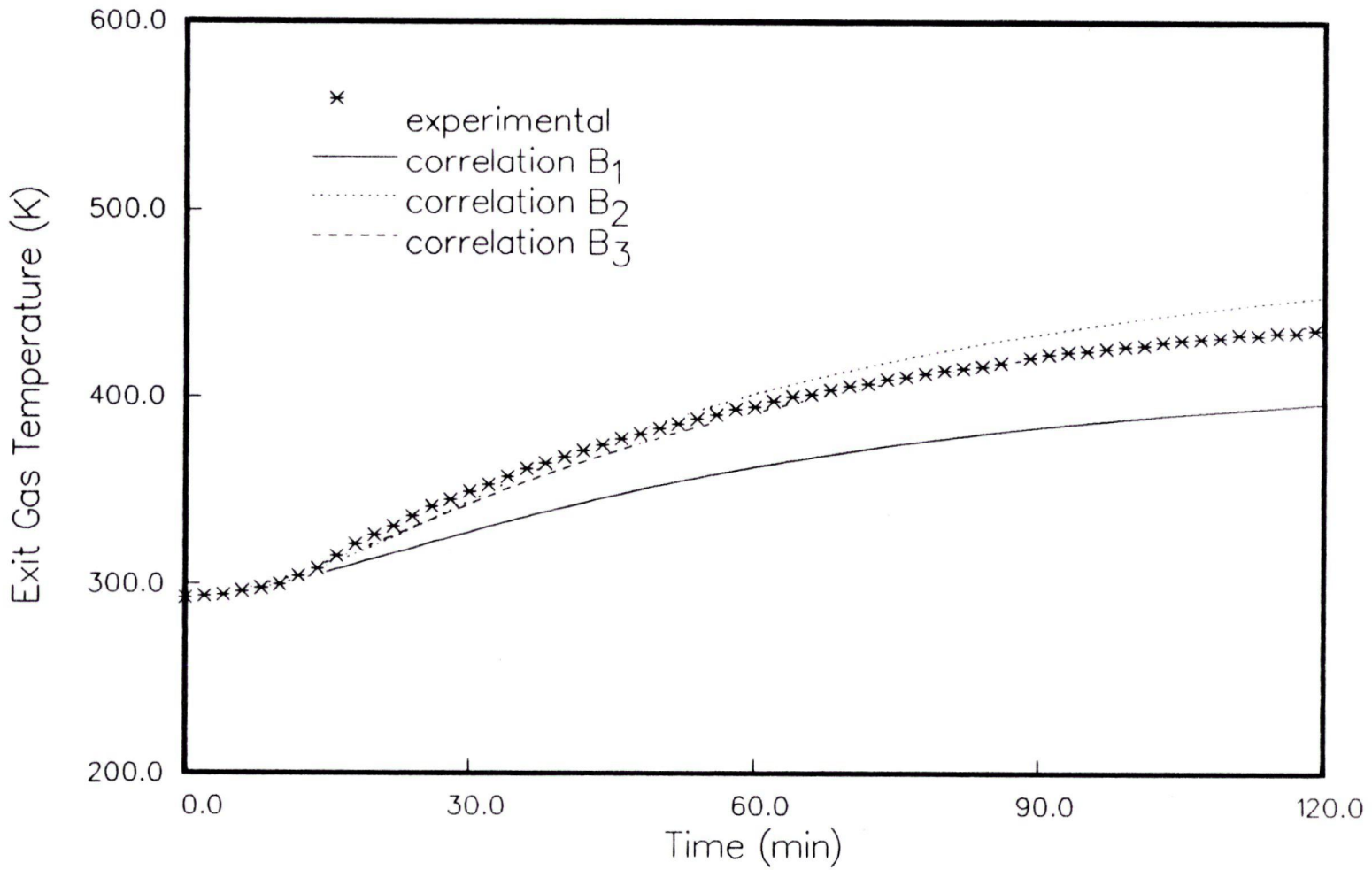

the overall increase in the exit gas temperature:

$$F_p = 0.03 \qquad (5.2)$$

In view of this, alternative entrainment rate correlations are investigated. Buchanan and Wilson (1965) and Yang and Keairns (1983) both observe that particle entrainment is directly proportional to the inlet gas flow rate in isothermal beds. Since the modelling undertaken in this study is not isothermal, an alternate strategy is devised. In this alternate strategy, the effect of nonisothermal operation is accounted for by correlating the entrainment rate to the volumetric gas velocity at the base of the draft tube. Accordingly, both the spout gas divergence and the spout gas temperature affect the total amount of entrainment, as they should. Hence, correlation B_2, in which total particle entrainment is proportional to the gas velocity at the base of the draft tube, is derived:

$$F_p = 0.03 + 0.05(U_s - 5.54) \qquad (5.3)$$

The last correlation referred to in Figure 5.8, correlation B_3, is based upon the observation of Claflin and Fane (1984), who observe proportionality according to the 0.7^{th} power of the gas flow rate:

$$F_p = 0.03 + 0.05(U_s - 5.54)^{0.7} \qquad (5.4)$$

An interesting distinction is observed between the correlations B_2 and B_3. While not clearly evident in Figure 5.8, the correlation B_2 predicts a slower initial increase in the entrainment rate, which is reflected by a milder initial slope in the exit gas temperature response. Furthermore, as temperatures continue to

increase, the particle entrainment rate continues to increase linearly resulting in even higher exit gas temperatures. Conversely, correlation B_3 predicts steeper initial exit gas temperature gradients, but lower final exit gas temperatures for equivalent increases in the external wall temperature. These trends, of course, are reflections of the relationships expressed in the correlations.

The question as to which correlation more clearly represents the actual nature of particle entrainment, is better understood by referring to Figures 5.9 and 5.10. In Figure 5.9, the exit gas temperature response in the pilot-scale reactor to the following change in external wall temperature (expression obtained by fitting experimentally-measured values) is illustrated:

$$T_w = 1266 - 51 \cdot e^{-t/528} \qquad (5.5)$$

Application of similar entrainment rate correlations is seen to be able to predict responses comparable to those obtained experimentally. For the pilot-scale reactor, these correlations, correlations P_1 and P_2 respectively, are given by

$$F_p = 0.06 + 0.01(U_s - 19.9) \qquad (5.6)$$

$$F_p = 0.06 + 0.0106(U_s - 19.9)^{0.7} \qquad (5.7)$$

In developing these responses, it is noted that varying the initial entrainment rate, which in this case is 0.06 kg/s, shifts the entire curve in the vertical direction. While the entrainment correlation does affect the shape of the response, the rate of change of the exit

Fig. 5.9 – Transient Exit Gas Temperatures in Pilot–Scale Reactor For Various Entrainment Rate Correlations
(Inlet gas flowrate = 0.0107 kg/s steam,
T_w given by Equation 5.5)

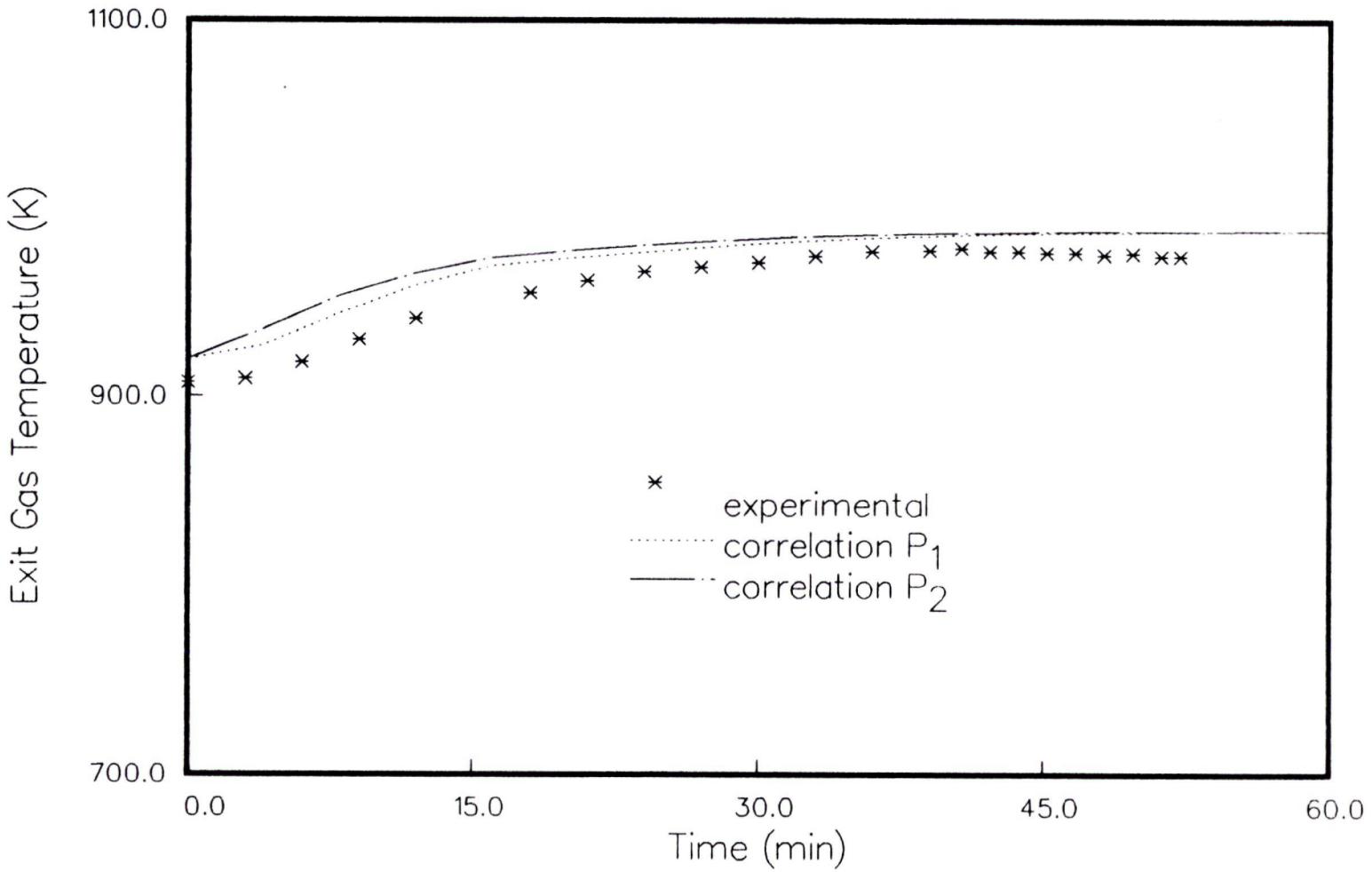

Fig. 5.10 – Transient Exit Gas Temperatures in Pilot–Scale Reactor for Second Increase in Wall Temperature
(Inlet gas flowrate = 0.0107 kg/s steam,
T_w given by Equation 5.8)

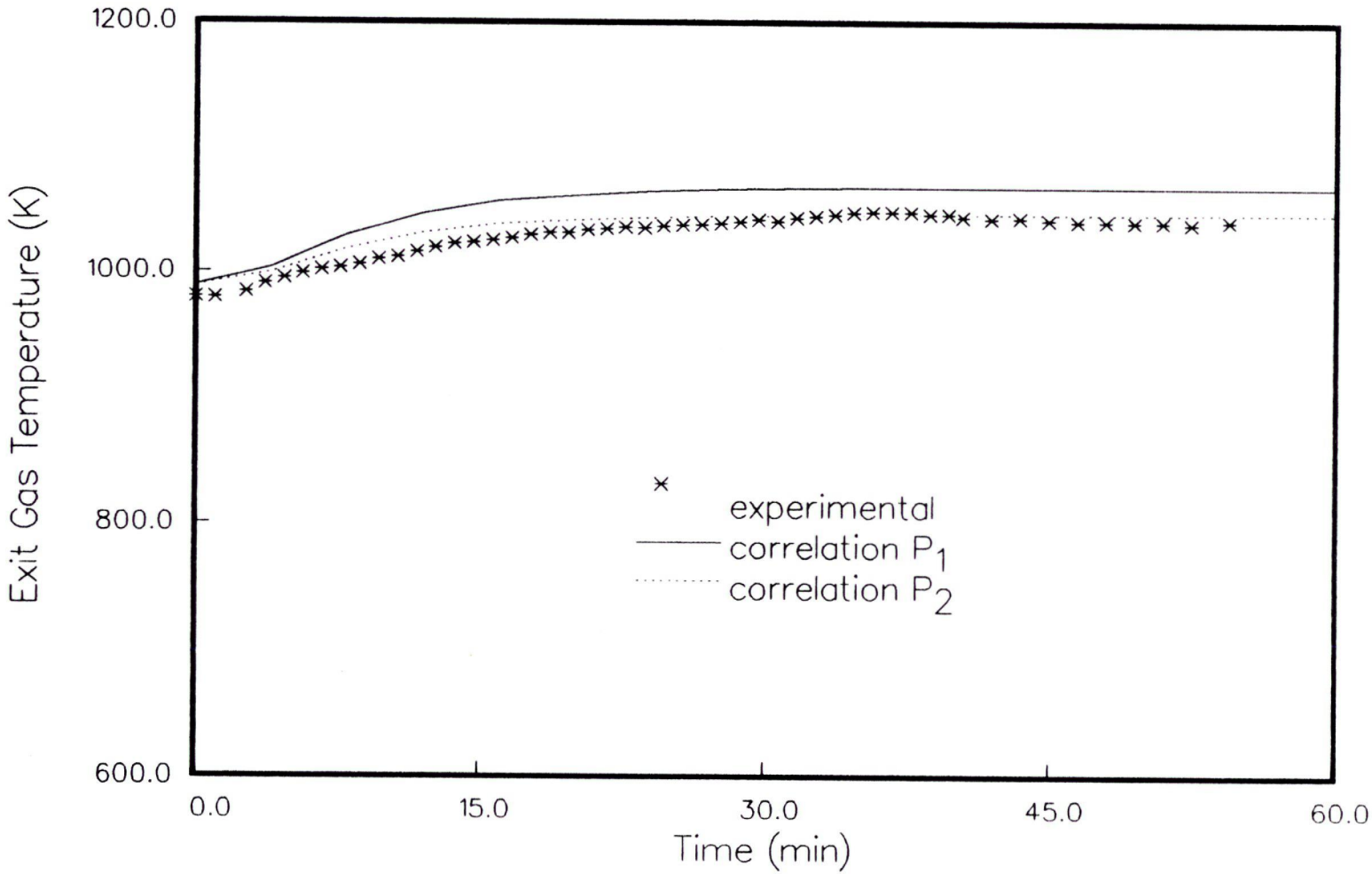

gas temperature is mostly dependent upon the nature of heat transfer in the bed, as described by the governing differential equations. Finally, the form of the correlation affects the response by defining the overall increase in total particle entrainment and hence, the overall increase in exit gas temperature. Discriminating between the two correlations then requires comparison with experimental data, as performed in both of these figures.

In Figure 5.9, both correlations are fitted to match the response of exit gas temperature to a change in the wall temperature. Differentiating between the two correlations is then elucidated by comparison with the responses to the following second increase in the wall temperature (expression obtained by fitting experimentally-measured values), as illustrated in Figure 5.10:

$$T_w = 1326 - 60 \cdot e^{-t/360} \qquad (5.8)$$

In this second transient case, while the trends of the responses are similar, the linear correlation begins to overpredict the final exit gas temperature. Therefore, for large temperature changes or large increases in flow rates, the corresponding entrainment rate increases are best correlated to the 0.7^{th} power of the gas velocity in the draft tube.

5.4 DYNAMIC RESPONSES

With the incorporation of the 0.7^{th} power correlation for particle entrainment (i.e. correlation P_2), studies of

the dynamic behavior of a spouted bed with a draft tube are carried out in consideration of three different operating conditions. These include changes in the bed wall temperature due to fluctuations or changes in the power of the external heat source, and fluctuations in either the inlet gas stream temperature or flow rate. The inlet gas concentration may also vary; however, unless they significantly alter the reactions occurring in the reactor (i.e. the heats of reaction become significant), they are of little consequence. Therefore, only the responses resulting from changes in the wall temperature, the inlet gas temperature and the inlet gas flow rate are presented.

It should be noted that in carrying out these analyses, only gaseous feeds are considered due to the complex effects of liquids on both spouting hydrodynamics and two-phase reactions. Additionally, in analyzing the responses, reactions are not considered in the modelling work. Since the model proposed in this study is developed to predict responses to operational disturbances (i.e. not start-up), small fluctuations in the heats of reaction will not greatly affect the dominant thermal responses of the reactor, which are due mainly to the inherent properties of the bed. Consequently, temperature responses predicted in consideration of only inert feeds will reasonably approximate the temperature responses in the reactor during pyrolysis runs.

5.4.1 WALL TEMPERATURE CHANGES

One of the most important parameters which can be

adjusted in the spouted bed reactor is the temperature at the external wall. This type of a change is of importance in the case of a pyrolysis reactor because it determines the temperature at which reactions will take place and hence, greatly affects the product distribution. Dynamic simulations can then elucidate the trends associated with such a change.

Figure 5.11 illustrates the changes in the axial spout gas temperature profiles associated with a step increase of 10 K in the external bed wall temperature. Results are presented in terms of the deviation of temperatures from their initial steady state profiles (Figure 5.3 on page 75). It is also noted that the initial steady state profiles pertain to the injection of steam into the pilot-scale reactor and that responses are considered for the case of steam as the spouting fluid.

Referring to Figure 5.11, the slow response of the spout gas temperature profile to the step change in wall temperature is observed. In fact, approximately 15 minutes are required for this temperature profile to reach steady state. This is indicative of the slow thermal response time of the annular solids as shown in Figure 5.12. The corresponding response in the spout particle temperature profiles is illustrated in Figure 5.13.

Of interest in these graphs is the relationship between the three temperature profiles. The annular temperature profile and the particle temperature profile are characterized by first

Fig. 5.11 – Dynamic Response of Spout Gas Temperature in Pilot–Scale Reactor to Step Increase of 10 K in Wall Temperature
(Inlet gas flowrate = 0.0107 kg/s steam,
Initial wall temperature = 1214 K)

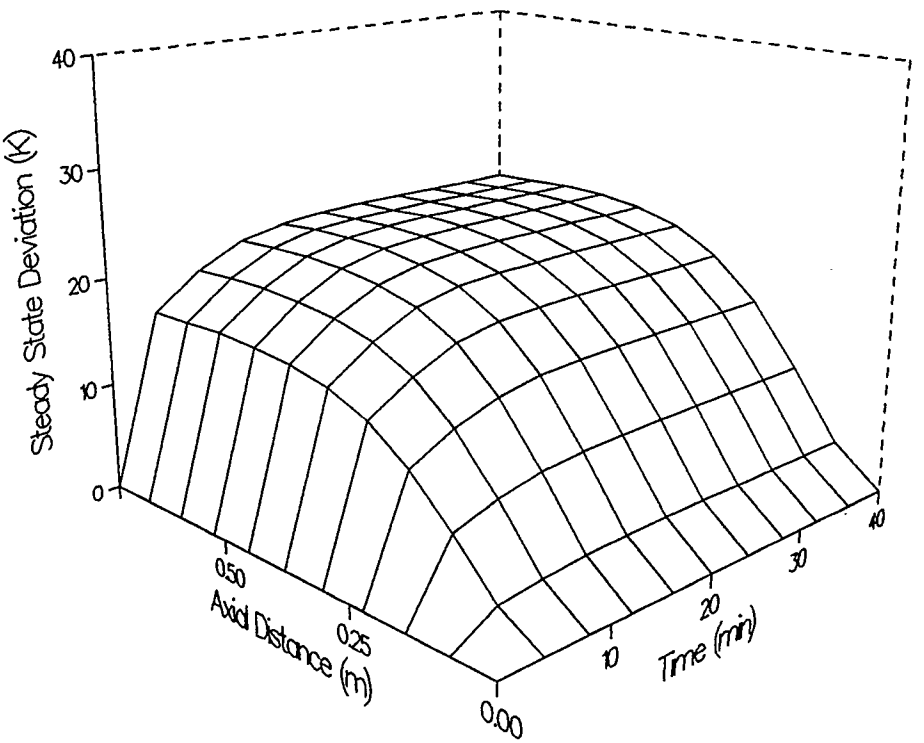

Fig. 5.12 – Dynamic Response of Annular Temperature in Pilot–Scale Reactor to Step Increase of 10 K in Wall Temperature
(Inlet gas flowrate = 0.0107 kg/s steam,
Initial wall temperature = 1214 K)

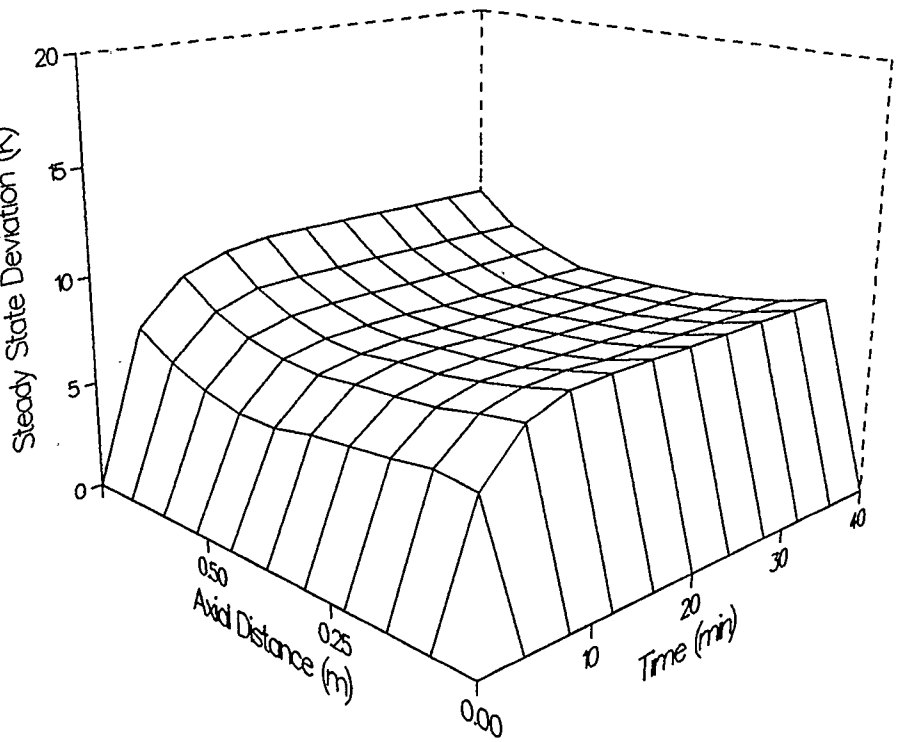

Fig. 5.13 – Dynamic Response in Spout Particle Temperature in Pilot–Scale Reactor to Step Increase of 10 K in Wall Temperature
(Inlet gas flowrate = 0.0107 kg/s steam,
Initial wall temperature = 1214 K)

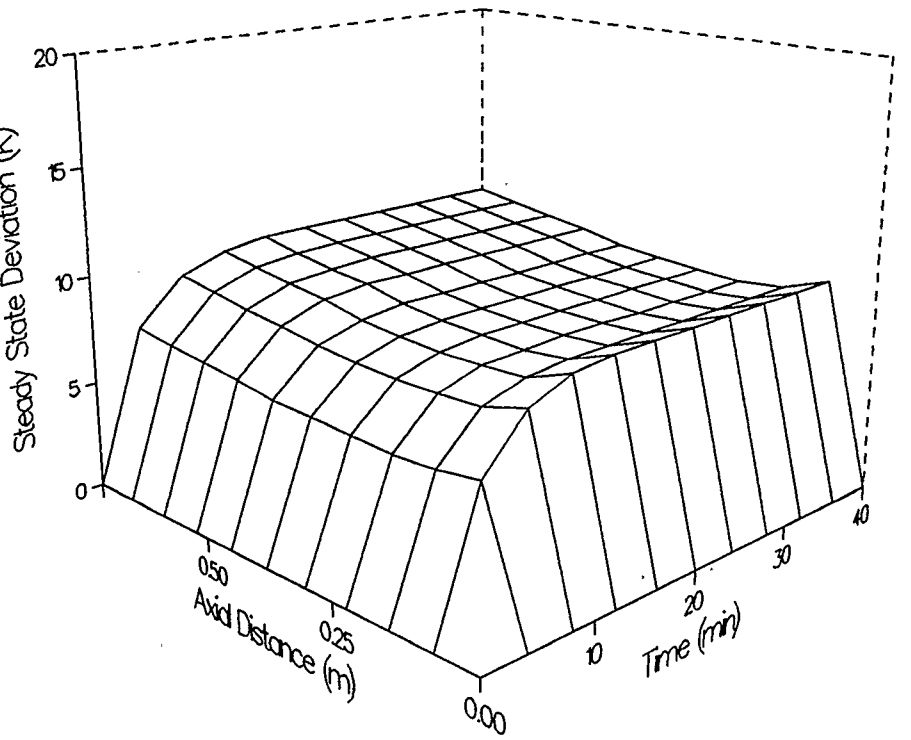

order responses of temperature versus time. The spout gas temperature profile matches these profiles illustrating not only the dependence of the gas temperature on both of the other temperatures, but also the short time constant associated with the approach to equilibrium of the gas temperature as compared with the annular temperature.

In addition to the response times of each of these variables, it is also interesting to note the absolute change in temperatures. For both the annular and particle temperatures, the absolute increase is about 10 K throughout the entire axial length of the bed or approximately the equivalent of the step change introduced. The gas temperature, however, increases by twice this amount. This apparent anomaly is explained by reference to Figure 5.14 in which the change in entrainment rate with respect to time is displayed. As the disturbance is introduced, the total entrainment increases as the gas temperature increases. Since the energy transferred to the gases is largely dependent upon the heat transferred from the spout particles, increases in entrainment will tend to compound the effect of the initial disturbance.

5.4.2 INLET GAS TEMPERATURE CHANGES

In addition to wall temperature changes, other operational disturbances which may arise are fluctuations in the inlet gas temperature. The effect of a step increase of 3 K on the gas temperature profile is illustrated in Figure 5.15. Again the overall increase in the exit gas temperature is observed to exceed that of the

Fig. 5.14 – Variation of Entrainment Rate in Pilot–Scale Reactor for Step Increase of 10 K in Wall Temperature
(Inlet gas flowrate = 0.0107 kg/s steam,
Initial wall temperature = 1214 K)

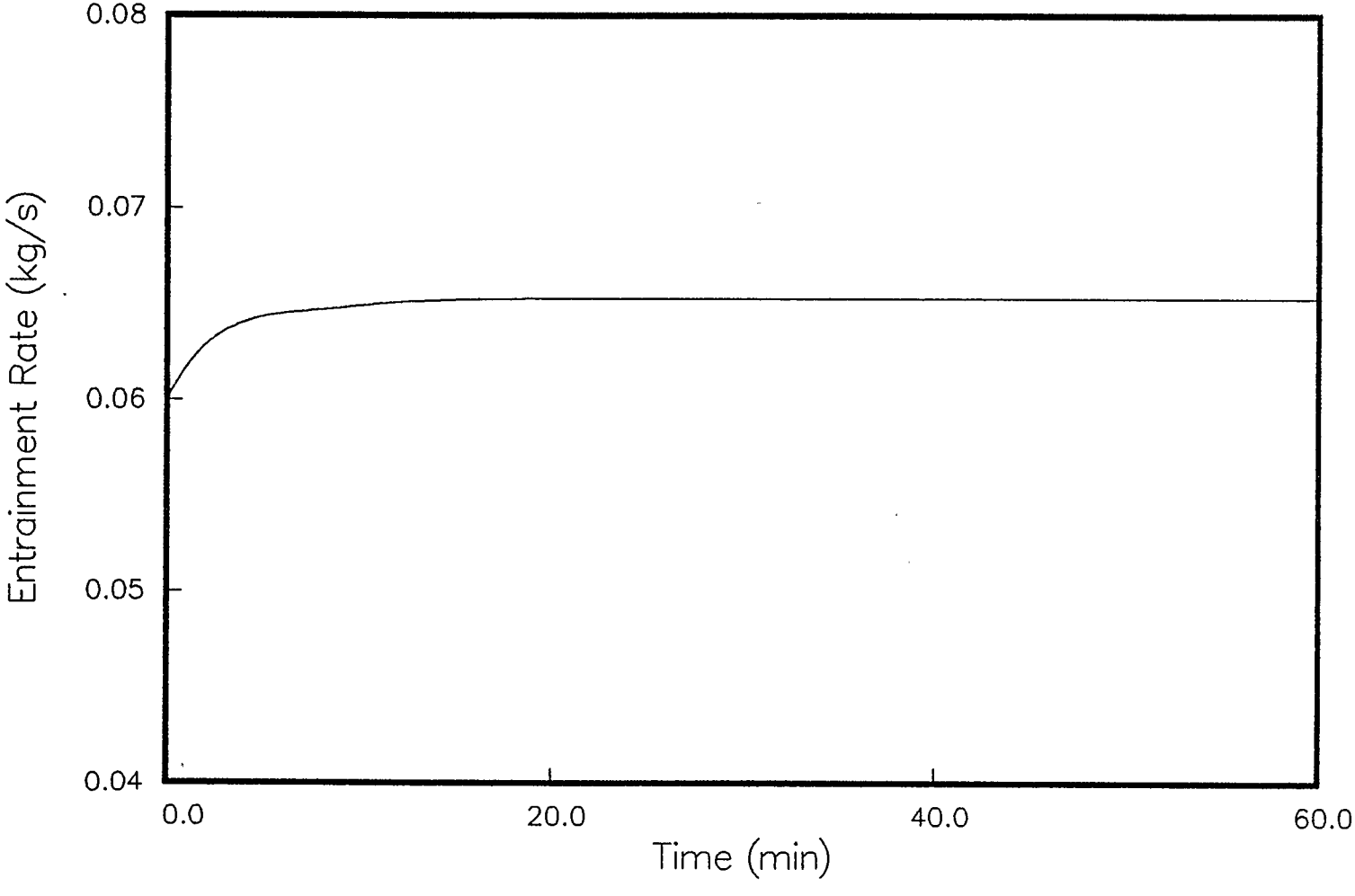

Fig. 5.15 – Dynamic Response of Spout Gas Temperature in Pilot–Scale Reactor to Step Increase of 3 K in Inlet Gas Temperature

(Inlet gas flowrate = 0.0107 kg/s steam,
Wall temperature = 1214 K,
Final inlet gas temperature = 476 K)

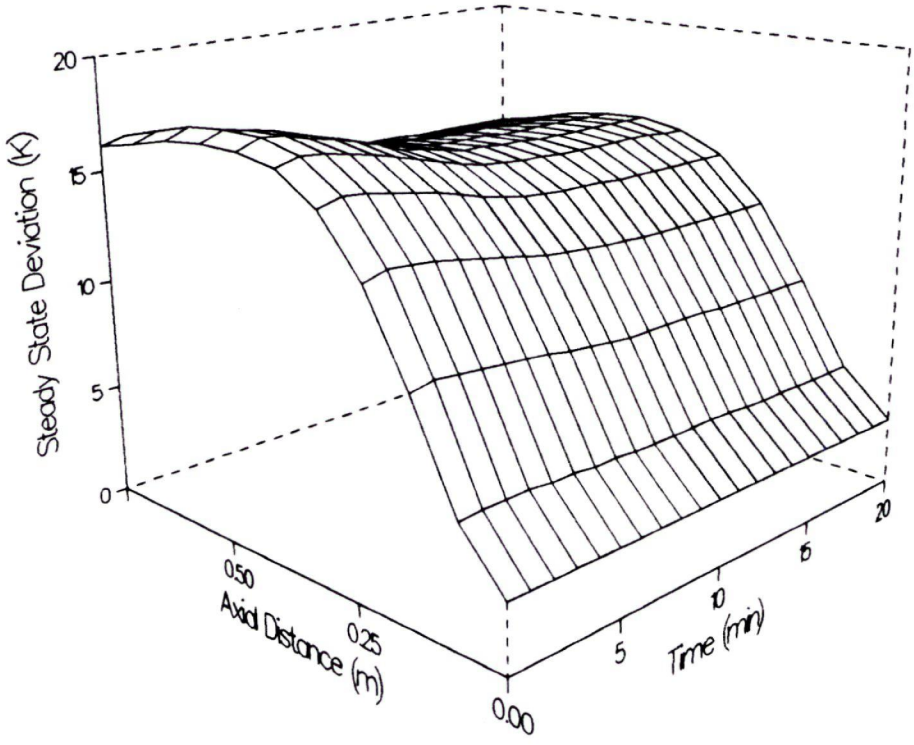

change in the inlet gas temperature. This also is due to the sudden increase in the overall entrainment rate as shown in Figure 5.16.

An even more curious trend is the decrease in gas temperature as a function of time. In Figure 5.15, the axial gas temperature profile is observed to almost instantaneously attain what Arkun *et al.* (1983) refer to as a "pseudo-steady state". In the context of this study, this translates to a instantaneous increase in the momentum of the spout gas stream causing the particle entrainment to suddenly rise. As temperatures in the bed stabilize, the particle entrainment decreases and the final steady state is reached.

5.2.3 INLET FLOW RATE CHANGES

The appearance of "pseudo-steady states" is even more pronounced in the responses in the bed to a step change in inlet gas flow rate. The response of the spout gas temperature to a 10 percent increase in the inlet gas flow rate is presented in Figure 5.17. Similar to the response to a step change in inlet gas temperature, the spout gas temperature practically instantaneously attains the "pseudo-steady state". As explained by Arkun, this corresponds to the mass residence time of the spout gases.

The introduction of the changes or the pseudo-steady state, results in temperature differentials which subsequently cause responses in the annular temperatures as shown in Figure 5.18. The additional heat load created by the increase in flow

Fig. 5.16 – Variation of Entrainment Rate in Pilot–Scale Bed for Step Increase of 3 K in Inlet Gas Temperature

(Inlet gas flowrate = 0.0107 kg/s steam,
T_w = 1214 K, Final inlet gas temperature = 476 K)

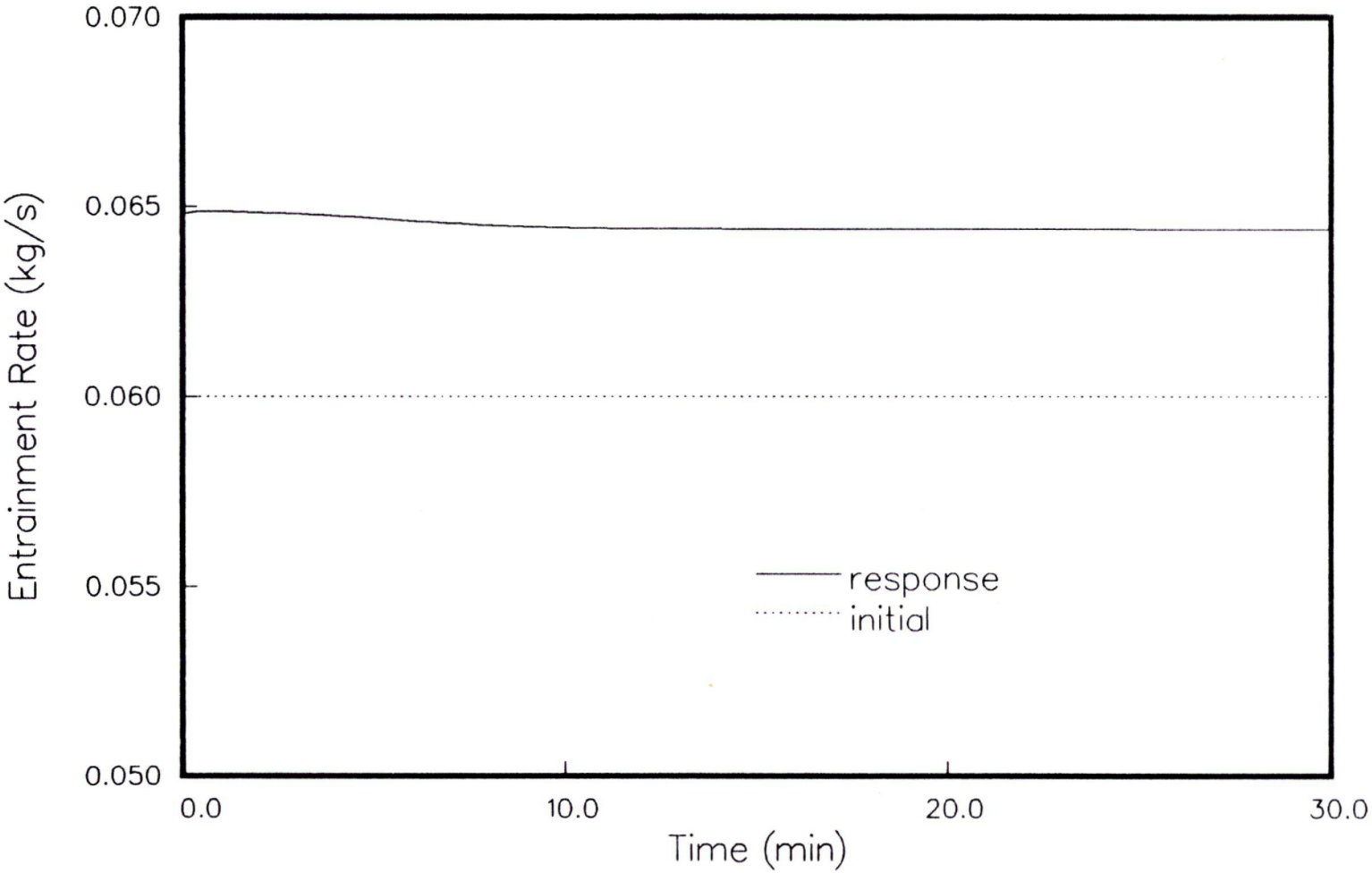

Fig. 5.17 – Dynamic Response of Spout Gas Temperature in Pilot–Scale Reactor to Step Increase of 10 % in Inlet Gas Flow Rate
(Initial inlet gas flowrate = 0.0107 kg/s steam, Wall temperature = 1214 K)

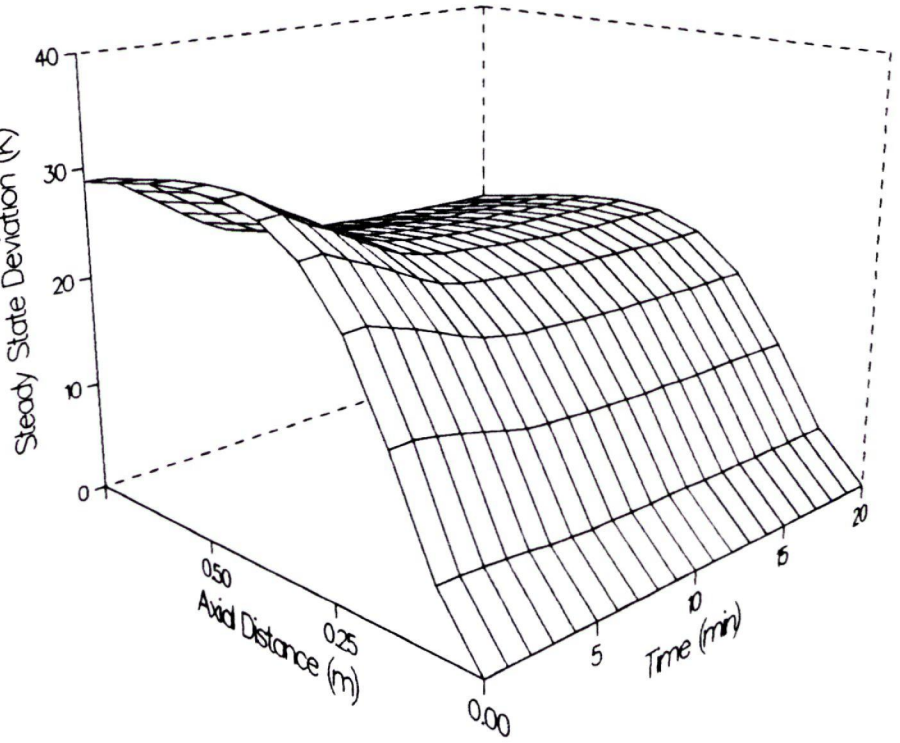

Fig. 5.18 – Dynamic Response of Annular Temperature in Pilot–Scale Reactor to Step Increase of 10 % in Inlet Gas Flow Rate
(Initial inlet gas flowrate = 0.0107 kg/s steam, Wall temperature = 1214 K)

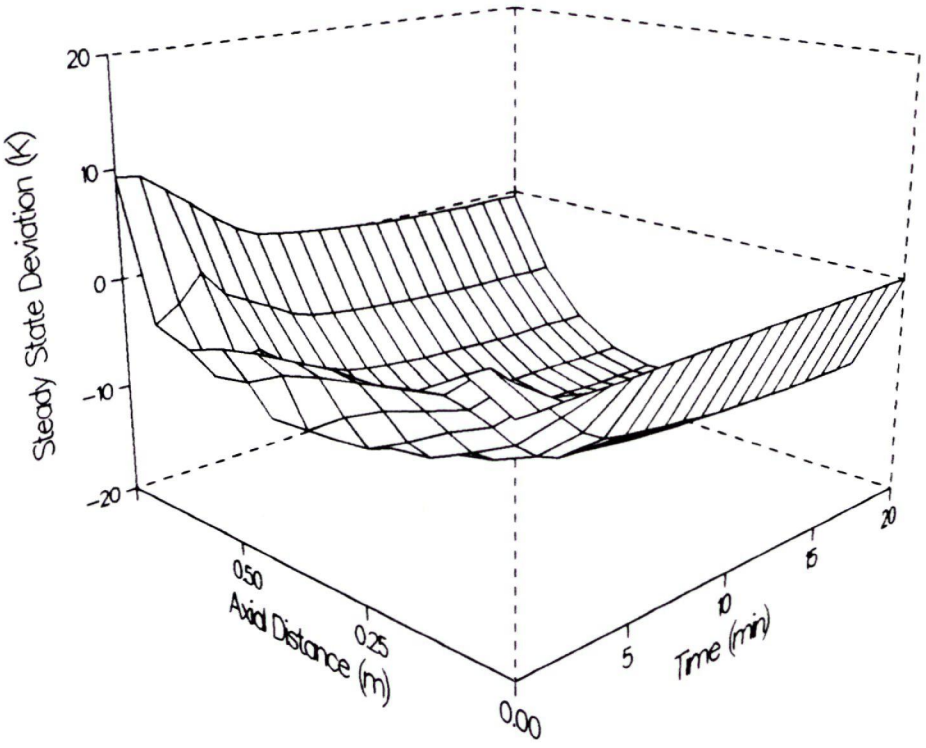

rate causes the annular temperatures to decrease and consequently, the spout gas temperatures decrease accordingly.

As Arkun *et al.* (1983) find, the responses for disturbances are most greatly affected by the thermal response time of the annulus. For disturbances in the feed properties, a "pseudo-steady state" appears; however, the final temperature reached is not dependent upon this phenomenon. They therefore conclude that the dynamics of the spout temperature may be ignored relative to the dynamics of the annular temperature. In the case of this study, though, the "pseudo-steady states" may be significant depending upon the nature and magnitude of the disturbance introduced. Therefore, neglecting of the spout gas temperature dynamics is dependent upon the application of the model and the accuracy required.

Chapter 6

CONCLUSIONS AND RECOMMENDATIONS

In extension of the work of Stocker (1987), this study presents a dynamic model for a spouted bed reactor with a draft tube. Steady state simulations confirm the findings of Stocker in that extremely high heat-up rates (greater than 5.8×10^4 K/s) are possible in the spout of this reactor, therefore making it ideal in pyrolysis applications.

6.1 CONCLUSIONS

The major contribution of this study is the development of a model to predict the dynamic heat transfer characteristics of a spouted bed reactor with a draft tube. In addition, the dynamic model is employed in steady state calculations as well. Comparisons with experimental data indicate the ability of the model to predict both steady state and dynamic responses.

In addition to these findings, studies regarding

spouted bed hydrodynamics are presented. Various correlations describing gas divergence from the spout into the annulus are studied indicating the effect of this hydrodynamic property upon heat-up rates in the spout. Unfortunately, however, it is impossible to discriminate between the correlations due to the lack of data available regarding this subject.

Studies concerning particle entrainment rates are also carried out illustrating the effect this parameter. Again lack of information limits the extent of this study; however, correlation of particle entrainment rates to the 0.7^{th} power of spout gas velocities matches well the dynamic responses of the bed.

Simulations of dynamic responses for various disturbances indicate that short term dynamic behaviour is strongly affected by changes in the inlet gas stream properties. Long term responses, however, are dependent upon the dynamics of the annular temperature.

In view of the dynamic responses observed, control of a spouted bed reactor for changes in feed properties can only be achieved by corresponding changes in other feed stream properties. Control of the bed by manipulation of the external wall temperature results in much slower responses, the time constant of which is highly dependent upon the diameter of the bed. Decreasing the diameter of the bed, while ensuring that sufficient annular residence time is allowed for particles to regain lost energy, is then one method by which to

increase the effectiveness of manipulating the external heat load as a means of controlling the spouted bed.

On an industrial level, in which heat is generally supplied by means other than external heaters, the results presented in this study still indicate the major thermal characteristics of a spouted bed reactor with a draft tube. Consequently, even the trends noted for the bench-scale and the pilot-scale reactors can assist in understanding industrial reactor dynamics.

6.2 RECOMMENDATIONS

Taking into account the assumptions required in the development of the dynamic model presented in this study, the first area of additional study must lie in the area of developing more reliable hydrodynamic correlations. The most important of these correlations are those relating to the particle entrainment rates and the gas divergence. While certain attempts at understanding hydrodynamics have been attempted in this study, the deficiency of information in this area limits the ability to correctly predict spouted bed operation under differing conditions.

In addition, with correct hydrodynamic correlations, the major assumptions made in the development of the dynamic model of this study should be further investigated to ascertain their effects upon the simulations presented.

The logical extension of the work presented in this study is the development of control strategies for operational use. In employing the dynamic model in this study, the degree of accuracy should first be defined and then the specification of collocation points can be minimized to reduce computational time. Another simplification which may be employed, is the inclusion of the spout gas temperature as a quasi-steady state variable. In so doing, however, caution must be taken since short term responses may be inaccurate with such an approach.

REFERENCES

Aimes, W.F., Numerical Methods for Partial Differential Equations, Academic Press, Inc., New York, 1977

Albright, L.F., B.L. Crynes, and W.H. Corcoran, Pyrolysis : Theory and Industrial Practice, Academic Press Inc., New York, 1983

Arkun, Y., K.J. Smith, and G. Sawyer, "Studies on Modelling and Control of Spouted Bed Reactors - II", Chem. Eng. Sci., 38, 6, 897, 1983

Behie, L.A., M.A. Bergougnou, and C.G.J. Baker, "Mass Transfer From a Grid Jet in a Large Gas Fluidized Bed", in Fluidization Technology, Hemisphere, Washington, 1, 261, 1976

Brereton, C.M.H., and J.R. Grace, "A Note on Comparison of Spouted Bed Reactor Models", Chem. Eng. Sci., 39, 1315, 1984

Buchanan, R.H., and B. Wilson, "The Fluid-Lift Solids Recirculator", Mech. Chem. Eng. Trans., 117, May, 1965

Burden, R.L., J.D. Faires, and A.C. Reynolds, Numerical Analysis, Prindle, Weber, and Schmidt, Inc., Boston, 1978

Chatterjee, A., "Effect of Particle Diameter and Apparent Particle Density on Internal Solid Circulation Rate in Air-Spouted Beds", I.E.C.Proc.Des.Dev., 9, 531, 1970

Chatterjee, A., R.S.S. Adusumilli, and A.V. Deshmukh, "Wall-to-Bed Heat Transfer Characteristics of Spout-Fluid Beds", Can. J. Chem. Eng., 61, 390, 1983

Chen, J.J.J., and Y.W. Lam, "On Jet Flow in Porous Media as Related to the Spouted Bed", Can. J. Chem. Eng., 63, 361, 1985

Claflin, J.K., and A.G. Fane, "Spouting With a Porous Draft Tube", Can. J. Chem. Eng., 61, 356, 1983

Claflin, J.K., and A.G. Fane, "Gas Distribution and Heat Transfer in a Draft Tube Spouted Bed", A.I.Ch.E Symp. Ser., 80, 17, 1984

Clift, R., J.R. Grace, and M.E. Weber, Bubbles, Drops, and Particles, Academic Press, Inc., New York, 1978

Cook, H.H., and J. Bridgwater, "Particle Residence Times in the Continuous Spouting of Mixtures", Can. J. Chem. Eng., 63, 326, 1985

Epstein, N., "Void Fraction Variation in the Spouted Bed Annulus", I.E.C. Proc. Des. Dev., 7, 1, 157, 1968

Epstein, N., and K.B. Mathur, "Heat and Mass Transfer in Spouted Beds - A Review", Can. J. Chem. Eng., 49, 467, 1971

Epstein, N., and S. Levine, "Non-Darcy Flow and Pressure Distribution in a Spouted Bed", in Fluidization, Cambridge University Press, 98, 1978

Epstein, N., C.J. Lim, and K.B. Mathur, "Data and Model For Flow Distribution and Pressure Drop in Spouted Beds", Can. J. Chem. Eng., 56, 436, 1978a

Fan, L.S., S.J. Hwang, and A. Matsuura, "Hydrodynamic Behaviour of a Draft Tube Gas-Liquid-Solid Spouted Bed", Chem. Eng. Sci., 39, 12, 1677, 1984

Filla, M., L. Massimilla, and S. Vaccaro, "Gas Jets in Fluidized Beds and Spouts : A Comparison of Experimental Behaviour and Models", Can. J. Chem. Eng., 61, 370, 1983

Finlayson, B.A., The Method of Weighted Residuals and Variational Principles, Academic Press, Inc., New York, 1972

Fogler, H.S., Elements of Chemical Reaction Engineering, Prentice-Hall, Inc., New Jersey, 1986

Froment, G.F., "Thermal Cracking for Olefins Production. Fundamentals and Their Application to Industrial Problems.", Chem. Eng. Sci., 36, 1271, 1981

Grace, J.R., and K.B. Mathur, "Height and Structure of the Fountain Region Above Spouted Beds", Can. J. Chem. Eng., 56, 533, 1978

Grbavcic, Z.B., D.V. Vukovic, F.K. Zdanski, and H., Littman, "Fluid Flow Pattern, Minimum Spouting Velocity, and Pressure Drop in Spouted Beds", Can. J. Chem. Eng., 54, 33, 1976

Hadzisdmajlovic, D.E., Z.B. Grbavcic, D.V. Vukovic, and H. Littman, "The Mechanics of Spout-Fluid Beds at the Minimum Spout-Fluid Flowrate", Can. J. Chem. Eng., 61, 343, 1983

Hansen, K.W., and S.B. Jorgensen, "Dynamic Modelling of a Gas Phase Catalytic Fixed-Bed Reactor - I", Chem. Eng. Sci., 31, 579, 1976

Heil, C., and M. Tels, "Pressure Distribution in Spout-Fluid Bed Reactors", Can. J. Chem. Eng., 61, 331, 1983

Kays, W.M., and M.E. Crawford, Convective Heat and Mass Transfer, McGraw-Hill, Inc., New York, 1980

Kirkbur, F., and B. Kisakurek, "Dynamic Analysis of an Ethane Cracking Reactor", in Chemical Reactor Design and Technology, Martinus Nijhoff Publishers, Dordrecht, Netherlands, 1986

Kmiec, A., "Simultaneous Heat and Mass Transfer in Spouted Beds", Can. J. Chem. Eng., 53, 18, 1975

Kmiec, A., "Hydrodynamics of Flows and Heat Transfer in Spouted Beds", Chem. Eng. J., 19, 189, 1980

Kmiec, A., "The Minimum Spouting Velocity in Conical Beds", Can. J. Chem. Eng., 61, 274, 1983

Kumpinsky, E., and N. Amundson, "Reactor Model Assessment For the Combustion of Char in Spouted Beds of Sand", I.E.C. Proc. Des. Dev., 23, 4, 784, 1984

Kunii, D., and J.M. Smith, "Heat Transfer Characteristics of Porous Rocks", A.I.Ch.E. Journal, 6, 1, 71 , 1960

Kursad, D., and B. Kilkis, "Numerical Analysis of Spouted Bed Hydrodynamics", Can. J. Chem. Eng., 61, 297, 1983

Lefroy, G.A., and J.F. Davidson, "The Mechanics of Spouted Beds", Trans. Inst. Chem. Eng., 47, T120, 1969

Lim, C.J., and K.B. Mathur, "Residence Time Distribution of Gas in Spouted Beds", Can. J. Chem. Eng., 52, 150, 1974

Lim, C.J., and K.B. Mathur, "A Flow Model For Gas Movement in Spouted Beds", A.I.Ch.E. Journal, 22, 4, 674, 1976

Lim, C.J., and K.B. Mathur, "Modelling of Particle Movement in Spouted Beds", in Fluidization, Cambridge University Press, 104, 1978

Lim, C.J., and J.R. Grace, "Spouted Bed Hydrodynamics in a 0.91 m Diameter Vessel", Can. J. Chem. Eng., 65, 366, 1987

Littman, H., D.V. Vukovic, F.K. Zdanski, and Z.B. Grbavcic, "Basic Relations for the Liquid Phase Spout-Fluid Bed at the Minimum Spout Fluid Flowrate", in Fluidization Technology, Hemisphere, Washington, 1, 373, 1976

Littman, H., P.V. Narayanan, A.H. Tomlins, and M.L. Friedman, "A Complete Theoretical Model for a First Order Isothermal Catalytic Reaction in a Spouted Bed", A.I.Ch.E Symp. Ser., 77, 174, 1981

Littman, H., M.H. Morgan, P.V. Narayanan, S.J. Kim, J.Y. Day, and G.M. Lazarek, "An Axisymmetric Model of Flow in the Annulus of a Spouted Bed of Coarse Particles. Model, Experimental Verification and Residence Time Distribution", Can. J. Chem. Eng., 63, 188, 1985

Malek, M.A., and B.C.Y. Lu, "Heat Transfer in Spouted Beds", Can. J. Chem. Eng., 42, 14, 1964

Mann, U., and E.J. Crosby, "Modelling Circulation of Solids in Spouted Beds", I.E.C. Proc. Des. Dev., 11, 314, 1972

Mann, U., and E.J. Crosby, "Cycle Time Distribution in Spouted Beds", Can. J. Chem. Eng., 53, 579, 1975

Markowski, A., and W. Kaminski, "Hydrodynamic Characteristics of Jet-Spouted Beds", Can. J. Chem. Eng., 61, 377, 1983

Massimilla, L., G. Donsi, and N. Migliaccio, "The Dispersion of Gas Jets in Two-Dimensional, Fluidized Beds of Coarse Solids", A.I.Ch.E Symp. Ser., 77, 17, 1981

Mathur, K.B., and C.J. Lim, "Vapour Phase Chemical Reaction in Spouted Beds : A Theoretical Model", Chem. Eng. Sci., 29, 789, 1974

Mathur, K.B., and N. Epstein, Spouted Beds, Academic Press, Inc., New York, 1974

Mathur, K.B., and N. Epstein, "Developments in Spouted Bed Technology", Can. J. Chem. Eng., 52, 129, 1974a

McCabe, W.L., and J.C. Smith, Unit Operations of Chemical Engineering, McGraw-Hill, Inc., New York, 1976

McNab, G.S., "Prediction of Spout Diameter", Brit. Chem. Eng. Proc. Tech., 17, 532, 1972

McNab, G.S., and J. Bridgwater, "A Theory for Effective Solid Stresses in the Annulus of a Spouted Bed", Can. J. Chem. Eng., 57, 274, 1979

Michelsen, M.L., and J. Villadsen, "A Convenient Computational Procedure for Collocation Constants", Chem. Eng. J., 4, 64, 1972

Morgan, M.H., J.Y. Day, and H. Littman, "Spout Voidage Distribution, Stability and Particle Circulation Rates in Spouted Beds of Coarse Particles - I. Theory", Chem. Eng. Sci., 40, 8, 1367, 1985

Nagarkatti, A., and A. Chatterjee, "Pressure and Flow Characteristics of a Gas Phase Spout-Fluid Bed and the Minimum Spout-Fluid Condition", Can. J. Chem. Eng., 52, 185, 1974

Nemeth, J., E. Pallai, and E. Aradi, "Scale-Up Examination of Spouted Bed Dryers", Can. J. Chem. Eng., 61, 419, 1983

Patrose, B., and H.S. Caram, "The Mechanics of Particle Motion in a Grid Jet", A.I.Ch.E Symp. Ser., 80, 48, 1984

Perry, R.H., D.W. Green, and J.O. Maloney, Ed.s, Perry's Chemical Engineers' Handbook, 6th ed., McGraw-Hill, Inc., New York, 1984

Piccinini, N., J.R. Grace, and K.B. Mathur, "Vapour Phase Chemical Reaction in Spouted Beds : Verification of Theory", Chem. Eng. Sci., 34, 1257, 1979

Reid, R.C., J.M. Prausnitz, and T.K. Sherwood, The Properties of Liquids and Gases, 3rd ed., McGraw-Hill, Inc., New York, 1977

Rovero, G., C.M.H. Brereton, N.Epstein, J.R. Grace, L. Casalegno, and N. Piccinini, "Gas Flow Distribution in Conical-Base Spouted Bed", Can. J. Chem. Eng., 61, 289, 1983

Rovero, G., N. Piccinini, J.R. Grace, N. Epstein, and C.M.H. Brereton, "Gas Phase Solid-Catalyzed Chemical Reaction in Spouted Beds", Chem. Eng. Sci., 38, 4, 557, 1983a

Ryan, W.J., and U.A. Heinzle, "Use of a Draught Tube Contactor For Heterogeneous Catalytic Gas Reaction", Aust. Miner. Dev. Lab. Bull., 8, 1, 1969

Sadek, S.E., "Heat Transfer to Air-Solids, Suspensions in Turbulent Flow", I.E.C. Proc. Des. Dev., 11, 1, 133, 1972

Smith, K.J., Y. Arkun, and H. Littman, "Studies on Modelling and Control of Spouted Beds - I", Chem. Eng. Sci., 37, 4, 567, 1982

Stocker, R.K., Ultrapyrolysis of Propane in a Spouted Bed Reactor With a Draft Tube, Ph.D. Thesis, University of Calgary, Calgary, Alberta, 1987

Sucec, J., Heat Transfer, Wm. C. Brown Publishers, Dubuque, Iowa, 1985

Sundaram, K.M., and G.F. Froment, "Kinetics of Coke Deposition in the Thermal Cracking of Propane", Chem. Eng. Sci., 34, 635, 1979

Uemaki, O., M. Fugikawa, and M. Kugo, "Pyrolysis of Petroleum (Crude Oil, Heavy Oil, and Naphtha) For Production of Ethylene and Propylene in an Externally Heated Spouted Bed", Kogyo Kagaku Zasshi, 73, 453, 1970

Van Velzen, D., H.J. Flamm, and H. Langenkamp, "Gas Flow Patterns in Spouted Beds", Can. J. Chem. Eng., 52, 145, 1974

Villadsen, J.V., and W.E. Stewart, "Solution of Boundary Value Problems By Orthogonal Collocation", Chem. Eng. Sci., 22, 1483, 1967

Villadsen, J., and M.L. Michelsen, Solution of Differential Equation Models By Polynomial Approximation, Prentice-Hall, Inc., New Jersey, 1978

Viswanathan, K., "Semicompartmental Model For Spouted Bed Reactors", Can. J. Chem. Eng., 62, 623, 1984

Viswanathan, K., "Model For Continuous Drying of Solids in Fluidized / Spouted Beds", Can. J. Chem. Eng., 64, 87, 1986

Viswanathan, K., M.S. Lyall, and B.C. Raychaudhuri, "Spouted Bed Drying of Agricultural Grains", Can. J. Chem. Eng., 64, 223, 1986

Vukovic, D.V., F.D. Zdanski, G.V. Vunjak, Z.B. Grbavcic, and H. Littman, "Pressure Drop, Bed Expansion and Liquid Holdup in a Three Phase Spouted Bed Contactor", Can. J. Chem. Eng., 52, 180, 1974

Watkinson, A.P., G. Cheng, and C.B. Prakash, "Comparison of Coal Gasification in Fluidized and Spouted Beds", Can. J. Chem. Eng., 61, 468, 1983

Whiting, K.J., and D. Geldart, "A Comparison of Cylindrical and Semi-Cylindrical Spouted Beds of Coarse Particles", Chem. Eng. Sci., 35, 1499, 1980

Wu, S.W.M., C.J. Lim, and N. Epstein, "Hydrodynamics of Spouted Beds at Elevated Temperatures", Chem. Eng. Comm., 62, 251, 1987

Yagi, S., and D. Kunii, "Studies on Effective Thermal Conductivities in Packed Beds", A.I.Ch.E. Journal, 3, 3, 373, 1957

Yang, W.C., and D.L. Keairns, "Studies on the Solid Circulation Rate and Gas Bypassing in Spouted Fluid Bed With a Draft Tube", Can. J. Chem. Eng., 61, 349, 1983

APPENDIX A

MODEL EQUATIONS DEVELOPMENT

A.1 MATERIAL BALANCE EQUATIONS

A.1.1 GAS MATERIAL BALANCES

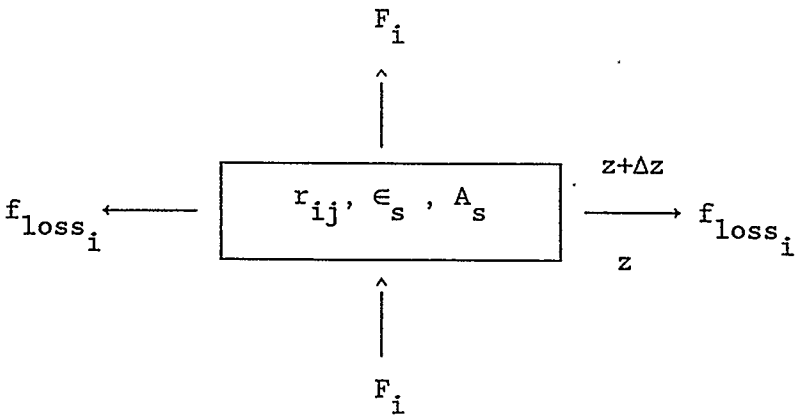

Performing a material balance for each component, i, in the elemental volume in the spout, as shown above, results in the following equation:

$$F_i\Big|_z - F_i\Big|_{z+\Delta z} - f_{loss_i}\cdot\Delta z - \sum_{j=1}^{N_r}(r_{ij}\cdot A_s\cdot\Delta z\cdot\epsilon_s) = \frac{d}{dz}\left(A_s\cdot\epsilon_s\cdot\Delta z\cdot C_i\right) \qquad (A.1)$$

In arriving at equation A.1, plug flow in the spout is assumed. This infers that concentrations and temperatures within the elemental volume are relatively homogeneous throughout. The gas divergence function, $f_{loss_i}(z)$, defines the amount of spout gas bypassing into the annulus and therefore applies only in the entrainment region. In addition, the reaction term is included to account for the endothermic reactions occurring in pyrolysis. Dividing Equation A.1 by Δz, the following

partial differential equation describing the flow of each gaseous component, N_c, is derived:

$$A_s \frac{\partial}{\partial t}\left(\epsilon_s \cdot C_i \right) = - \frac{\partial F_i}{\partial z} + A_s \cdot \epsilon_s \cdot \sum_{j=1}^{N_r} r_{ij} - f_{loss_i} \qquad (A.2)$$

By further applying the quasi-steady state assumption, the term on the left-hand side of Equation A.2 reduces to zero leaving the following differential equation.

$$\frac{dF_i}{dz} = A_s \cdot \epsilon_s \cdot \sum_{j=1}^{N_r} r_{ij} + f_{loss_i} \qquad (A.3)$$

Of particular interest in this equation is the fact that removal of the gas divergence term (i.e. flow in the draft tube), reduces the equation to that describing reaction in a plug flow reactor. The reaction terms referred to in Equation A.3 then, are those describing pyrolysis of the particular hydrocarbon fed into the reactor. In the case of propane pyrolysis, for instance, the kinetic scheme developed by Sundaram and Froment (1979) can be utilized.

The gas divergence term employed in Equation A.3 is developed from existing hydrodynamic correlations. The following equation, as discussed in Chapter 3, describes annular gas flow in a conventional, isothermal spouted bed:

$$U_a = U_{aH} \left[1 - \left(1 - \frac{z}{L_e} \right)^3 \right] \qquad (A.4)$$

The annular gas velocity at the top of the entrainment height, U_{aH}

(where $H = L_e$), is given by the modified Mamuro-Hattori equation, Equation 3.3 on page 34. This gas velocity is then converted into the total fractional molar gas bypass term by applying the ideal gas law and assuming isobaric operation:

$$U_a = \frac{\sum_{i=1}^{N_c} F_i \cdot R \cdot T_g}{P \cdot A_a} \qquad (A.5)$$

The total fractional molar gas bypass is then defined as the ratio of the total molar flow rate in the annulus at the top of the entrainment region to the total molar flow rate into the reactor as shown in Equation A.6:

$$g_L = \frac{\left(\sum_{i=1}^{N_c} F_i \right)_{aH}}{\left(\sum_{i=1}^{N_c} F_{i_0} \right)} = \frac{U_{aH} \cdot P \cdot A_a}{R \cdot T_{aH} \cdot \left(\sum_{i=1}^{N_c} F_{i_0} \right)} \qquad (A.6)$$

For a cylindrical spouted bed, the cross-sectional area of the annulus, A_a, is approximately constant given the relatively small change in spout diameter over the length of the entrainment region. Therefore, Equation A.4 can be rewritten in terms of the gas flow rates for an isothermal, isobaric spouted bed as follows

$$\sum_{i=1}^{N_c} F_i = g_L \cdot \left(\sum_{i=1}^{N_c} F_{i_0} \right) \left[1 - \left(1 - \frac{z}{L_e} \right)^3 \right] \qquad (A.7)$$

Since the temperatures in the entrainment region are low (i.e. less than 600° C), reactions are insignificant in the entrainment region and

so Equation A.7 can be rewritten in terms of each individual component in the feed:

$$F_i = g_L \cdot F_{i_0} \left[1 - \left(1 - \frac{z}{L_e} \right)^3 \right] \qquad (A.8)$$

Now the gas divergence function, $f_{loss_i}(z)$, can be calculated as the gas dispersing into the annulus per unit height by differentiating with respect to the axial distance z:

$$f_{loss_i}(z) = \frac{dF_i}{dz} = \frac{3 \cdot F_{0_i} \cdot g_L}{L_e} \left(1 - \frac{z}{L_e} \right)^2 \qquad (A.9)$$

A.1.2 SPOUT PARTICLE MATERIAL BALANCE

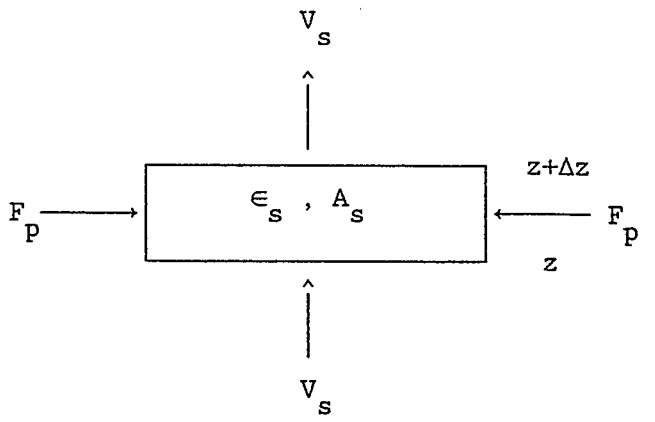

Performing a material balance on the spout particles over the elemental volume shown above and neglecting the accumulation term, by implementing the quasi-steady state assumption, allows derivation of the equation describing spout voidage profiles along the length of the reactor. As explained in Chapter 3, the particle entrainment rate is assumed to be a constant value per unit height. Therefore, considering the particles to enter an elemental spout volume with a mass-averaged velocity, V_s, the particle material balance for solids in the spout is given by

$$(1-\epsilon_s)\cdot A_s\cdot V_s\cdot \rho_p \Big|_z - (1-\epsilon_s)\cdot A_s\cdot V_s\cdot \rho_p \Big|_{z+\Delta z} + F_p \frac{\Delta z}{L_e} = 0 \qquad (A.10)$$

Dividing by Δz and by assuming the particle density to remain relatively constant, the differential equation given by Equation A.11 is developed:

$$\frac{d}{dz}\left[A_s \cdot V_s (1-\epsilon_s)\right] = \frac{F_p}{\rho_p \cdot L_e} \qquad (A.11)$$

Equation A.11 can be rearranged to yield the following differential equation:

$$\frac{d\epsilon_s}{dz} = \frac{(1-\epsilon_s)}{V_s} \cdot \frac{dV_s}{dz} + \frac{(1-\epsilon_s)}{A_s} \cdot \frac{dA_s}{dz} - \frac{F_p}{V_s \cdot A_s \cdot \rho_p \cdot L_e}$$

$$(A.12)$$

As outlined in Chapter 3, the second and third terms on the right hand side of Equation A.12 apply only in the entrainment region, with equations describing the spout cross-sectional area given by Equations 3.10 and 3.11.

A.2 MOMENTUM BALANCE EQUATION

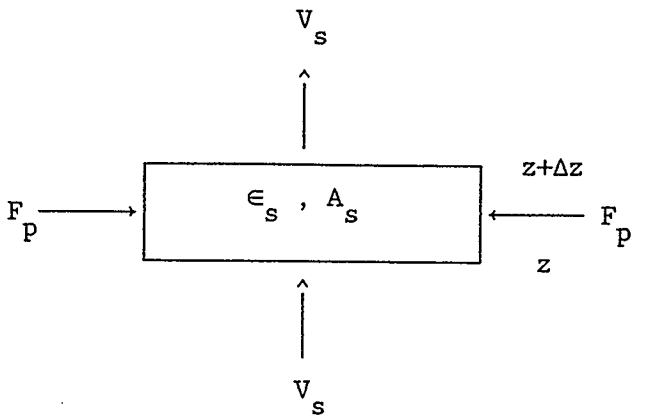

In order to develop an equation describing the mass-averaged particle velocity profile along the length of the spout, a momentum balance equation is analyzed with the momentum of the particles entering an elemental volume given by

$$\text{momentum} = (1-\epsilon_s)\, A_s \cdot \rho_p \cdot V_s^2 \Big|_z \qquad (A.13)$$

By neglecting pressure changes, particle-particle, and particle-wall effects, the remaining terms to be considered are those accounting for the momentum transferred to the particles from the passing spout gases, the momentum added by the entrained particles, the effects on momentum caused by gravity and bouyancy. With the drag coefficient defined as the ratio of the average drag per unit projected area of the particle divided by the product of the fluid density and the velocity head, the total drag force on the particles is expressed by Equation A.14

$$\text{drag force} = \frac{C_D \cdot \rho_g (U_s - V_s)^2 A_p}{2} \qquad (A.14)$$

where A_p, the total projected area of the particles given the spout voidage is

$$A_p = \frac{\frac{\pi}{4} d_p^2 (1-\epsilon_s) A_s \cdot \Delta z}{\frac{\pi}{6} d_p^3} = \frac{3(1-\epsilon_s) A_s \cdot \Delta z}{2 \cdot d_p} \qquad (A.15)$$

The entrainment, gravity, and buoyancy effects are given by Equations A.16, A.17, and A.18, respectively:

$$\text{entrainment force} = V_s \cdot F_p \frac{\Delta z}{L_e} \qquad (A.16)$$

$$\text{gravity force} = A_s(1-\epsilon_s)\, \rho_p \cdot g \cdot \Delta z \qquad (A.17)$$

$$\text{buoyancy force} = \frac{A_s(1-\epsilon_s)\rho_p \cdot \rho_g \cdot g \cdot \Delta z}{\rho_p} \qquad (A.18)$$

Combining Equations A.13 through A.18 results in the following momentum balance:

$$A_s(1-\epsilon_s)\rho_p \cdot V_s^2\Big|_z - A_s(1-\epsilon_s)\rho_p \cdot V_s^2\Big|_{z+\Delta z} + \frac{3 \cdot C_D \cdot \rho_g (U_s - V_s)^2 A_s (1-\epsilon_s)}{4 \cdot d_p}$$

$$+ \frac{V_s \cdot F_p \cdot \Delta z}{L_e} - A_s(1-\epsilon_s)\rho_p \cdot g \cdot \Delta z + A_s(1-\epsilon_s)\rho_g \cdot g \cdot \Delta z = 0 \qquad (A.19)$$

Dividing Equation A.19 by $\rho_p \cdot A_s(1-\epsilon_s)\Delta z$ leaves the following expression

$$\frac{1}{A_s(1-\epsilon_s)}\frac{d}{dz}\left[A_s(1-\epsilon_s)V_s^2\right] = \frac{3\cdot C_D\cdot\rho_g(U_s-V_s)^2}{4\cdot d_p\cdot\rho_p} + \frac{(\rho_g-\rho_p)g}{\rho_p}$$

$$+ \frac{F_p\cdot V_s}{L_e\cdot A_s\cdot\rho_p(1-\epsilon_s)} \qquad (A.20)$$

Expanding the left-hand side of Equation A.20 as follows

$$\frac{1}{A_s(1-\epsilon_s)}\frac{d}{dz}\left[A_s(1-\epsilon_s)V_s^2\right] = \frac{V_s^2}{A_s}\frac{dA_s}{dz} - \frac{V_s^2}{(1-\epsilon_s)}\frac{d\epsilon_s}{dz}$$

$$+ 2\cdot V_s\frac{dV_s}{dz} \qquad (A.21)$$

Substituting in Equation A.12 then yields

$$\frac{1}{A_s(1-\epsilon_s)}\frac{d}{dz}\left[A_s(1-\epsilon_s)V_s^2\right] = V_s\frac{dV_s}{dz} + \frac{F_p\cdot V_s}{L_e\cdot A_s\cdot\rho_p(1-\epsilon_s)}$$

(A.22)

Finally substituting this expression back into Equation A.20 results in Equation A.23:

$$\frac{dV_s}{dz} = \frac{1}{V_s}\left[\frac{3\cdot C_D\cdot\rho_g(U_s-V_s)^2}{4\cdot d_p\cdot\rho_p} + \frac{(\rho_g-\rho_p)g}{\rho_p}\right]$$

(A.23)

A.3 ENERGY BALANCE EQUATIONS

A.3.1 SPOUT GAS ENERGY BALANCE

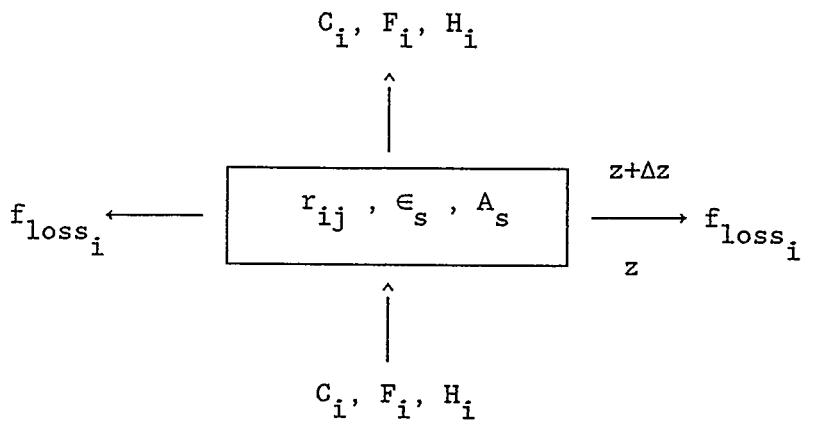

With the enthalpy of stream components given by H_i, the energy balance over the elemental spout gas volume assuming homogeneity in the element is given by

$$Q + \sum_{i=1}^{N_c} F_i \cdot H_i \Big|_z - \sum_{i=1}^{N_c} F_i \cdot H_i \Big|_{z+\Delta z} - \sum_{i=1}^{N_c} f_{loss_i} \cdot H_i \cdot \Delta z$$

$$= \frac{d}{dt} \left(A_s \cdot \in_s \cdot \Delta z \cdot \sum_{i=1}^{N_c} C_i \cdot H_i \right) \qquad (A.24)$$

Dividing the entire expression by Δz, then leaves the following

equation:

$$\frac{Q}{\Delta z} - \frac{\partial}{\partial z}\left(\sum_{i=1}^{N_c} F_i \cdot H_i \right) - \sum_{i=1}^{N_c} f_{loss_i} \cdot H_i$$

$$= A_s \frac{\partial}{\partial t}\left(\epsilon_s \cdot \sum_{i=1}^{N_c} C_i \cdot H_i \right) \qquad (A.25)$$

The right-hand side of Equation A.25 can be expanded using the chain rule:

$$\frac{\partial}{\partial t}\left(\epsilon_s \cdot \sum_{i=1}^{N_c} C_i \cdot H_i \right) = \epsilon_s \sum_{i=1}^{N_c} C_i \frac{\partial H_i}{\partial t} + \sum_{i=1}^{N_c} H_i \frac{\partial}{\partial t}\left(\epsilon_s \cdot C_i \right) \qquad (A.26)$$

Now dividing by A_s and rearranging the terms

$$\frac{Q}{\Delta z \cdot A_s} - \sum_{i=1}^{N_c} H_i \left[\frac{1}{A_s} \frac{\partial F_i}{\partial z} + \frac{\partial}{\partial t}\left(\epsilon_s \cdot C_i \right) + \frac{f_{loss_i}}{A_s} \right]$$

$$- \frac{1}{A_s} \sum_{i=1}^{N_c} F_i \frac{\partial H_i}{\partial z} = \epsilon_s \sum_{i=1}^{N_c} C_i \frac{\partial H_i}{\partial t} \qquad (A.27)$$

The term inside of the brackets on the left-hand side of the equation can be substituted by the dynamic material balance equation for each gaseous component as specified in Equation A.2. In addition, the enthalpy of each stream component at any point in the bed is a function of the heat capacity of that compound and the temperature at that point in the reactor. The partial differential equation describing the spout

gas temperature within the bed is then given by Equation A.28:

$$\epsilon_s \sum_{i=1}^{N_c} C_i \cdot c_{p_i} \frac{\partial T_g}{\partial t} = \frac{Q}{\Delta z \cdot A_s} - \sum_{i=1}^{N_c} \left(H_i \cdot \epsilon_s \sum_{j=1}^{N_r} r_{ij} \right) - \frac{1}{A_s} \sum_{i=1}^{N_c} F_i \cdot c_{p_i} \frac{\partial T_g}{\partial z} \qquad (A.28)$$

Further simplification can be achieved by substitution of the definition of heat of reaction:

$$\epsilon_s \sum_{i=1}^{N_c} C_i \cdot c_{p_i} \frac{\partial T_g}{\partial t} = \frac{Q}{\Delta z \cdot A_s} - \epsilon_s \sum_{j=1}^{N_r} r_j \cdot \Delta H_j - \frac{1}{A_s} \sum_{i=1}^{N_c} F_i \cdot c_{p_i} \frac{\partial T_g}{\partial z} \qquad (A.29)$$

The heat transfer term referred to in Equation A.29 encompasses all heat transfer to the spout gases from both the particles and the annulus. As such, it includes convective heat transfer terms for both the particle-to-gas and the annulus-to-gas energy fluxes as shown in Equation A.30:

$$Q = h_p \cdot A_s \cdot \Delta z (1-\epsilon_s) \left(\frac{6}{d_p} \right) (T_p - T_g) + U_w \cdot \pi \cdot D_s \cdot \Delta z (T_a - T_g) \qquad (A.30)$$

The heat transfer term to be substituted into Equation A.29 is then

$$\frac{Q}{\Delta z \cdot A_s} = \frac{6 \cdot h_p (1-\epsilon_s)}{d_p} (T_p - T_g) + \frac{4 \cdot U_w}{D_s} (T_a - T_g) \qquad (A.31)$$

As noted in Chapter 3 of this text, radiation to the spout gases is found to be negligible.

A.3.2 PARTICLE ENERGY BALANCE

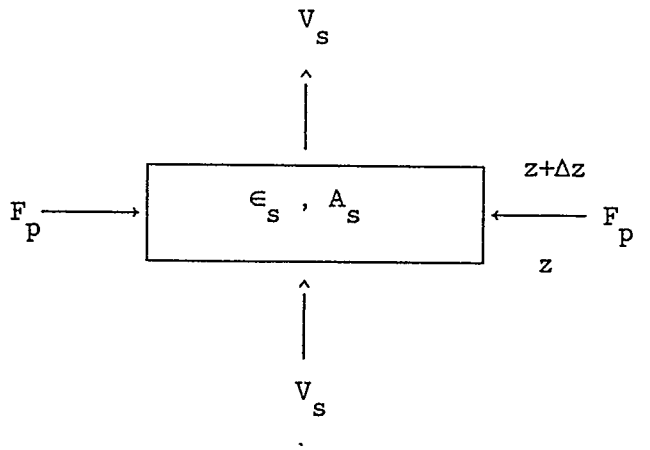

In a manner likewise to that of the spout gas energy balance, the particle energy balance is developed assuming homogeneity both within the particles and throughout the elemental volume. The energy in and out of the elemental volume associated with the particles already entrained in the spout is quantified in the expression below:

$$A_s \cdot V_s (1-\epsilon_s) \cdot \rho_p \cdot H_p \Big|_z - A_s \cdot V_s (1-\epsilon_s) \cdot \rho_p \cdot H_p \Big|_{z+\Delta z} \qquad (A.32)$$

Note that in Equation A.32, the change in enthalpy is due only to the change in particle temperature along the spout. The change in stream energy due to the increase in mass flow rate up the spout is considered by an additional term for the entrainment. In order to account for the particles entering into the spout in the entrainment region, it is assumed that they enter at the annular temperature and leave the elemental volume at the mass-averaged temperature of the particles.

The energy supplied to the spout particles due to entrainment is then

$$\frac{F_p \cdot \Delta z}{L_e} c_{p_p} \int_{T_p}^{T_a} dT = \frac{F_p \cdot \Delta z}{L_e} c_{p_p} (T_a - T_p) \qquad (A.33)$$

Including also the heat loss/gain terms and the accumulation terms and then dividing by Δz leaves

$$- A_s(1-\epsilon_s)V_s \cdot \rho_p \cdot c_{p_p} \frac{\partial T_p}{\partial z} + \frac{F_p \cdot c_{p_p} (T_a - T_p)}{L_e} + \frac{Q}{\Delta z}$$

$$= A_s(1-\epsilon_s)\rho_p \cdot c_{p_p} \frac{\partial T_p}{\partial t} \qquad (A.34)$$

Equation A.34 is next divided through by the coefficient of the partial derivative term on the right-hand side of the equation:

$$\frac{\partial T_p}{\partial t} = - V_s \frac{\partial T_p}{\partial z} + \frac{F_p (T_a - T_p)}{L_e \cdot A_s (1-\epsilon_s)\rho_p} + \frac{Q}{A_s(1-\epsilon_s)\rho_p \cdot c_{p_p} \cdot \Delta z}$$

$$(A.35)$$

The only term remaining to be defined in Equation A.35 is the heat loss/gain term. In deriving this term, the most important sources or sinks of energy are the heat lost by convection to the spout gases, and the heat gained by the particles by radiation from the draft tube wall.

Therefore, the following expression for the heat transfer is obtained:

$$Q = \frac{6 \cdot h_p \cdot A_s \cdot \Delta z}{d_p} (1-\epsilon_s)(T_g - T_p) + \pi \cdot D_s \cdot \Delta z \cdot \sigma \cdot F_{ap}(T_a^4 - T_p^4)$$

(A.36)

Consequently, the expression which is substituted into Equation A.35 is the following:

$$\frac{Q}{A_s(1-\epsilon_s)\rho_p \cdot c_{p_p} \cdot \Delta z} = \frac{6 \cdot h_p (T_g - T_p)}{d_p \cdot \rho_p \cdot c_{p_p}} + \frac{4 \cdot \sigma \cdot F_{ap}(T_a^4 - T_p^4)}{D_s(1-\epsilon_s)\rho_p \cdot c_{p_p}}$$

(A.37)

A.3.3 ANNULAR ENERGY BALANCE

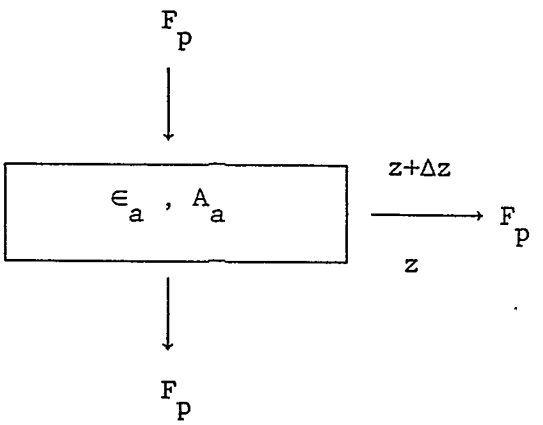

Inclusion of the energy balance for the annular region is extremely important in view of its effect on the overall heat transfer characteristics of the bed. Accordingly, it is modelled by taking into consideration all forms of energy flux, including that associated with the downward flow of particles in the annulus. First of all, however, the assumption of lumped parameters (i.e. - radial temperature gradients are ignored) is made as discussed in Chapter 3. In addition, the energy associated with the flow of gases in the annulus is assumed to be negligible with respect to the energy of the flowing particles. Moreover, axial conduction is found to be negligible with respect to this energy of flowing particles. With these assumptions, the expression describing energy flux due to particle motion is given by

$$F_p \cdot H_p \Big|_{z+\Delta z} - F_p \cdot H_p \Big|_z \qquad (A.38)$$

Accordingly, the energy balance for the elemental annular volume is

$$F_p \cdot H_p \Big|_{z+\Delta z} - F_p \cdot H_p \Big|_z + Q = A_a(1-\epsilon_a)\rho_p \cdot c_{p_p} \cdot \Delta z \frac{\partial T_a}{\partial t} \qquad (A.39)$$

The annular cross-sectional area referred to in Equation A.39 is given by the following equation:

$$A_a = \frac{\pi}{4}\left(D_b^2 - D_s^2 \right) \qquad (A.40)$$

The bed diameter, while constant for the cylindrical bed, varies in the conic section of conic-based beds. This diameter is then simply calculated by consideration of the geometry of the cone:

$$D_c = D_{in} + 2 \cdot z \cdot \tan\left(\frac{\theta}{2} \right) \qquad (A.41)$$

Dividing Equation A.39 by Δz now results in the partial differential equation of A.42:

$$\frac{\partial T_a}{\partial t} = \frac{1}{A_a(1-\epsilon_a)\rho_p \cdot c_{p_p}} \left[\frac{Q}{\Delta z} + \frac{z}{L_e} F_p \cdot c_{p_p} \frac{\partial T_a}{\partial z} \right] \qquad (A.42)$$

The additional ratio of axial distance to entrainment length in Equation A.42 is included to approximate the decrease in energy flow resulting from the reduction of particle flow in the entrainment region of the annulus as particles are swept into the spout. In the draft tube region, this term becomes unity as all particles in the annulus

are assumed to be in plug flow and therefore, the same particle mass flow is encountered throughout this region.

The heat transfer term in Equation A.42 is developed to include heat transfer to the annulus by both radiation and convection from the external heat source. In addition, heat is lost to both the spout gases and the spout particles. The heat term, Q, is then

$$Q = \pi \cdot D_b \cdot \Delta z \cdot \sigma \cdot F_{wa}(T_w^4 - T_a^4) + \pi \cdot D_b \cdot \Delta z \cdot h_a(T_w - T_a)$$

$$- \pi \cdot D_s \cdot \Delta z \cdot U_w(T_a - T_g) - \pi \cdot D_s \cdot \sigma \cdot F_{ap}(T_a^4 - T_p^4) \quad (A.43)$$

Substitution of Equation A.43 into Equation A.42 is a simple matter once definition of the heat transfer coefficients is established. While discussion of the heat transfer correlations employed in the model is left to the explanation in Chapter 3, the view factors referred to in Equation A.43 require additional explanation.

Assuming that all surfaces in which radiative heat transfer is involved, are gray, the overall interchange factor or view factor is then a function of both the surface areas and the emissivities of the bodies concerned. For the case of one body of surface area A_1 surrounding a second body of surface area A_2, the

overall interchange factor is given by Equation A.44:

$$F_{12} = \left[\left(\frac{1}{\epsilon_1} \right) + \frac{A_1}{A_2} \left(\frac{1}{\epsilon_2} - 1 \right) \right]^{-1} \qquad (A.44)$$

In the case where 1 represents the outer bed wall and 2, the annulus, the ratio of surface areas reduces to unity. In the case of radiative heat transfer from the annulus to the particles, the ratio of surface areas reduces to that shown in Equation A.45:

$$\frac{A_1}{A_2} = \frac{2 \cdot d_p}{3 \cdot D_s (1-\epsilon_s)} \qquad (A.45)$$

APPENDIX B

DYNAMIC MODEL PROGRAM LISTING

```
c Dynamic model of draft tube spouted bed reactor
c  written by : John H. Eng

      open (1,form="formatted",mode="in",file="twb.in")
c Main body of program for dynamic simulation
      parameter (nc=1,nrd=1)
      parameter (nv=6+nc)
      parameter (n1=9,n2=9)
      parameter (nvd=3)
      parameter (nt=n1+n2-1)
      parameter (nvd1=nvd*nt)
      integer meth,miter,index,ier,k
      integer iwk(nv), iwk1(nvd1)
      dimension wk(17*nv+1), wk1(nvd1*(nvd1+11))
      real le, ka, km, kp, mw(nc), mwave
      dimension y(nv)
      dimension stc(nc,nrd)
      dimension pc(nc), tc(nc), cp(nc,4), aen(nrd), ff(nrd)
      dimension dhr0(nrd), dhr(nrd,4), c(nc), rk(nrd)
      dimension rke(nrd), rkr(nrd)
      dimension r(nrd), dt(4), f0(nc)
      dimension z1i(2,n1), almat(2,n1,n1), b1mat(2,n1,n1)
      dimension y0(3), yd(nvd1)
      dimension fdt(nc)
      dimension vs(nt), es(nt), f(nc,nt), tgax(nt), taax(nt)
      external steady, fcnj, dynamic
      common /phycon/ p, pi, rid, g
      common /initial/ f0, tg0, vs0, es0
      common /spout/  le, hdt, din, ddt, db, cang
      common /param/  cpp, rhop, dp
      common /annul/  ea, kp, tw, fp, gloss
      common /critcal/ mw, tc, pc, cp
      common /react/  nr, aen, ff, rkr, stc, tref, trefe
      common /heats/ dhr0, dhr
      common /collode/ z1i, almat, b1mat
      common /trans/ t0ref, fref, deld, delt, zt, tbw
      common /hydro/ vs, es, f, y0
      common /tgas/ tgax
      common /propg/ cpmix, vmix, kmix
      common /proh/ hwss, hpss, kass, hass

c Set constants for transformed variables
      t0ref = tg0
      fref  = f0(1)
      deld  = db - ddt
      delt  = tw - tg0

c Calculate collocation points in entrainment and draft tube regions
      a1 = 1.5
      b1 = 1.5
      a2 = 1.5
      b2 = 1.5
c Note - n1 and n2 must be defined in subroutine ortho1
      call ortho1(a1,b1,a2,b2,z1i,almat,b1mat)
```

```
c Set coefficients for variation in heats of reactions
      if (nr.gt.0) then
       call heatcof(nr,dhr,cp,stc)
      end if

c Read in the initial steady-state values
c  or set all temperatures to zero (ie-room temp) for ss calculation
      do 10 i = 1, nt
       read (1,*) zzz, tg, tp, ta
       nz       = 3*(i-1)
       yd(nz+1) = (tg-t0ref)/delt
c       yd(nz+1) = 0.0
       tgax(i)  = yd(nz+1)
       yd(nz+2) = (tp-t0ref)/delt
c       yd(nz+2) = 0.0
       yd(nz+3) = (ta-t0ref)/delt
c       yd(nz+3) = 0.0
       taax(i)  = yd(nz+3)
       if (i.eq.n1) then
        tale = yd(nz+3)*delt + t0ref
       end if
   10 continue

c Set the time to zero for integration
      t     = 0.0
      call printt(t,yd,z1i)

c Calculate the fractional loss of gas into the annulus
      call gasbp(tale)

c Calculate the spout hydrodynamic profiles
      vs(1) = vs0
      es(1) = es0
      do 17 i = 1, nc
       f(i,1) = f0(i)
   17 continue
c Set the initial entrainment rate
      fp = 0.06
      call quasiss(es,vs,f)

c Calculate the heat transfer characteristics
      call conprop(tgax,taax,vs,es,f)
      print *,"vs = ",vs
      print *,"es = ",es
      print *,"f  = ",f

c Begin integration for the dynamic case
      tol   = 1.e-3
      meth  = 2
      miter = 2
      do 80 i = 1, 130
       h     = 1.0e-6
       index = 1
```

```
c Start with small time intervals and increase later on
      if (t.lt.960) then
       tend  = 15. + t
      else
       tend  = 60. + t
      end if
      call dgear (nvdl,dynamic,fcnj,t,h,yd,tend,tol,meth,miter,
     &  index,iwkl,wkl,ier)
c Update hydrodynamic properties assuming quasi-steady state
      do 90 j = 1, nt
       nz      = nvd*(j-1)
       tgax(j) = yd(nz+1)
       taax(j) = yd(nz+3)
   90 continue
      tale  = yd(nl*3)*delt + t0ref
      call gasbp(tale)
      do 100 j = 1, nc
       fdt(j) = f(j,nl)
  100 continue
      tdt   = yd(nl*3-2)*delt + t0ref
      adt   = pi*ddt**2/4.
      call gasprop(fdt,tdt,adt,es(nl),rhog,us,mwave)
c Calculate the entrainment rate for the new hydrodynamics
      fp    = 0.06 + 0.01*(us-19.8529)
c Output the entrainment rate and gas velocity as a check
      print *,"fp, usdt = ",fp, us
      call quasiss(es,vs,f)
      call conprop(tgax,taax,vs,es,f)
c Output temperature profiles every 4 minutes
      pri = tend/240.
      ipr = int(pri)
      dip = pri - ipr
      if (dip.eq.0) then
c Write desired values to an output data file
       call printt(t,yd,z1i)
       print *,"vs = ",vs
       print *,"es = ",es
       print *,"f  = ",f
      end if
      if (t.ge.5400) go to 110
   80 continue

  110 continue
      stop
      end


c Subroutine to calculate the drag coefficient
      subroutine cdrag(cd,rep)

c Use correlations given in Clift, Grace, & Weber (1982)
      wre  = log10(rep)
      wre2 = wre**2
      wre3 = wre**3
```

```
      if (rep.le.260) then
       cd = 24.*(1.+0.1935*(rep**(0.6305)))/rep
      else if (rep.gt.260.and.rep.lt.1500) then
       cd = 10.**(1.6435-1.1242*wre+0.1558*wre2)
      else if (rep.gt.1500.and.rep.lt.1.2e4) then
       cd = 10.**(-2.4571+2.5558*wre-0.9295*wre2+0.1049*wre3)
      else if (rep.gt.1.2e4.and.rep.le.4.4e4) then
       cd = 10.**(-1.9181+0.6370*wre-0.0636*wre2)
      else if (rep.gt.4.4e4.and.rep.le.3.38e5) then
       cd = 10.**(-4.3390+1.5809*wre-0.1546*wre2)
      else if (rep.gt.3.38e5.and.rep.le.4.e5) then
       cd = 29.78-5.3*wre
      else
       cd = 0.1*wre-0.49
      end if

      return
      end


c Subroutine for calculation of heat transfer properties
      subroutine conprop(tg,ta,vs,es,fg)
      parameter (nc=1)
      parameter (n1=9,n2=9)
      parameter (nt=n1+n2-1)
      dimension tg(nt), ta(nt), vs(nt), es(nt), fg(nc,nt), f(nc)
      dimension zli(2,n1), almat(2,n1,n1), blmat(2,n1,n1)
      dimension cpmix(nt), vmix(nt), hwss(nt), hpss(nt), hass(nt)
      real le, kp, kmix(nt), kass(nt), mwave
      common /spout/  le, hdt, din, ddt, db, cang
      common /param/  cpp, rhop, dp
      common /annul/  ea, kp, tw, fp, gloss
      common /collode/ zli, almat, blmat
      common /trans/ t0ref, fref, deld, delt, zt, tbw
      common /propg/ cpmix, vmix, kmix
      common /proph/ hwss, hpss, kass, hass

      ied = 1
      irc = 0
      zt  = le
      do 10 i = 1, nt
      if (i.gt.n1) then
       ied = 2
       irc = 1-n1
       zt  = hdt
      end if
      do 20 j = 1, nc
       f(j) = fg(j,i)
   20 continue
c Calculate the gas and annular temperatures
      tgas  = tg(i)*delt + t0ref
      tann  = ta(i)*delt + t0ref
      call proprty(f,tgas,cpmix(i),vmix(i),kmix(i))
      z = zli(ied,i+irc)
```

```
      call cxarea(z,as,dia,dasdz)
      call gasprop(f,tgas,as,es(i),rhog,us,mwave)

c Calculate the convective heat transfer coefficients in the spout
      duv  = us - vs(i)
      esv  = 1. - es(i)
      rep  = rhog*duv*dp/vmix(i)
      pr   = cpmix(i)*vmix(i)/(kmix(i)*mwave)
      re   = rhog*us*dia/vmix(i)
      call convhtc(pr,re,rep,kmix(i),esv,dia,hwss(i),hpss(i))
c Calculate the effective thermal conductivity of annulus
      call kann(kass(i),kp,dp,ea,tann,f)
c Calculate the effective heat transfer coefficient in the annulus
      if (zt.eq.le) then
       zh = hdt + le*(1.-z)
      else
       zh = hdt
      end if
      call hann(kass(i),zh,hass(i))

   10 continue
      return
      end


c Subroutine for calculating spout heat transfer coefficients
      subroutine convhtc(pr,re,rep,km,esv,dia,hw,hp)
      real km
      common /phycon/ p, pi, rid, g
      common /param/  cpp, rhop, dp

c Calculate the voidage
      es = 1.-esv
c Calculate the convective heat transfer coefficients in the spout
c Use Seider-Tate correlation (McCabe and Smith (1976)
      hw0 = 0.023*re**(0.8)*pr**(1./3.)*km/dia
c Use Sadek (1972) correlation for enhancement
      hinc = 0.2*(6.*esv*dia/(pi*es*dp))**(1.19)
      hw  = (1.+hinc)*hw0
c Use correlation of Rowe and Claxton (1965) for particle effect
      hpa = 2./(1.-esv**(1./3.))
      hpb = 2./(3.*es)
      hp  = (hpa + hpb*pr**(1./3.)*rep**(0.55))*km/dp

      return
      end


c Subroutine to calculate the cross-sectional area in
c  the spout assuming a linear increase in diameter
      subroutine cxarea(z,as,dia,dasdz)
      common /phycon/ p, pi, rid, g
      common /spout/  le, hdt, din, ddt, db, cang
      common /trans/ t0ref, fref, deld, delt, zt, tbw
```

```
      real le

      if (zt.eq.hdt) then
       dia = ddt
       dasdz = 0.0
      else
       dia = (ddt-din)*z + din
       dasdz = pi*(ddt-din)*dia/2.
      end if
      as  = pi*dia**2/4.

      return
      end


c Calculate Gaussian quadrature weights for Jacobi polynomials
c Taken from Villadsen and Michelsen (1978)
      subroutine dfopr(nd,n,n0,nl,i,id,difl,dif2,dif3,root,vect)
      implicit double precision (a-h,o-z)
      dimension difl(nd),dif2(nd),dif3(nd),root(nd),vect(nd)

c     subroutine evaluates discretization matrices and Gaussian
c     quadrature weights, normalized to sum 1
c     id = 1 :  discretization matrix for y(1) (x)
c     id = 2 :  discretization matrix for y(2) (x)
c     id = 3 :  gaussian quadrature weights

      nt=n+n0+nl
      if(id.eq.3) goto 10
      do 20 j=1,nt
      if (j.ne.i) goto 21
      if (id.ne.1) goto 5
      vect(i)=dif2(i)/difl(i)/2.
      goto 20
 5    vect(i)=dif3(i)/difl(i)/3.
      goto 20
 21   y=root(i)-root(j)
      vect(j)=difl(i)/difl(j)/y
      if (id.eq.2) vect(j)=vect(j)*(dif2(i)/difl(i)-2/y)
 20   continue
      goto 50
 10   y=0.
      do 25 j=1,nt
      x=root(j)
      ax=x*(1-x)
      if (n0.eq.0) ax=ax/x/x
      if (nl.eq.0) ax=ax/(1-x)/(1-x)
      vect(j)=ax/difl(j)**2.
 25   y=y+vect(j)
      do 60 j=1,nt
 60   vect(j)=vect(j)/y
 50   return
      end
```

```
c Subroutine containing dynamic equations
      subroutine dynamic(n,t,y,dy)
      parameter (nc=1,nrd=1)
      parameter (n1=9,n2=9)
      parameter (nt=n1+n2-1)
      real le, mw(nc), km, ka, kp, mwave
      dimension y(n), dy(n), f0(nc)
      dimension pc(nc), tc(nc), cp(nc,4)
      dimension dhr0(nrd), dhr(nrd,4), aen(nrd), ff(nrd)
      dimension stc(nc,nrd), c(nc), r(nrd)
      dimension dt(4), rkr(nrd)
      dimension z1i(2,n1), almat(2,n1,n1), blmat(2,n1,n1)
      dimension y0(3), fz(nc)
c The hydrodynamic properties (Vs, es, F) are assumed to
c  reach steady-state immediately (ie-their dynamic time
c  constants are very short relative to those of the
c  temperature profiles)
      dimension vs(nt), es(nt), f(nc,nt)
      dimension cpmix(nt), vmix(nt), hwss(nt), hpss(nt), hass(nt)
      real kmix(nt), kass(nt)
      common /phycon/ p, pi, rid, g
      common /initial/ f0, tg0, vs0, es0
      common /spout/  le, hdt, din, ddt, db, cang
      common /param/  cpp, rhop, dp
      common /annul/  ea, kp, tw, fp, gloss
      common /critcal/ mw, tc, pc, cp
      common /react/  nr, aen, ff, rkr, stc, tref, trefe
      common /heats/ dhr0, dhr
      common /collode/ z1i, almat, blmat
      common /trans/ t0ref, fref, deld, delt, zt, tbw
      common /hydro/ vs, es, f, y0
      common /radiate/ sigma, emw, emp
      common /propg/ cpmix, vmix, kmix
      common /proph/ hwss, hpss, kass, hass

c The variables referred to are as follows:
c       y(1)  = gas temperature in the spout
c       y(2)  = particle temperature in the spout
c       y(3)  = annular temperatures at grid

c Set function for change in wall temperature wrt time
c       tbw   = (1326.-(60.*exp(-t/360.))-t0ref)/delt
      tbw   = (1266.-(51.*exp(-t/528.))-t0ref)/delt

c Set parameters to indicate integration in the entrainment region
      ied = 1
      irc = 0
      nax = n1
      ned = 0
      nz0 = 0
      zt  = le
      zt0 = 0.0
      nv  = 3
```

```
    4 continue

c Derivatives for each variable are calculated at various heights
c Increments in the axial direction are denoted by "i"
      do 5 i = 1, nax
      nz = nv*(i-1) + nz0

c Calculate axial gradients in temperature profiles
      dtgdz = 0.0
      dtpdz = 0.0
      dtadz = 0.0
c      dt2dz = 0.0
      if (i.eq.1.and.ied.eq.1) then
       do 6 j = 1, nl
        nzi   = nv*(j-1)
        dtpdz = dtpdz + almat(ied,1,j)*y(nzi+2)
        dtadz = dtadz + almat(ied,1,j)*y(nzi+3)
c         dt2dz = dt2dz + blmat(ied,1,j)*y(nzi+3)
   6   continue
       go to 20
      end if
      do 10 j = 1, nax
c Use the initial condition in calculating the gradients
       if (j.eq.1.and.ied.eq.2) then
        nzi = nv*(nl-1)
        dtgdz = dtgdz + almat(ied,i+1,j)*y(nzi+1)
        dtpdz = dtpdz + almat(ied,i+1,j)*y(nzi+2)
        dtadz = dtadz + almat(ied,i+1,j)*y(nzi+3)
c         dt2dz = dt2dz + blmat(ied,i+1,j)*y(nzi+3)
       end if
       nzi   = nv*(j-1) + nz0
       dtgdz = dtgdz + almat(ied,i+irc,j+irc)*y(nzi+1)
       dtpdz = dtpdz + almat(ied,i+irc,j+irc)*y(nzi+2)
       dtadz = dtadz + almat(ied,i+irc,j+irc)*y(nzi+3)
c        dt2dz = dt2dz + blmat(ied,i+irc,j+irc)*y(nzi+3)
   10 continue
   20 continue

c Use collocation in the draft tube region for the annulus
      if (ied.eq.1.and.i.eq.nl) then
      dtadz = 0.0
c      dt2dz = 0.0
      do 21 j = 1, n2
       nzi   = nv*(j-2) + nl*nv
       dtadz = dtadz + almat(2,1,j)*y(nzi+3)
c        dt2dz = dt2dz + blmat(2,1,j)*y(nzi+3)
   21 continue
      end if

c Calculate the cross-sectional area in the spout
      z = zli(ied,i+irc)
      call cxarea(z,as,dia,dasdz)

c Calculate the gas properties at the height z
```

```
      ftot = 0.0
      do 25 j = 1, nc
       fz(j) = f(j,i+ned)
       ftot = ftot + fz(j)
   25 continue

c Calculate the gas temperature from the transformed variable
      tg   = y(nz+1)*delt + t0ref
      cpm  = cpmix(i+ned)
      vm   = vmix(i+ned)
      km   = kmix(i+ned)

c Calculate gas velocity, density, and molecular weight
      call gasprop(fz,tg,as,es(i+ned),rhog,us,mwave)

c Calculate the component concentrations
      conc  = p/(rid*tg*ftot)
      cptot = 0.0
      do 30 j = 1, nc
       c(j) = fz(j)*conc
       cpi = 0.0
       do 35 ij = 1, 4
        cpi = cpi + cp(j,ij)*tg**(ij-1)
   35  continue
       cptot = cptot + c(j)*cpi*4.184
   30 continue

c Calculate the particle Reynolds number
      rep = rhog*duv*dp/vm
      duv = us - vs(i+ned)
      esv = 1.- es(i+ned)

c Calculate the rates of reactions
      if (nr.gt.0) then
       call rrate(tg,c,r)
      end if

c Set the convective heat transfer coefficients in the spout
      hw  = hwss(i+ned)
      hp  = hpss(i+ned)
c Set the effective thermal conductivity of annulus
      tann = y(nz+3)*delt + t0ref
      ka  = kass(i+ned)
      ha  = hass(i+ned)

c Calculate the heat transferred to the gas from the wall
      if (ied.eq.1) then
       uw = hw
      else
       uw = hw*ha/(hw+ha)
      end if
      qwg = 4.*uw*(y(nz+3)-y(nz+1))/dia

c Calculate the heat transferred to the gas from the particles
```

```
      qpg = 6.*esv*hp*(y(nz+2)-y(nz+1))/dp
      qg  = qwg + qpg

c Calculate the total heat of reaction
      hr  = 0.0
      if (nr.gt.0) then
      dt(1) = tg - tref
      dt(2) = tg**2 - tref**2
      dt(3) = tg**3 - tref**3
      dt(4) = tg**4 - tref**4
      do 50 j = 1, nr
       dhrt = dhr0(j)
       do 60 ij = 1, 4
        dhrt = dhrt + dhr(j,ij)*dt(ij)
   60  continue
       hr = hr + r(j)*dhrt
   50 continue
      hr = hr*es(i+ned)/delt
      end if
      dtgdz    = cpm*ftot*dtgdz/(as*zt)
      if (i.eq.1.and.ied.eq.1) then
       dy(1)    = 0.0
      else
       dy(nz+1) = (qg - dtgdz - hr)/(es(i+ned)*cptot)
      end if

c Calculate the temperature in the particles
c Calculate the heat transferred by convection
      qpg = 6.*hp*(y(nz+2)-y(nz+1))/(dp*rhop*cpp)
      if (zt.eq.hdt) then
       qfp = 0.0
      else
       qfp = fp*(y(nz+3)-y(nz+2))/(rhop*le*as*esv)
      end if
      dtpdz    = vs(i+ned)*dtpdz/zt
c Calculate the heat transferred to the particles by radiation
c Calculate the relative surface areas of the particles and wall
      ar    = 2.*dp/(3.*esv*dia)
      fap   = 1./((1./emw) + ar*((1./emp)-1.))
      dtap  = ((tann**4)-((y(nz+2)*delt+t0ref)**4))/delt
      qap   = 4.*sigma*fap*dtap/(dia*esv*cpp*rhop)
      dy(nz+2) = -dtpdz + qfp - qpg + qap

c Calculate the annular temperatures
      zact  = z*zt + zt0
      dc    = din + 2.*zact*tan(pi*cang/360.)
      if (dc.gt.db) then
       dc    = db
      end if
      if (ied.eq.1) then
       zsing = z
       qwa   = 0.0
      else
       zsing = 1.0
```

```
        qwa   = dc*ha*(tbw-y(nz+3))
       end if
       qag   = dia*uw*(y(nz+3)-y(nz+1))
c Calculate the radiative effects
       qap   = sigma*dia*fap*dtap
       if (ied.eq.1) then
        qwar = 0.0
       else
        fwa   = 1./((1./emp) + (1./emw) - 1.)
        dtwa  = (((tbw*delt+t0ref)**4)-(tann**4))/delt
        qwar  = sigma*dc*fwa*dtwa
       end if
c Use forward differencing in the entrainment region of annulus
       if (ied.eq.1.and.i.ne.nax) then
        dtadz   = (y(nz+nv+3)-y(nz+3))/(zli(ied,i+irc+1)-z)
       end if
       dtadz    = dtadz*zsing*fp*cpp/(zt*pi)
c       dt2dz    = dt2dz*ka*((dc**2)-(dia**2))/(4.*zt)
       denom    = (1.-ea)*rhop*cpp*((dc**2)-(dia**2))/4.
       if (denom.lt.1.e-3) denom = 1.e-3
       if (i.eq.nax.and.ied.eq.2) then
        dy(nz+3) = dy(nz+2)
       else
c         dy(nz+3) = (qwa + qwar - qag - qap + dtadz + dt2dz)/denom
        dy(nz+3) = (qwa + qwar - qag - qap + dtadz)/denom
       end if
       if (i.eq.1.and.ied.eq.1) then
        dy(nz+2) = dy(nz+3)
       end if

   5  continue

c Perform calculations for the draft tube section
       if (ied.eq.1) then
        ied = 2
        irc = 1
        nax = n2-1
        ned = n1
        zt  = hdt
        zt0 = le
        nz0 = nv*n1
        go to 4
       end if
       i = i+1

       return
       end


c Dummy subroutine for partial derivative calculations
c This subroutine is used for steady state calculations
       subroutine fcn(n,x,y,pd)
       integer n
       real y(n), pd(n,n), x
```

```
      return
      end


c Dummy subroutine for partial derivative calculations
c This subroutine is used for dynamic calculations
      subroutine fcnj(n,x,y,pd)
      integer n
      real y(n), pd(n,n), x
      return
      end


c Subroutine to calculate fractional flow of gas into annulus
      subroutine gasbp(t)
c where  t = temperature in annulus at z = le
      parameter (nc=1)
      common /phycon/ p, pi, rid, g
      common /initial/ f0, tg0, vs0, es0
      common /spout/  le, hdt, din, ddt, db, cang
      common /param/  cpp, rhop, dp
      common /annul/  ea, kp, tw, fp, gloss
      dimension f0(nc)
      real k, kp, le, mwave

c Calculate annular gas properties
      ann = pi/4.*(db**2 - ddt**2)
      call proprty(f0,t,cp,v,k)
      call gasprop(f0,t,ann,ea,rhog,us,mwave)

c Calculate maximum spoutable bed height
c Use correlation of Lefroy and Davidson
      hm  = 0.72*(db**2)/ddt
c Use correlation of Malek and Lu
c      hm  = 0.105e3*db*((db/dp)**(0.75))*((db/din)**(0.4))/rhop
c Calculate the maximum spoutable bed height (McNab and Bridgwater)
c      ar  = g*(dp**3)*rhog*(rhop-rhog)/(v**2)
c      ar1 = (sqrt(1.+35.9e-6*ar) - 1.)**2
c      hm  = (db**2/dp)*((db/din)**(2./3.))*(700./ar)*ar1

c Calculate the minimum fluidization velocity
      u1  = 3.111e-4*((ea*dp)**3)*g*rhog*(rhop-rhog)/(((1.-ea)*v)**2)
      u2  = sqrt(1. + u1) - 1.
      umf = 42.9*(1.-ea)*v/(rhog*dp)*u2

c Calculate Ua and fractional gas loss (modified Mamuro-Hattori eqn)
      ua  = 0.88*umf*(1.-((1.-le/hm)**3))
      fta = ua*ann*rhog/mwave
      ft0 = 0.0
      do 10 i = 1, nc
       ft0 = ft0 + f0(i)
   10 continue
      gloss = fta/ft0
      print *,"gloss = ",gloss
```

```
      return
      end


c Subroutine to calculate the gas density and velocity
      subroutine gasprop(f,tg,as,es,rhog,us,mwave)
      parameter (nc=1)
      dimension f(nc)
      dimension pc(nc), tc(nc), cp(nc,4)
      real mw(nc), mwave
      common /phycon/ p, pi, rid, g
      common /critcal/ mw, tc, pc, cp

c Calculate the gas mixture properties
      ftot = 0.0
      fwtot = 0.0
      do 10 i = 1, nc
       ftot = ftot + f(i)
       fwtot = fwtot + f(i)*mw(i)
   10 continue
      mwave = fwtot/ftot

c Calculate the gas density
      rhog = fwtot*p/(ftot*rid*tg)

c Calculate the gas velocity in the spout
      us = ftot*rid*tg/(p*as*es)

      return
      end


c This subroutine calculates the effective heat transfer
c  coefficient in the annulus
      subroutine hann(ka,z,ha)
      real ka, kp, nun, nud
      common /phycon/ p, pi, rid, g
      common /spout/  le, hdt, din, ddt, db, cang
      common /param/  cpp, rhop, dp
      common /annul/  ea, kp, tw, fp, gloss

c Use correlation for wall-to-bed heat transfer coefficient
      vz  = 4.*fp/((1-ea)*rhop*pi*(db**2-ddt**2))
      rho = (1.-ea)*rhop
      ha  = 1.129*sqrt(vz*rho*cpp*ka/z)

      return
      end


c Subroutine to calculate coefficients for variation
c  in heats of reaction
      subroutine heatcof(nr,dhr,cp,stc)
```

```
      parameter (nc=1)
      parameter (nrd=1)
      dimension dhr(nrd,4), cp(nc,4), stc(nc,nrd)

c Set coefficients for variation in heats of reactions
      do 10 i = 1, nr
       do 20 j = 1, 4
        sum = 0.0
        do 30 k = 1, nc
         sum = sum + stc(k,i)*cp(k,j)/real(j)
   30   continue
        dhr(i,j) = sum
   20  continue
   10 continue

      return
      end


c Calculate zeroes of Jacobi polynomials
c Taken from Villadsen and Michelsen (1978)
      subroutine jcobi(nd,n,n0,nl,al,be,difl,dif2,dif3,root)
      implicit double precision (a-h,o-z)
      dimension difl(nd),dif2(nd),dif3(nd),root(nd)

c     evaluation of roots and derivatives of jacobi polynomials
c     p(n) (al,be): machine accuracy 16 d;

c     first evaluation of coefficients in recursion formulas
c     recursion coefficients are stored in difl and dif2

      ab=al+be
      ad=be-al
      ap=be*al
      difl(1)=(ad/(ab+2)+1.)/2.
      dif2(1)=0.
      if (n.lt.2) goto 15
      do 10 i=2,n
      zl=i-1
      z=ab+2*zl
      difl(i)=(ab*ad/z/(z+2.)+1.)/2.
      if (i.ne.2) goto 11
      dif2(i)=(ab+ap+zl)/z/z/(z+1)
      goto 10
 11   z=z*z
      y=zl*(ab+zl)
      y=y*(ap+y)
      dif2(i)=y/z/(z-1.)
 10   continue

c     root determination by newton"s method with suppression
c     of previously determined roots

 15   x=0.
```

```
      do 20 i=1,n
 25   xd=0.
      xn=1.
      xd1=0.
      xn1=0.
      do 30 j=1,n
      xp=(dif1(j)-x)*xn-dif2(j)*xd
      xp1=(dif1(j)-x)*xn1-dif2(j)*xd1-xn
      xd=xn
      xd1=xn1
      xn=xp
 30   xn1=xp1
      zc=1.
      z=xn/xn1
      if (i.eq.1) goto 21
      do 22 j=2,i
 22   zc=zc-z/(x-root(j-1))
 21   z=z/zc
      x=x-z
      if (dabs(z).gt.1.d-09) goto 25
      root(i)=x
      x=x+0.0001
 20   continue

c     add eventual interpolation points at x=0 or x=1

      nt=n+n0+n1
      if(n0.eq.0) goto 35
      do 31 i=1,n
      j=n+1-i
 31   root(j+1)=root(j)
      root(1)=0
 35   if (n1.eq.1) root(nt)=1.

c     now evaluate derivatives of polynomial

      do 40 i=1,nt
      x=root(i)
      dif1(i)=1.
      dif2(i)=0.
      dif3(i)=0.
      do 40 j=1,nt
      if (j.eq.i) goto 40
      y=x-root(j)
      dif3(i)=y*dif3(i) + 3*dif2(i)
      dif2(i)=y*dif2(i) + 2*dif1(i)
      dif1(i)=y*dif1(i)
 40   continue
      return
      end


c Subfunction to calculate the effective annular
c  thermal conductivity (Kunii & Smith 1960)
```

```
      subroutine kann(ka,kp,dp,ea,tw,f0)
      parameter (nc=1)
      real ka, km, kp
      dimension f0(nc)
      common /radiate/ sigma, emw, emp

c Calculate the gas thermal conductivity in the annulus assuming
c  the gas has the same composition as the feed
      call proprty(f0,tw,cpm,vm,km)
      aa   = kp/km
      den1 = log(aa-(aa-1.)*sqrt(1./3.))
      den2 = (aa-1.)*(1.-sqrt(1./3.))/aa
      phi  = ((aa-1.)/aa)**2/(3.*(den1-den2)) - 2./(3.*aa)

c Calculate the radiative heat transfer coefficients (kW/m**2*K)
c Use Yagi and Kunii (1957) correlations
      conv = 1./860.4208
      hvd  = 1. + ea*(1.-emp)/(2.*(1.-ea)*emp)
      hrv  = conv*0.1952*(tw/100.)**3/hvd
      hrs  = conv*0.1952*emp*(tw/100.)**3/(2.-emp)

c Calculate the effective annular thermal conductivity
      tc1 = ea*(1.+0.895*hrv*dp/km)
      tc2 = 1./(1./phi+dp*hrs/km) + 2./(3.*aa)
      tc3 = 0.895*(1.-ea)/tc2
      ka = km*(tc1 + tc3)

      return
      end


c This subroutine combines matrices A and B for both
c   entrainment and draft tube regions
      subroutine ortho1(a1,b1,a2,b2,z1i,almat,b1mat)
      parameter (n1=9,n2=9)
      dimension z1i(2,n1), almat(2,n1,n1), b1mat(2,n1,n1)
      dimension x1(n1), am1(n1,n1), bm1(n1,n1), difla(n1)
      dimension x2(n2), am2(n2,n2), bm2(n2,n2), diflb(n2)
      common /interp/ difla, diflb

      call ortho(n1,a1,b1,x1,am1,bm1,difla)
      call ortho(n2,a2,b2,x2,am2,bm2,diflb)
      do 10 i = 1, n1
       z1i(1,i) = x1(i)
       do 20 j = 1, n1
        almat(1,i,j) = am1(i,j)
        b1mat(1,i,j) = bm1(i,j)
   20  continue
   10 continue

      do 30 i = 1, n2
       z1i(2,i) = x2(i)
       do 40 j = 1, n2
        almat(2,i,j) = am2(i,j)
```

```
          blmat(2,i,j) = bm2(i,j)
   40   continue
   30 continue

      return
      end


c This subroutine calculates matrices A and B for each region
      subroutine ortho(nt,alpha,beta,xi,amat,bmat,dif)
      double precision difl, dif2, dif3, root, a, b, vl, v2
      parameter (nd=30)
      dimension difl(nd), dif2(nd), dif3(nd), root(nd), vl(nd), v2(nd)
      dimension xi(nt), amat(nt,nt), bmat(nt,nt), dif(nt)

c Calculate collocation points for particular choice of weight function
      a = alpha
      b = beta
c This subroutine uses Lobatto quadrature (see Villadsen et al (1978))
      n = nt - 2
      call jcobi(nd,n,1,1,a,b,difl,dif2,dif3,root)
c Calculate the matrices A and B
      do 10 i = 1, nt
       xi(i)  = root(i)
       dif(i) = difl(i)
       call dfopr(nd,n,1,1,i,1,difl,dif2,dif3,root,vl)
       call dfopr(nd,n,1,1,i,2,difl,dif2,dif3,root,v2)
       do 11 j = 1, nt
        amat(i,j) = vl(j)
        bmat(i,j) = v2(j)
   11  continue
   10 continue

      return
      end


c Subroutine for output of temperature profiles at time t
      subroutine printt(t,y,zi)
      parameter (nl=9,n2=9)
      parameter (nvd=3)
      parameter (nvdl=nvd*(nl+n2-1))
      dimension y(nvdl), zi(2,nl), x(3)
      common /spout/  le, hdt, din, ddt, db, cang
      common /trans/ t0ref, fref, deld, delt, zt, tbw
      real le
c      open (1,form="formatted",mode="out",file="t2.out")
c Write the steady-state temperature profiles to file temp.out
      write (6,60)
      time = t/60.
      write (6,30) time
      write (6,60)
      write (6,40)
      write (6,60)
```

```
      ied = 1
      nax = n1
      nz0 = 0
      zt  = le
      zt0 = 0.0

    5 continue
      do 10 i = ied, nax
       nz   = nvd*(i-ied) + nz0
       do 20 j = 1, 3
        x(j) = y(j+nz)*delt + t0ref
   20 continue
       z = zt*zi(ied,i) + zt0
       write (6,50) z,x
   10 continue

      if (ied.eq.1) then
       ied = 2
       nax = n2
       nz0 = nvd*n1
       zt  = hdt
       zt0 = le
       go to 5
      end if

   30 format (2x,"At a time of ",f5.1," minutes :")
c   30 format (2x,"At a time of ",f5.3," seconds :")
   40 format (2x,"Z(m)",9x,"Tg(K)",7x,"Tp(K)",7x,"Ta(K)")
   50 format (1x,f7.5,3f12.1)
   60 format (2x)

      return
      end


c Subroutine for calculating the gas properties (in SI units)
c  - heat capacity, viscosity, thermal conductivity
c Note - data entered into subroutine are not all in SI
c  See block data for units to be used
      subroutine proprty(f,t,cpmix,vmix,kmix)
      parameter (nc=1,nrd=1)
      dimension pc(nc), tc(nc), cp(nc,4), f(nc)
      real ki, kmix, mw(nc)
      common /critcal/ mw, tc, pc, cp
c where
c      pc  = critical pressures of all components (atm)
c      tc  = critical temperatures of all components (K)
c      mw  = molecular weights of all components
c      cp  = heat capacity coefficients (cal/gmol*K)
c      f   = flow rates of all components
c      cpmix = mixture heat capacity (kJ/kmol*K)
c      vmix  = mixture viscosity (Pa*s)
c      kmix  = mixture thermal conductivity (kW/m*K)
```

```
c Conversion factor for heat capacity (cal/gmol*K to kJ/kmol*K)
      conv  = 4.184
      sumc1 = 0.0
      sumc2 = 0.0
      sumv1 = 0.0
      sumv2 = 0.0
      sumk1 = 0.0
      sumk2 = 0.0
      do 10 i = 1, nc
c Calculate component heat capacities (cal/gmol*K)
       cpi = 0.0
       do 20 j = 1, 4
        cpi = cpi + cp(i,j)*t**(j-1)
   20  continue
       tr    = t/tc(i)
       psi   = tc(i)**(1./6.)*mw(i)**(-0.5)*pc(i)**(-2./3.)
       gam   = psi*mw(i)
       aa    = 4.610*tr**0.618 - 2.04*exp(-0.449*tr)
c Calculate viscosity of each individual component (microPoise)
       vi    = (aa + 1.94*exp(-4.058*tr) + 0.1)/psi
c Calculate thermal conductivity of each component (stupid imperial)
       ki    = 1.e-6*cpi*(14.52*tr - 5.14)**(2./3.)/gam
c Use mixing rule to estimate mixture heat capacity
       sumc1 = sumc1 + f(i)*cpi
       sumc2 = sumc2 + f(i)
c Use mixing rule to estimate mixture viscosity
       sumv1 = sumv1 + f(i)*vi*sqrt(mw(i))
       sumv2 = sumv2 + f(i)*sqrt(mw(i))
c Use mixing rule to estimate mixture thermal conductivity
       sumk1 = sumk1 + f(i)*ki*sqrt(mw(i))
       sumk2 = sumk2 + f(i)*sqrt(mw(i))
   10 continue

c Calculate mixture heat capacity in kJ/kmol*K
      cpmix = sumc1/sumc2*conv
c Calculate mixture viscosity in Pa*s
      vmix = sumv1/sumv2*1.e-7
c Calculate mixture thermal conductivity in kW/m*K
      kmix = sumk1/sumk2*0.41868

      return
      end


c Driver subroutine for integrating quasi-steady state equations
      subroutine quasiss(es,vs,f)
      parameter (nc=1,nrd=1)
      parameter (n1=9,n2=9)
      parameter (nt=n1+n2-1)
      parameter (nv=2+nc)
      dimension iwk2(nv), wk2(17*nv+1)
      dimension x(nv)
      dimension es(nt), vs(nt), f(nc,nt), f0(nc)
      dimension difla(n1), diflb(n2)
```

```
      dimension zli(2,nl), almat(2,nl,nl), blmat(2,nl,nl)
      real le, mw(nc), km, ka, kp, mwave
      common /phycon/ p, pi, rid, g
      common /initial/ f0, tg0, vs0, es0
      common /spout/  le, hdt, din, ddt, db, cang
      common /collode/ zli, almat, blmat
      common /trans/ t0ref, fref, deld, delt, zt, tbw
      common /interp/ difla, diflb
      external quasi, fcn

c Set initial conditions for integration
      x(1)  = vs0
      x(2)  = es0
      do 10 i = 1, nc
       x(2+i) = f0(i)
   10 continue

c Set parameters for integration in the entrainment region
      ied = 1
      nax = nl
      ned = 0
      zt  = le
   20 continue
c Set constants for use with subroutine DGEAR
      tol  = 1.e-5
      h    = 1.e-8
      mth  = 1
      mitr = 0
      indx = 1
      z    = 0.0
      do 30 i = 2, nax
       zend = zli(ied,i)
       call dgear(nv,quasi,fcn,z,h,x,zend,tol,mth,mitr,
     &  indx,iwk2,wk2,ier)
       vs(i+ned) = x(1)
       es(i+ned) = x(2)
       do 40 j = 1, nc
        f(j,i+ned) = x(2+j)
   40  continue
   30 continue

c Integrate once more over the draft tube region
      if (zt.eq.le) then
       ied = 2
       nax = n2
       ned = nl-1
       zt  = hdt
       go to 20
      end if
      return
      end


c Subroutine containing equations for Vs, es, f(i)
```

```
      subroutine quasi(n,z,y,dy)
c The variables referred to are as follows:
c       y(1)  = solids velocity
c       y(2)  = voidage
c       y(j)  = flow rate of component , j = 3, 2+nc

      parameter (nc=1,nrd=1)
      parameter (n1=9,n2=9)
      parameter (nt=n1+n2-1)
      dimension y(n), dy(n)
      dimension f(nc), stc(nc,nrd), f0(nc)
      dimension pc(nc), tc(nc), cp(nc,4), aen(nrd), ff(nrd)
      dimension dhr0(nrd), dhr(nrd,4), c(nc)
      dimension rkr(nrd)
      dimension r(nrd), dt(4)
      dimension tgax(nt), difla(n1), diflb(n2), xint(n1)
      dimension zli(2,n1), almat(2,n1,n1), blmat(2,n1,n1)
      real le, mw(nc), km, ka, kp, mwave
      common /phycon/ p, pi, rid, g
      common /initial/ f0, tg0, vs0, es0
      common /spout/  le, hdt, din, ddt, db, cang
      common /param/  cpp, rhop, dp
      common /annul/  ea, kp, tw, fp, gloss
      common /critcal/ mw, tc, pc, cp
      common /react/  nr, aen, ff, rkr, stc, tref, trefe
      common /heats/ dhr0, dhr
      common /collode/ zli, almat, blmat
      common /trans/ t0ref, fref, deld, delt, zt, tbw
      common /tgas/ tgax
      common /interp/ difla, diflb

c Set parameters for either entrainment or draft tube region
      if (zt.eq.le) then
       ied = 1
       nax = n1
       ned = 0
       zt0 = 0.0
      else
       ied = 2
       nax = n2
       ned = n1-1
       zt0 = le
      end if

c Calculate the cross-sectional area in the spout
      call cxarea(z,as,dia,dasdz)

c Calculate the gas mixture properties
      ftot = 0.0
      do 10 i = 1, nc
       f(i) = y(2+i)
       ftot = ftot + f(i)
   10 continue
c Calculate the gas temperature at height z
```

```
c First evaluate Lagrangian interpolation coefficients
      pol = 1.0
      do 20 i = 1, nax
       yy      = z - zli(ied,i)
       xint(i) = 0.0
       if (yy.eq.0.) xint(i) = 1.0
       pol     = pol*yy
   20 continue
      if (pol.eq.0.) go to 40
      do 30 i = 1, nax
       if (ied.eq.1) then
        xint(i) = pol/(difla(i)*(z-zli(1,i)))
       else
        xint(i) = pol/(diflb(i)*(z-zli(2,i)))
       end if
   30 continue
   40 continue
      tg = 0.0
      do 50 i = 1, nax
       tg = tg + tgax(i+ned)*xint(i)
   50 continue
      tg   = tg*delt + t0ref
      call proprty(f,tg,cpm,vm,km)

c Calculate the gas velocity in the spout
      call gasprop(f,tg,as,y(2),rhog,us,mwave)

c Calculate the drag coefficient
      duv = us - y(1)
      rep = rhog*duv*dp/vm
      call cdrag(cd,rep)

c Calculate the particle velocity in the spout
      term1 = 0.75*rhog*cd*duv*abs(duv)/(rhop*dp)
      term2 = (rhop - rhog)*g/rhop
      dy(1) = (term1-term2)*zt/y(1)

c Calculate the void space in the spout
      esv = 1.-y(2)
      if (esv.le.0) then
       esv = 1.e-8
      end if
      if (ied.eq.2) then
       extra  = 0.0
      else
       extra  = esv*dasdz/as - fp/(as*y(1)*rhop)
      end if
      dy(2) = esv*dy(1)/y(1) + extra

c Calculate the component concentrations
      conc = p/(rid*tg*ftot)
      do 60 i = 1, nc
       c(i) = f(i)*conc
   60 continue
```

```
c Calculate the rates of reactions
      if (nr.gt.0) then
       call rrate(tg,c,r)
      end if

c Calculate the flow rate for each component
      do 70 i = 1, nc
c Include reaction rate term for each component
       term = 0.0
       if (nr.gt.0) then
       do 80 j = 1, nr
        term = term + stc(i,j)*r(j)
   80  continue
       end if
       if (ied.eq.2) then
        floss  = 0.0
       else
        floss  = f0(i)*gloss*3.*((1-z)**2)
       end if
       dy(2+i) = as*y(2)*term*zt - floss
   70 continue

      return
      end


c Subroutine to calculate the rates of reactions
      subroutine rrate(tg,c,r)
c The variables are defined as follows:
c    * tg  = gas temperature (K)
c    * c   = concentrations of all components
c      r   = rates of reaction
c Note * - input variables
      parameter (nc=1,nrd=1)
      dimension c(nc), r(nrd)
      dimension rk(nrd), rke(nrd)
      dimension aen(nrd), ff(nrd), rkr(nrd), stc(nc,nrd)
      dimension dhr0(nrd), dhr(nrd,4)
      common /phycon/ p, pi, rid, g
      common /react/  nr, aen, ff, rkr, stc, tref, trefe
      common /heats/ dhr0, dhr

c Calculate the rates of reactions
      do 10 i = 1, nc
       rk(i) = ff(i)*exp(-aen(i)/(rid*tg))
   10 continue
c Calculate the equilibrium rate constants
      dti = 1./tg - 1./trefe
      dtl = alog(tg/trefe)
      dtl = tg - trefe
      dt2 = tg**2 - trefe**2
      do 20 i = 1, nr
       if (rkr(i).ne.0.) then
```

```
          rkea = -(dhr0(i)+dhr(i,1))*dti + dhr(i,2)*dtl + dhr(i,3)*dtl
          rke(i) = rkr(i)*exp((rkea + dhr(i,4)*dt2)/rid)
          dkea = -dhr(i,1)/tg**2 + dhr(i,2)/tg + dhr(i,3)
         else
          rke(i) = 0.0
         end if
   20 continue

c Calculate the rates of reaction
       do 30 i = 1, nr
        r(i) = 1.0
        norder = 0
        do 40 j = 1, nc
         if (stc(j,i).lt.0) then
          if (c(j).eq.0.) then
           r(i) = 0.0
          else
           r(i) = r(i)*(c(j)**(-stc(j,i)))
          end if
         end if
   40   continue
c Add effect of reverse reactions
        if (rkr(i).gt.0.) then
         product = 1.0
         nrev    = 0
         do 60 j = 1, nc
          if (stc(j,i).gt.0) then
           if (c(j).eq.0) then
            product = 0.0
           else
            product = product*(c(j)**stc(j,i))
           end if
          end if
   60    continue
         r(i) = (r(i) - product/rke(i))*rk(i)
        else
         r(i) = r(i)*rk(i)
        end if
   30 continue

      return
      end


c Block data subprogram for input data
      block data

c Enter total number of components and reactions
      parameter (nc=1,nrd=1)
      real mw(nc), le, kp
      dimension f0(nc), pc(nc), tc(nc), cp(nc,4)
      dimension dhr0(nrd), dhr(nrd,4), aen(nrd)
      dimension ff(nrd), rkr(nrd), stc(nc,nrd)
      common /phycon/ p, pi, rid, g
```

```
      common /initial/ f0, tg0, vs0, es0
      common /spout/  le, hdt, din, ddt, db, cang
      common /param/  cpp, rhop, dp
      common /annul/  ea, kp, tw, fp, gloss
      common /critcal/ mw, tc, pc, cp
      common /react/  nr, aen, ff, rkr, stc, tref, trefe
      common /heats/ dhr0, dhr
      common /radiate/ sigma, emw, emp

c Set physical constants (pressure is assumed to be constant)
c   p   = kPa
c   pi  = what else?
c   rid = kJ/kmol*K
c   g   = m/s2
      data p,pi,rid,g /101.325,3.1415927,8.31432,9.81/
c The parameters to be specified are:
*      le = height of entrainment section (m)
*      hdt = height of draft tube (m)
*      din = diameter of inlet nozzle (m)
*      ddt = diameter of draft tube (m)
*      db  = diameter of bed (m)
*      cpp = particle heat capacity (kJ/kg*K)
*      rhop = particle density (kg/m**3)
*      dp = particle diameter (m)
*      ea = voidage in the annulus
*      kp = thermal conductivity of the particles (kW/m*K)
*      tw = outer wall temperature (C)
*      fp = overall rate of solid entrainment (kg/s)
      data le,hdt,din,ddt,db,cang /0.1516,0.60,0.0250,0.0400,0.20,60./
      data cpp,rhop,dp /1.07,2635.,0.001034/
      data ea,kp,tw,fp /0.42,3.3e-4,1214.0,0.06/
c Enter data corresponding to the radiation properties
*      sigma = Stephan-Boltzman constant (kW/m2*K4)
*      emw   = emissivity of wall material
*      emp   = emissivity of particles
      data sigma,emw,emp /5.672e-11,0.90,0.93/
c Enter data for component properties ( 100 % steam )
c Set inlet conditions
      data tg0,tp0,ta0,vs0,es0 /473.2,1373.2,1295.4,0.1,0.999/
      data f0(1) /5.94e-4/
c Enter component molecular weights
      data mw(1) /18.015/
c Enter component critical pressures (atm), and temperatures(K)
      data pc(1) /217.6/
      data tc(1) /647.3/
c Enter component heat capacity data (Reid,Sherwood,Prausnitz (1977))
c  (units given in terms of cal/gmol*K)
      data (cp(1,i),i=1,4) /7.701,4.595e-4,2.521e-6,-0.859e-9/
c Enter total number of reactions
      data nr /0/
c Enter reference temperatures for enthalpy calculations (K)
      data tref, trefe /298.0,1048.15/
c Set the standard heats of reaction at 298 K (kJ/kmol)
c Reaction numbers are as given in Sundaram and Froment
```

```
      data dhr0(1) /0.0/
c Enter the activation energies and frequency factors for reactions
c Note that the same numerical notation as Sundaram & Froment is used
      data aen(1) /0.0/
      data ff(1)  /0.0/
c Enter the equilibrium constants for reversible reactions
c  (if the reaction is not reversible then the equilibrium
c    constant must be entered as 0)
      data rkr(1) /0.0/

c Enter the stoichiometric coefficients for each component
c   with respect to each reaction
      data stc(1,1) /1.0/

      end
```